

8. INSTRUMENTATION REQUIREMENTS FOR ROD BUNDLE HEAT TRANSFER FACILITY

8.1 Introduction

The objective of the Rod Bundle Heat Transfer Program is to provide data on the key thermal-hydraulic phenomena of interest for dispersed flow film boiling and reflood heat transfer. Instrumentation requirements were developed to provide the needed data. The required information was identified in the PIRT given in Section 2. As the PIRT indicates, information is needed to develop and/or validate specific heat transfer and two-phase flow models. Since the objective is to develop the component models which comprise "reflood heat transfer", data will be obtained to view the component models as identified in the PIRT.

One of the more important objectives of the Rod Bundle Heat Transfer Program is to obtain new information on the mechanism of liquid entrainment at the quench front. This requires detailed measurements of the void fraction, droplet size, droplet velocity, and local heat transfer from the heater rods. The liquid entrainment at the quench front and the resulting droplet field downstream is responsible for the improved cooling at the upper elevations in the rod bundle where the peak cladding temperature occurs. Codes currently have difficulty predicting the correct amount of liquid entrainment as well as the timing of the entrainment. The instrumentation used in the Rod Bundle Heat Transfer Program will help resolve this modeling issue.

The instrumentation plan and layout will follow the lessons learned from the FLECHT⁽⁸⁻¹⁾ and FLECHT-SEASET⁽⁸⁻²⁾ reflood heat transfer programs as well as the ACHILLES⁽⁸⁻³⁾ experimental program. Both sets of FLECHT experiments and the Rod Bundle Heat Transfer experiments are separate effects tests with prescribed boundary and initial conditions. While there are needs for very specific data which is difficult to measure, proven instrumentation will be used with redundant measurement techniques where possible and developmental instrumentation will be verified using bench-top experiments before installing in the test bundle. In addition bundle mass and energy balances will be used to calculate parameters of interest from the data.

8.2 Instrumentation Requirements

Perhaps the most basic requirement is to perform transient mass and energy balances on the test facility. Inlet flow, pressure, coolant temperature, outlet vapor flow, pressure, and liquid flow will be measured. Since the reflood tests are transients, there will be mass accumulation within the bundle. The mass accumulation will be measured using sensitive differential pressure (DP) cells with fine axial spacing. This approach was used successfully in the FLECHT and FLECHT-SEASET programs and mass balances were typically within five percent. The DP resolution in the current facility is finer than FLECHT.

To obtain an axial void fraction distribution requires the use of several different measurements. These include inlet and exit measurements and axial heat flux into the coolant. The axial quality distribution above the quench front and the amount of evaporation can be calculated from the data. Similarly, the void distribution along the heated bundle can also be determined to indicate the flow and heat transfer regimes and the information used to correlate the measured heat transfer data.

The differential pressure drop measurements must be corrected for frictional pressure drop, as well as any acceleration pressure drop, to infer local void fraction.

Since the quality is non-equilibrium, measurements of the true vapor temperature are needed as well as the wall heat flux into the fluid. Different techniques were tried to measure the vapor temperature in a dispersed non-equilibrium two-phase flow as part of the FLECHT-SEASET program⁽⁸⁻²⁾, as well as elsewhere^{(8-4) (8-5) (8-6) (8-7)}. The technique that appears to be best is the use of miniature thermocouples which are placed normal to the flow and which point into the flow. As the froth region approaches, the thermocouples will wet since the droplet number density increases as the void fraction decreases. Very small thermocouples have a fast response time to allow the thermocouple to recover rapidly from being wetted by entrained droplets. In this fashion, a reasonable measure of the non-equilibrium vapor temperature can be achieved. Therefore, ample miniature thermocouples will be placed into the different subchannels along the axial length of the bundle. In addition, since the spacer grids can promote improved cooling downstream of the spacer, fluid thermocouples will be placed in these locations. A local quality can be calculated wherever a local vapor temperature exists in the bundle.

The experimental program will be structured to help separate the thermal-hydraulic phenomena which are observed during "reflood heat transfer". The test facility will be characterized hydraulically by measuring the rod bundle frictional losses. The spacer grid form losses will also be measured. Therefore, the two-phase differential pressure measurements can be corrected for frictional losses and form losses using single-phase data and an appropriate two-phase multiplier. Sufficient, sensitive, differential pressure cells will be arranged along the bundle to measure the rod bundle frictional losses and the grid losses over a range of Reynolds numbers.

Radiation-only experiments will determine, in-situ, the fraction of radiation heat flux which is transmitted from the inner rods to the housing, unheated dummy rods, and the outer peripheral row of rods. Values of the heater rod emissivity will be obtained from independent measurements using the pre-production heater rod which was tested at similar conditions. This data will help validate a multi-node model radiation network which can then be used to calculate the total radiation heat transfer in the bundle during reflood, and hence, the convective or dispersed flow film boiling portion of the total measured heat transfer. The data will also be used to validate the detailed COBRA-TF subchannel model for the test facility. Therefore, there is a requirement for sufficient thermocouple instrumentation on the heater rods, housing, and the dead or support rods at different planes within the bundle.

The fuel rods will be simulated using electrical heater rods with the capability to simulate decay power at 40 seconds following reactor scram. These rods will have an internal heating coil with a prescribed axial power shape. Thermocouples will be placed along the rods to cover the complete axial length of the bundle. There will be thermocouples at specific elevations to obtain the radial temperature distribution dependence in the bundle. Heat flux will be determined from an inverse conduction calculation using the thermocouple data. In addition, the experiments are designed for computer code validation purposes; therefore, the thermocouples and the differential pressure cells will be arranged within the bundle with the following considerations:

- The overall bundle energy distribution will be determined during the transient;
- Thermocouples will be placed upstream and downstream of spacers to see their effects;
- Thermocouples will be placed on the spacer grids to determine their temperature and quench time;
- Thermocouples will be placed on the housing and dummy rods for rod-to-dummy rod, and rod-to-housing radiation heat transfer calculations;
- Thermocouples will be placed at the center of the differential pressure cell spans such that one can then more easily relate the measured heat transfer to the local void fraction.

The experiments and instrumentation plan will allow a transient mass and energy balance to be performed.

In addition to heat transfer and the vapor and structure temperatures, data are needed on the flow behavior in the test bundle. In the froth region, data are needed on local void fraction distribution, interfacial area, and droplet/liquid ligament size. Also in the dispersed flow regime, data are needed on the droplet size, velocity, and number density for wall-to-drop radiation heat transfer, and the vapor-to-drop radiation and convective heat transfer. There is also evidence that entrained droplets enhance the convective heat transfer⁽⁸⁻¹⁾⁽⁸⁻²⁾ either by increasing turbulence, adding a distributed heat sink, or both. There is a requirement, therefore, that data be obtained on drop sizes, velocities, and number densities, to characterize the droplet mechanics of the dispersed two-phase region so interfacial area and droplet Weber numbers can be calculated from the test data. If the vapor flow rates and temperatures are known from other measurements, slip or relative droplet velocity can be calculated from the drop velocity measurements.

The flow regime must be characterized in the froth region where the liquid changes from continuous liquid dispersed droplet flow (continuous vapor). Therefore, the test section will require windows which will permit viewing and photographing the transient flow at important time periods in the transient.

8.3 Proposed New Instrumentation

While the Rod Bundle Heat Transfer program is not intended to be an instrumentation development program, several new techniques will be used to obtain the data needed as identified by the PIRT. A soft-gamma ray measuring device or x-ray system will be used at selected fixed elevations along the lower portion of the bundle.

The gamma densitometer will give chordal average densities of the two-phase flow mixture as the flow regime changes from a dispersed droplet flow to the froth region and finally to solid water. This technique has been used in the past for void fraction measurements in rod bundles with success in the article listed in Reference 8-8. To minimize attenuation of the soft gamma ray, beryllium inserts will be used in the test housing instead of quartz. The transient gamma ray measurements will provide an independent validation of the void fraction obtained from the finely spaced differential pressure measures.

Droplet information has been traditionally obtained using high speed photography and laborious methods to obtain drop sizes and velocities, by examining droplet behavior frame-by-frame from the high speed film. Newer techniques will be used in the Rod Bundle Heat Transfer program utilizing a pulsed laser technique in conjunction with a fine grid digital camera. This system is called a Laser Illuminated Digital Camera System (LIDCS). The pulsed laser provides backlighting as well as the focus volume for pictures in the center subchannels of the rod bundle. This measurement technique employs software to determine the droplet size spectrum, Sauter mean drop size, droplet velocities, drop velocity distribution and an estimate of the droplet number density. These data can be used to estimate the interfacial area of the entrained droplet phase. The pulsed laser and digital camera technique has not been applied to rod bundle heat transfer before; therefore, to verify the performance of the system and confirm the accuracy of the measurements, a series of "bench-top" experiments are being performed to develop the data reduction and analysis methods to analyze the droplet data.

There will also be new techniques used for more traditional measurements in the rod bundle. There will be very finely instrumented regions of differential pressure cells with three-inch spans along the bundle to calculate a more localized void fraction from the data in the froth region and dispersed regions (note, however, the dispersed region void fraction could be within the uncertainty of the pressure cell after corrections). These data will be used to help correlate the measured heat transfer with the local void fraction. There will also be miniature fluid thermocouples which will act as steam probes to measure the local vapor temperature. In addition there will also be traversing vapor measurements within the bundle at selected locations to give the subchannel local temperature. This technique will be verified in a small heated bench experiment.

These techniques and measuring systems will provide new, more accurate, more reliable data for computer code model development and validation.

8.4 Instrumentation Plan Comparison to the PIRT

The PIRT tables in Section 2 listed the key thermal-hydraulic models and or parameters which are needed for developing and validating component models which comprise “reflood heat transfer”. Most of the items identified in the PIRT tables can be measured directly. Some can be determined from analysis of the test data, and some can be determined from the literature, while others will not be fully separable from the measurements made. Tables 8-1 to 8-8 reproduce the PIRT tables from Section 2 and indicate how the specific phenomena will be measured. All PIRT items are given in these tables regardless of ranking; however, instrumentation and use of new measuring techniques have been oriented specifically to obtaining data for the highly ranked PIRT phenomena.

As the tables indicate, nearly all the highly ranked phenomena will be measured directly or calculated from the experimental data. When a parameter is directly calculated from the experimental data, the calculation uses the transient mass and energy balance on the test section to calculate the radially averaged fluid properties. A code is not used at this stage of the analysis so the data analysis is independent of the code to be validated by the experiments.

There will be some difficulties in measuring the effects of the different cladding used in the rod bundle experiments as compared to the Zircaloy cladding used in the fuel rods. This difference was discussed in the scaling analysis in Sections 6 and 7. The effects of the difference in the materials is small except for the minimum film boiling temperature. For this parameter, data from the literature, FLECHT tests with Zircaloy cladding⁽⁸⁻⁹⁾ and NRU experiments⁽⁸⁻¹⁰⁾ can provide guidance on the most appropriate value to be used. A similar situation exists for the differences in the heater rod surface emissivity and the emissivity for zircaloy rods. Here, however, the differences become smaller once the heater rod surface is oxidized. The emissivity of the oxidized surface approaches 0.9 for either metal. The determination of T_{\min} for different surface conditions, and material types is a candidate for a bench-type test and analysis.

In the dispersed flow film boiling region, the portion of the wall heat flux due to radiation heat transfer (to vapor, surfaces, housing, and droplets) can be separated from the measured total wall heat flux obtained from the inverse conduction calculation using the heater rod thermocouples. What cannot be easily separated from the remaining portion of the wall heat flux, in the froth flow regime, is the direct contact heat transfer. This mode of heat transfer occurs just above the quench front where the wall is near the minimum film boiling temperature. There have been models developed for this phenomena by Forslund and Rohsenow⁽⁸⁻¹¹⁾, Iloeji⁽⁸⁻¹²⁾ and Pederson⁽⁸⁻¹³⁾ and others (see Section 2), which can be used to separate this specific component from the remaining film boiling and convective heat transfer term. Different options and models will be used to assess the magnitude of this heat transfer component.

For forced flooding experiments, instrumentation will be required to measure the variable flow into and out of the bundle. Previous experiments have concentrated on only the positive oscillatory flow⁽⁸⁻¹⁴⁾ such that there is no reverse flow out of the bundle. ERSEC⁽⁸⁻¹⁴⁾ are the closest tests which simulate positive and negative flows. The FLECHT-SEASET tests simulated stepped flows which reflected the effects of the steam binding in PWRs. An injection scheme and measurement plan will be developed to measure the instantaneous flow into the bundle.

8.5 Conclusions

The instrumentation requirements were developed using the PIRT tables as a guide for the important phenomena for the different test types which the experiments must capture for code development and verification. The Rod Bundle Heat Transfer facility will employ ample instrumentation proven to perform in previous rod bundle experiments. There will also be state-of-the-art instrumentation to measure details of the two-phase flow field in a non-intrusive manner. The combination of the different techniques provides a robust instrumentation plan for the Rod Bundle Heat Transfer program so the most important phenomena identified in the PIRT can be measured or calculated from the data.

8.6 References

- 8-1. Lilly, G.P., Yeh, H.C., Hochreiter, L.E., and Yamaguchi, N., "PWR FLECHT Skewed Profile Low Flooding Rate Test Series Evaluation Report," WCAP-9183.
- 8-2. Lee, N., Wong, s., Yeh, H.C., and Hochreiter, L.E., "PWR FLECHT-SEASET Unblocked Bundle, Forced and Gravity Reflood Task Data Evaluation and Analysis Report," NRC/EPRI/Westinghouse Report No. 10, WCAP-9891, NUREG/CR-2256, RPRI NP-2013, November 1981.
- 8-3. Denham, M.K., Sowitt, D. and K.G. Pearson, "ACHILLES Unballooned Cluster Experiments, Part I, Description of ACHILLES Rig Test Section and Experimental Procedures," AEEW-R2336, November 1989.
- 8-4. Loftus, M.J., Hochreiter, L.E., Conway, C.E., Rosal, E.R., and Wenzel, A.H., "Non-Equilibrium Vapor Temperature Measurements in Rod Bundle and Steam Generator Two-Phase Flows," Proceedings of the Third CSNI Specialist Meeting on Transient Two-Phase Flow, March 1981.
- 8-5. Ihle, P., and Rust, K., "Influence of Spacers on the Heat Transfer During the Reflood Phase of a Pressured Water Reactor Loss of Coolant Accident," Nuclear Research Center, Karlsruhe, KFK Report 3178. September 1982.

- 8-6. Lilly, G.P., Yeh, H.C., Hochreiter, L.E., and Yamaguchi, N., "PWR FLECHT Cosine Low Flooding Rate Test Series Evaluation Report," WCAP-8838, 1977.
- 8-7. Unal, C., "An Experimental Study of Thermal Nonequilibrium Convective Boiling in Post-Critical-Heat-Flux Region in Rod Bundles," Ph.D. Dissertation, Lehigh University, 1985.
- 8-8. Jiang, Y and Rezkallah, K. S., "An Experimental Stude of the suitability of Using a Gamma Desitometer for Void Fraction Measurement in Gas-Liquid Flow in a Small Deameter Tube," Measurement Science and Technology, Vol. 4, pp. 496-505, 1993.
- 8-9. Cadek, F.F., Dominicis, D.P., and R.H. Leyse, "FLECHT Final Report," WCAP-7665, April 1971.
- 8-10. Mohr, C.L., et.al., "Data Report for Thermal-Hydraulic Experiment 2 (TH-2), NUREG/CR-2526, PNL-4164, November 1982.
- 8-11. Forslund, R.P., and Rohsenow, W.M., "Dispersed Flow Film Boiling," J.Heat Trans. 90 (6), 399-407, 1968.
- 8-12. Iloeje, O.C., Plummer, D.N., Griffith, P., and Rohsenow, W.M., "An Investigation of the Collapse and Surface Rewet in Film Boiling in Vertical Flow," J. Heat Trans. ,Vol. 97, pp. 166-172, 1975.
- 8-13. Pedersen, C.O., "The Dynamics and Heat Transfer Characteristics of Water Droplets Impinging on a Heated Surface," Ph.D. Thesis, Carnegie Institute of Technology, 1967
- 8-14. Clement, P., Deruaz, R., and Veteau, J.M., "Reflooding of a PWR Bundle Effect of Inlet Flow Rate Oscillations and Spacer Grids," European Two-Phase Flow Group Meeting, Paris, June 1982.

Table 8- 1 Single Phase Liquid Convective Heat Transfer in the Core Component During Reflood Below the Quench Front

<u>Process/Phenomena</u>	<u>Ranking</u>	<u>Basis</u>	<u>RBHT Instrumentation and Measurements</u>
- Convective Heat Transfer	M	1 ϕ Convective H.T. data has been correlated for rod bundles, uncertainty will not affect PCT, can effect point of boiling.	Will measure T_s , T_f and power below quench front so forced convective H.T. or natural convection H.T. can be calculated.
- Geometry	L	Hydraulic diameter has been shown to be acceptable for pitch-to-diameter ratio of 1.3.	
- Spacer Grids	L	Effects of spacers in 1 ϕ convective H.T. are known effects known for natural convection. No impact on PCT uncertainty.	Models exist for spacer H.T. multiplier. The effects of spacers will be measured with detailed axial T/C placement.
- Material Properties	L	Property effects are accounted for in analysis for 1 ϕ H.T. Little uncertainty.	Property effects can be calculated from T_s and T_b .
- Liquid Velocity (Reynolds Number)	M	Determine convective heat transfer	Will measure total flow, T_w , T_f , Can calculate heat transfer from data and correlate. Local flow can be calculated from subchannel code (COBRA, VIPRE) or by hand calculations

**Table 8-1 Single Phase Liquid Convective Heat Transfer in the Core Component During Reflood Below the Quench Front
(continued)**

- Liquid Subcooling	M	Liquid is heat sink	Fluid temperatures will be measured with miniature steam probes; selected T/C's can traverse.
- Decay Power	H	Source of energy for rods, boundary condition for test	Will be simulated.

Table 8 - 2 Subcooled and Saturated Boiling --Core Component Below the Quench Front

<u>Process/Phenomena</u>	<u>Ranking</u>	<u>Basis</u>	<u>RBHT Instrumentation and Measurements</u>
-Subcooled Boiling Heat Transfer and Heat Flux, Split of Energy Between Liquid and Vapor Production	M	A significant variation in the subcooled boiling heat transfer coefficient will not affect the PCT uncertainty since rod is quenched.	Will measure rod temperature (surface), local fluid temperatures (selectively) and power such that total wall heat flux can be calculated. Bundle average quality can be calculated from an energy balance. Codes use the Chen Model ⁽⁸⁾ which has a superposition of convection and boiling. The RBHT can be used to test this type of correlation since both T_s and q'' are measured. However, it will be difficult to determine directly the heat flux split between convection and boiling without using the correlation.
-Geometry, P/D, De	L	Boiling effects in rod bundles have been correlated for our P/d, De range with acceptable uncertainty.	The void fraction will be measured along the test section using ΔP cells, and at fixed locations with a soft gamma ray detector.
-Spacers	L	Locally enhances heat transfer; Correlations/ Models are available, acceptable uncertainty.	Effects of spacer grids can be measured with the detailed axial T/C placement on the heater rods.
-Material Properties	L	Data exists for the range of conditions, little uncertainty.	
-Local Void Fraction	M	Data exists for tubes and rod bundles	The void fraction will be measured along the test section using ΔP cells, and at fixed locations with a low energy gamma ray detector. This is a difficult measurement since the void is very low and attached to the heater rods.
- Liquid Subcooling	M	Determines the condensation of vapor, energy split	Subcooling will be measured with miniature T/C's, and traversing T/C's.

Table 8-2 Subcooled and Saturated Boiling – Core Component Below the Quench Front (continued)

- Interfacial Heat Transfer Area	M	Determines net vapor generation	Movies can be taken at different positions but very difficult to obtain interfacial area.
- Decay Power	H	Energy source for heat transfer	Will be simulated over a range of conditions.
-Saturated Boiling Heat Transfer and Heat Flux	M	Similar to subcooled boiling, data is available for our P/D, De range. The uncertainty of Saturated Boiling H.T. coefficient will not significantly impact the PCT since rod is quenched.	Rod wall temperature and heat flux will be measured as well as the fluid temperature (saturation).
-Geometry, P/D, De	L	Data exists in the range of P/D, De with acceptable uncertainties.	
-Spacer Grids	L	Locally enhances heat transfer, Correlations/ Models are available, with acceptable uncertainty.	The effect of the spacer grids can be detected from axial heater rod thermocouples.
-Material Properties	L	Data exists for our range of conditions, little uncertainty.	
-Local Void Fraction	H	Provides the fluid conditions as the flow enters the quench front region and total steam flow which effects the liquid entrainment.	The void fraction will be measured along the test section using ΔP cells, and at fixed locations with a low energy gamma ray detector.
-Decay Power	H	Source of energy for rods, boundary condition for the test.	Will be simulated.

Table 8 - 3 Quench Front Behavior in the Core Component

<u>Process/Phenomena</u>	<u>Ranking</u>	<u>Basis</u>	<u>RBHT Instrumentation and Measurements</u>
-Fuel/Heater Rod Materials, and Thickness ρ , C_p , k , Rod Diameter	H	These properties effect the stored energy in the fuel/heater rod and its quench rate, uncertainty directly impacts PCT.	Inconel Heater Rods will be used. Heater rod properties will be know from direct measurements.
-Gap Heat Transfer Coefficient	M	Second largest resistance in fuel rod. Affects heat release <u>rate</u> from fuel pellet. Gap heat transfer coefficient has large uncertainty, but its impact on PCT is smaller since all stored energy is redistributed much earlier than reflood, timing may change however.	Heater rods do have a gap like fuel rods since they are swagged. High gap conductivity is used for heater rods (5000 Btu/Hr -ft ² - °F since rods are swagged. Gap effects cannot be directly simulated with conventional heaters.
-Cladding Surface Effects <ul style="list-style-type: none"> • Oxides • Roughness • Materials • T_{min} • T_{CHF} 	H	Since Zircaloy oxidizes, the oxide layer will quench sooner due to its low conductivity, compared to Inconel. Also roughness of oxide layer promotes quenching. The surface condition effects T_{min} which is the point where quenching is initiated. Quenching is a quasi-steady two-dimensional process, Values of T_{min} and T_{CHF} can be estimated. Large uncertainty but relatively less impact on PCT.	Inconel will be used for the cladding since repeated tests will be performed. Other data on Zircaloy quench will be sought and compared to Inconel and specific T_{min} models, such that a simple model can treat both materials. Separate bench tests will be performed to characterize T_{min} for different surfaces and materials.
-Transition Boiling Heat Transfer (surface - liquid contact heat transfer)	H	Determines the <u>rate</u> of heat release at Quench Front directly impacts PCT, large uncertainty.	Depends on wall super heat. Low super heats, give high values, high super heats give low values. Quasi-steady, two-dimensional process. Estimates can be made using the closely spaced heater rod T/C's to obtain the axial conduction effects as well as a two-dimensional mode of the heat rod. Calculate heat flux by inverse conduction methods.

Table 8-3 Quench Front Behavior in the Core Component (continued)

-Steam Generation at Quench Front	H	It is the rapid amount of steam generation which creates the liquid entrainment, large uncertainty and impact on PCT.	This is a quasi-steady two-dimensional process. Steam generation rate can be calculated from the heater rod T/C's, total energy and the bundle mass and energy balance.
-T _{CHF}	H	Clad temperature when the critical heat flux is obtained, Used to develop the boiling curve and transition boiling.	Measured by heater rod T/C's some 2-dimensional correction may be needed.
-T _{min}	H	Clad temperature at minimum film boiling point, Demarcation between good and poor cooling is needed to develop boiling curve.	Measured by heater rod T/C's. Some 2-dimensional correction effects may be needed. Separate bench tests will also be performed to measure T _{min} and T _{CHF} for different surfaces.
-Surface Temperature	H	Cladding temperature indicates which heat transfer regime the surface is experiencing.	Measured by heater rod T/C's, may need some 2-dimensional correction effects.
-Spacer Grid	M	Steam generation at the quench front is the dominant effect and the resulting heat transfer is very large, location could impact entrainment due to wetting of the grid and vapor acceleration through the grid.	Axial placement of heater rod T/C's will show grid affects if any.
-Radiation Effects, Wall to Liquid, Vapor	L	The convective effects of the vapor generation dominates, wall temperatures are low.	Can calculate from the data via energy balance to obtain estimate.

Table 8-3 Quench Front Behavior in the Core Component (continued)

Decay Power	M	Stored energy is the primary source of energy for rods.	Will be simulated in tests.
Void Fraction/Flow Regime	H	Determines the wall heat transfer since large α results in dispersed flow, low α in film boiling. Directly impacts PCT.	Void fraction will be measured (estimated) using ΔP cells, and gamma densitometers, and high-speed movies.
Interfacial Area	H	Determines the initial configuration of the liquid as it enters the froth region directly impacts liquid/vapor heat transfer and resulting PCT downstream.	Interfacial area can be estimated from high-speed photography if windows remain dry.
Fluid Temperature	H	Influences the quench rate and net vapor generation. Important for high flooding rates, with high subcooling	Local miniature fluid temperatures will measure fluid temperature at many axial positions. Void fraction will also be measured with cells and gamma densitometer.

Table 8- 4 Two-Phase Froth (Transition) Region for Core Component

<u>Process/Phenomena</u>	<u>Ranking</u>	<u>Basis</u>	<u>RBHT Instrumentation and Measurements</u>
-Void Fraction/Flow Regime	H	Void fraction/flow regime helps determine the amount of vapor-liquid heat transfer, which affects the downstream vapor temperature at PCT, large uncertainty.	Average void fraction will be measured with DP cells. Vapor superheat will be estimated from miniature fluid T/C's.
-Liquid Entrainment	H	Significant generation of steam in the froth and quench regions helps create liquid entrainment.	Can be calculated from the rod bundle energy balance, however, assumption must be made on vapor temperature. Mass stored in froth region is measured by cells, and gamma measurements.
-Liquid Ligaments, Drop Sizes, Interfacial Area, Droplet Number Density	H	Liquid flow characteristics determine the interfacial heat transfer in the transition region as well as the dispersed flow region, large uncertainty.	The flow regime, interfacial area, droplet size, and droplet velocities will be estimated by high-speed photography, and laser measurements.
-Film Boiling Heat Transfer at Low Void Fraction Classical Film Boiling (Bromley)	H	Film boiling heat transfer is the sum of the effects listed below in the adjacent column. Each effect is calculated separately and is added together in a code calculation, large uncertainty.	Will measure the total heat transfer. Vapor heat transfer will be estimated from the bundle energy balance. The difference is the film boiling and direct contact heat transfer.
Droplet Contact Heat Transfer	H	Wall temperature is low enough that some direct wall-to-liquid heat transfer is possible, with high heat transfer rates, large uncertainty.	Some data exists on wall surface. Difficult to separate this component from total heat flux.

Table 8-4 Two-Phase froth (Transition) Region for Core Component (continued)

Convective Vapor Heat Transfer	M	Vapor convective heat transfer relatively less important since the liquid content in the flow is large and the vapor velocities are low, but large uncertainty.	Calculate from bundle energy balance using measured vapor temperatures, bundle exit liquid and vapor flows, total heat flux (corrected for radiation).
Interfacial Heat Transfer	M	Interfacial heat transfer effects are relatively small since the steam superheat is low, large uncertainty exists.	Interfacial heat transfer will be inferred from the vapor temperature measurements and flow as calculated from bundle energy balance.
Radiation Heat Transfer to Liquid/Vapor	M	The radiation heat transfer effects are also small since the rod temperatures are low.	Radiation tests will help isolate the different components. Increased radiation will exit in the tests due to the two phase mixture since there will be wall-to-mixture radiation in addition to surface-to-surface radiation.
Spacer Grids	M	The velocities and Reynolds numbers are low in this region such that droplet breakup and mixing are not as important. Drop deposition could occur.	Axial placement of <i>heater</i> rod T/C's will measure the effects of spacers.
-Decay Power	H	Source of power for rods.	Will be simulated.

Table 8 - 5 A Dispersed Flow Region for Core Component

<u>Process/Phenomena</u>	<u>Ranking</u>	<u>Basis</u>	<u>RBHT Instrumentation and Measurement</u>
-Decay Power	H	Energy source which determines the temperature of the heater rods, and energy to be removed by the coolant.	Power is a controllable parameter in the experiment
-Fuel Rod/Heater Rod properties, ρ , C_p , k	L	Properties can be modeled. Stored energy release is not important at this time.	Data on heater rod properties will be independently measured.
-Dispersed Flow Film Boiling (components given below)	H	Dispersed flow film boiling modeling has a high uncertainty which directly effects the PCT.	Current plan for tests is to perform a bundle energy balance to obtain local quality. The convective heat transfer will be calculated using steam-only tests such that a 1ϕ convective correlation for RBHT facility will be available. Specific tests will also be run to determine the effects of convective enhancement and radiation heat transfer such that the different heat transfer effects should be separable from the total heat transfer measured in a reflood test.
■ Convection to Superheated Vapor	H	Principal mode of heat transfer as indicated in FLECHT-SEASET experiments.	Similar convective behavior is expected in the RBHT tests, as in the FLECHT-SEASET tests, except that the spacer grids may have a larger effect because of mixing vane design.
■ Dispersed Phase Enhancement of Convective Flow	H	Preliminary models indicate that the enhancement can be over 50% in some cases.	A series of separate tests will be performed to examine this heat transfer effect which will be compared to the single-phase convection tests.

Table 8-5 A Dispersed Flow Region for Core Component (continued)

-Gap Heat Transfer	L	Controlling thermal resistance is dispersed flow film boiling heat transfer resistance. Large gap heat transfer uncertainties are not important, but fuel centerline temperature is affected.	Heater rods will not simulate the gap heat transfer, but not needed for this regime.
-Cladding Material	L	Cladding material in the tests is Inconel which has the same conductivity as Zircaloy. Nearly the same temperature drop will occur.	Test will use Inconel.
-Oxidation Rate	M	Inconel will not oxidize while Zircaloy will, and create a secondary heat source at very high PCTs, Zircaloy reaction can be significant at high temperature.	Oxidation not simulated in tests since cladding is Inconel.
-Fuel Clad Swelling/Ballooning	L	Ballooning can divert flow from the PCT location above the ballooning region. The ballooned cladding usually is not the PCT location. Large uncertainty.	Flow blockage is not simulated but was modeled in FLECHT-SEASET Heat transfer was improved.

Table 8-5 A Dispersed Flow Region for Core Component (continued)

<ul style="list-style-type: none"> ■ Direct Wall Contact ■ Heat Transfer 	L	Wall temperatures are significantly above T_{min} such that no contact is expected.	Will verify no contact from the literature. This component cannot be directly measured in the RBHT tests but we can estimate its effects. Separate small-scale tests are needed.
<ul style="list-style-type: none"> ■ Droplet Dry Wall Contact 	M	Iloeje indicates this heat transfer mechanism is less important than vapor convection.	This component cannot be separated out of the total heat flux data in the RBHT tests. Separate smaller scale tests are needed. This effect will be captured in the measured total heat flux.
<ul style="list-style-type: none"> ■ -Droplet-to-Vapor Interfacial Heat Transfer 	H	Interfacial heat transfer reduces the vapor temperature, which is the heat sink for the wall.	The axial vapor temperature distribution will be measured, and the bundle average quality will be calculated to obtain the evaporation. Also, drop sizes and velocities will be measured.
<p>- Radiation Heat Transfer</p> <ul style="list-style-type: none"> ■ Surfaces ■ Vapor ■ Droplets 	<p>H/M</p> <p>H/M</p> <p>H/M</p>	Important at higher bundle elevations (H) where convective heat transfer is small since the vapor is highly superheated. Very important for BWR reflood with sprays and colder surrounding channel. Large uncertainty.	Separate tests will be used to characterize the radiation behavior of the RBHT test facility with no convection. The surface emissivity will be independently measured. Radiation Heat Transfer will be calculated for the forced flooding tests.

Table 8 - 6 Top Down Quench in Core Components

<u>Process/Phenomena</u>	<u>Ranking</u>	<u>Basis</u>	<u>RBHT Instrumentation and Measurements</u>
Deentrainment of Film Flow	L ¹	Film flow quenches the heater rod. High uncertainty.	The top-down quench front will be measured but deentrainment of drops onto the liquid film will not be measured.
Sputtering Droplet Size and Velocity	L	Droplets are sputtered off at the quench front and reentrained upward. Since the sputtering front is above PCT location, no direct impact. Entrained, sputtered drops affect total liquid entrainment, as well as the steam production in the steam generators.	If the top quench front progresses downward such that it is within a viewing location then droplet size and velocity can be estimated from high-speed movies and laser measurements. Quench locations will be determined from heater rods T/C's and housing T/C's.
Fuel Rod/Heater Rod Properties for Stored Energy $\rho, C_p, k.$	L ¹	These properties are important since they determine the heat release into the coolant. However, since this occurs above PCT level, no impact.	Heater rod stored energy is approximately the same as the fuel rod. The conductivity of the heater rod is larger than the fuel rod so heat is released quicker.
Gap Heat Transfer	L ¹	Affects the <u>rate</u> of energy release from fuel/heater rod.	No gap heat transfer simulated.

Some of these individual items can be ranked as high (H) within the top down quenching process; however, the entire list is ranked as low for a PWR/BWR since it occurs downstream of the PCT location.

Table 8 - 7
Preliminary PIRT for Variable Reflood Systems Effects Tests

<u>Process/Phenomena</u>	<u>Ranking</u>	<u>Basis</u>	<u>RBHT Instrumentation and Measurements</u>
Upper Plenum - Entrainment/Deentrainment	M	Upper plenum will fill to a given mixture level after which the remaining flow will be entrained into the hot leg, large uncertainty.	A non-scaled upper plenum will be simulated in the tests; it should be easier liquid to entrain relative to a plant. Differential pressure cells will indicate mass storage.
Hot Leg - Entrainment, Deentrainment	L	Hot legs have a relatively small volume and liquid entering the hot leg will be entrained into the steam generator plena, medium uncertainty.	Hot leg entrainment can be simulated up to the separator which will separate the liquid flow.
Pressurizer	L	Pressurizer is filled with steam and is not an active component-small uncertainty.	Pressurizer will not be simulated.
Steam Generators	H	The generators evaporate entrained droplets and superheat the steam such that the volumetric vapor flow increases (particularly at low pressure). The result is higher steam flow downstream of the generators, high uncertainty since a good model is needed. FLECHT-SEASET data exist.	The steam generators will not be simulated, but the aspects of the higher steam flow will be accounted for when specifying the inlet flooding rates. Flow pressure drop across simulated resistance will be measured.
Reactor Coolant Pumps	H	Largest resistance in the reactor coolant system, directly affects the core-flooding rate, low uncertainty.	The resistance will be represented in the test to give approximate inlet flooding rate response observed in the system calculations.
Cold Leg Accumulator Injection	H	Initial ECC flow into the bundle.	Accumulator flow rates will be scaled, simulated, and measured.

Table 8 - 7
Preliminary PIRT for Variable Reflood Systems Effects Tests (continue)

Cold Leg Pumped Injection	H	Pumped injection is the liquid source for majority of the reflood transient.	Pumped injection will be simulated and measured.
Pressure	H	Low pressure (~35 psia) significantly affects vapor volumetric flow steam binding decreases the bundle flooding rate.	Pressure range will be simulated and measured.
Injection Subcooling	M/H	Lower subcooling will result in more boiling below the quench front, additional vapor to vent.	Subcooling range will be simulated.
Downcomer wall heat transfer	H	The heat transfer from the downcomer walls raises the ECC fluid temperature as it enters the core, resulting in more steam generation.	Simulate affect by varying the inlet temperature.
Lower Plenum Wall Heat Transfer	M	Same effect as downcomer.	Simulate the metal heat effect by varying the inlet temperature.
Break	L	Excess ECC injection spills out of vessel, break ΔP helps pressurize reactor system.	Simulate break ΔP .

**Table 8 - 8
High Ranked BWR Core Phenomena**

<u>Process/Phenomena</u>	<u>Basis</u>	<u>RBHT Instrumentation and Measurements</u>
■ Core Space Film Boiling	PCT occurs in film boiling.	Film boiling components will be measured by heater rod T/C's, data will be corrected for radiation.
■ Upper Tie Plate CCFL	Hot assembly is in cocurrent up-flow above CCFL limit.	Similar behavior as PWR reflooding.
■ Channel-bypass Leakage	Flow bypass will help quench the BWR fuel channel.	The housing in the RBHT test will approximate a BWR channel, no leakage flow simulated; housing T/C's will indicate quench location.
■ Steam Cooling	A portion of the dispersed flow film boiling heat transfer.	Simulated in RBHT tests.
■ Dryout	Transition from nucleate boiling and film boiling.	Simulated in RBHT tests, but hot assembly is calculated to be in up flow.
■ Natural Circulation Flow	Flow into the core and system pressure drops.	Flow range can be simulated in RBHT, using pumped flow.
■ Flow Regime	Determines the nature and details of the heat transfer in the core.	Since pressures, heat flux, temperature, and flows can be simulated, flow regimes will be representative, measurements of void fraction by cells, gamma densitometer, high speed photography.
■ Fluid Mixing	Determines the liquid temperature in the upper plenum for CCFL break down.	Not simulated in RBHT, but hot assembly is calculated to be in upflow.

Table 8 - 8
High Ranked BWR Core Phenomena (continued)

■ Fuel Rod Quench Front	Heat release from the quench front will determine entrainment to the upper region of the bundle.	Heater rod T/C's will indicate the quench front behavior.
■ Decay Heat	Energy source for heat transfer.	Will simulate in RBHT as a boundary condition.
■ Interfacial Shear	Affects the void fraction and resulting droplet and liquid velocity in the entrained flow.	Is not directly measured, can estimate for different flow regimes from data.
■ Rewet: Bottom Reflood	BWR hot assembly refloods like PWR.	Simulated in RBHT.
■ Rewet Temperature	Determines quench front location.	RBHT will use different materials than fuel rod; bench tests will be used to support the RBHT data.
■ Top Down Rewet	Top of the hot assembly will rewet in a similar manner as PWR.	Will be simulated in RBHT.
■ Void Distribution	Gives the liquid distribution in the bundle.	Will be measured with differential pressure cells, gamma densitometer and/or x-ray techniques.
■ Two-Phase Level	Similar to quench front location, indicates location of nucleate and film boiling.	Will be measured with heater rod T/C's and differential pressure cells obtain axial void distribution.

9. DEVELOPING A FACILITY INPUT MODEL

9.1 Introduction

The COBRA-TF^(9-1, 9-2, 9-3) computer code was used to model the RBHT facility. The objective was to perform pre-test calculations to obtain information about the range of the parameters to expect during reflood transient. This analysis also provided a basis to develop the test matrix and indicate the maximum temperature conditions reached in the bundle for a given set of conditions.

The COBRA-TF code was developed at the Pacific Northwest Laboratory under the sponsorship of the NRC to provide best-estimate thermal-hydraulic analyses of a LWR vessel during LOCAs. The two-phase flow is described with a two-fluid, three-field model. Thermal radiation and grid spacer effects are also included in the code, as well as a more detailed dispersed flow film boiling model as described in Section 4. The code was developed for use with either rectangular Cartesian or sub-channel coordinates.

Two COBRA-TF models of the RBHT test facility were developed: a two-channel model and a more detailed individual sub-channel model. The two-channel model was used to examine the local fluid conditions within the test facility for comparison with a plant. This model does not account for rod-to-rod or rod-to-housing radiation heat transfer from the inner channel which exists in the test bundle. The model does account for the test section housing and calculates the convection heat transfer to the housing as well as the energy released from the housing as it quenches.

A more detailed, 1/8th sector of the test facility was modeled on a sub-channel basis with each sub-channel, individual heater rod surface, and the gap between rods uniquely modeled. The subchannel capability of COBRA-TF allows more accurate representation of small rod bundle arrays since each individual rod can be modeled with different surfaces for radiation heat transfer, so rod-to-rod and rod-to-housing radiation heat transfer can be modeled more accurately. In this fashion, the radial temperature gradient which develops due to the radiation heat losses to the test section housing can be simulated. There are specific experiments planned in the RBHT program to examine radiation-only heat transfer within the rod bundle and to the test section housing. The emissivities of the rods and housing will be measured.

Both the two-channel and the sub-channel model were used for pre-test analysis. Since the two-channel calculations run much quicker and are easier to analyze, the majority of the pre-test calculations used this model. The more detailed model was used selectively for specified tests to examine the detail of the flow structure within the rod bundle.

9.2 Two-Channel Model

9.2.1 Input deck description

The analysis considered a 7x7 rod array comprised of forty-five heater rods, four unheated rods, and the surrounding housing. The facility modeling approach was to divide the test facility into four sections and five fluid channels. As shown in Figure 9-1, channels one and five represent the lower and upper plenums, respectively. Channel two models the low end fitting of the rod bundle. The third element is the actual heated length of the rod bundle and contains two fluid channels. Channel three is the inner channel and encompasses a total of sixteen 'hot' rods; this includes the nine center rods and summation of the fractional parts of the rods that lie on the channel's boundary (Figure 9-2). The second core channel, channel four, is comprised of the remaining twenty-nine heater rods, the four unheated rods, and the housing.

Three geometry types, *hrod*, *tube* and *wall*, were employed to represent the components of the test section. The *hrod* type signifies a solid cylinder and, thus, was employed to model the heater rods. As shown in Figure 9-3, successive layers of Boron Nitride, Monel K-500, Boron Nitride and Inconel 600 constitute the material composition of each rod. The unheated rods, of *tube* geometry, consist solely of Inconel 600.

The housing was modeled as a single wall with a cross-sectional area and wetted perimeter equal to the sum of the four individual sides. Both radial and axial noding were specified in the input model. As seen in Figure 9-4, there are three radial nodes for the Inconel 600 unheated rods and housing.

Radial noding in the heater rods is shown in Figure 9-3. The first two material segments of the rods (Boron Nitride and Monel K-500) both feature only one node, while three nodes each were allocated to the latter two segments. Axially, a total of twenty-eight nodes were specified, distributed as follows: two in the lower plenum, one in the lower end fitting, twenty-two in the heated length, and three in the upper plenum. Nodal boundaries in the heated length (see Figure 9-5) align with the grid locations, an ideal situation from a computational standpoint. Consequently, since the first grid is located 2.51 inches from the bottom of the rod bundle, the first axial node in the heated length is 2.51 inches from the bottom of the core.

The major approximation made by this input model was to neglect radiation heat transfer. COBRA-TF does not have the capability to calculate radiation effects across channel boundaries; rather, it can only calculate radiation within each channel. Each rod within a channel is considered to be at the same temperature, therefore wall-to-wall radiation effects within the channel boundaries are neglected.

9.2.2 Results of Two-Channel Model

At the time this report was written, work was still continuing, so the results presented in this section are preliminary.

The analysis considered three flooding transients with different flooding rates (20.32, 25.4, 38.1 mm/sec), (0.8, 1.0 and 1.5 in/sec). A constant pressure (40 psia) was set in the upper plenum. The water inlet subcooling was 48.89 C (120 F). The axial power shape is shown in Figure 9-6 which is the axial shape to be used in the RBHT tests. The initial power was chosen at 0.7 kW/ft at the peak power location of 108 inches from the bottom of the heated length. The decay power factor is the ANS-1971 +20% and is shown in Figure 9-7. This parameter will be ranged to cover the ANS-1979 decay heat standard as well as to provide overlap with existing data. In the actual experiments, the initial rod temperature will be determined by an adiabatic heat-up, not simulated in this analysis. The initial peak temperature was assumed to be 815 C (1500 F), and the local rod initial temperature was calculated based on the local power factor. The initial housing temperature was assumed to be a uniform value of 260 C (500 F). The simulation was carried out for 500 seconds.

The 25.4mm/sec (1.0 in/sec) flooding rate results are shown in Figures 9-8 through 9-15. Figure 9-8 shows the quench front location versus time. The quench front rises relatively rapidly during the first 180 seconds, then it slows down. The average quench front velocity between 200 and 500 seconds is 0.096 in/sec. Figure 9-9 shows the hot rod clad temperature at different elevations. The Peak Clad Temperature 1354 C (2470 F) is reached at about 170 seconds at the peak power location.

The housing temperature at different elevations is given in Figure 9-10, showing that the maximum temperature is reached at the same heater rod peak locations. The axial distribution of hot rod temperature is shown in Figure 9-11. Figure 9-12 shows the vapor temperature at different locations above the quench front. The effect of the grids is to reduce the vapor temperature downstream of the grids and, as a consequence, this reduces the clad temperature at the same locations. This effect is visible in Figures 9-11 and 9-12.

Figures 9-13 and 9-14 show respectively the vapor flow rate and the entrained liquid flow rate at the outlet of the bundle. An almost quasi-steady-state is reached at the end of the transient where the total of vapor, continuous liquid, and droplets flow rates almost matches the inlet subcooled liquid flow rate.

Finally Figure 9-15 shows the pressure at the inlet of the bundle. Since pressure is fixed at 40 psia at the outlet of the bundle, the inlet pressure is the result of the gravity head and pressure drop across the bundle.

Similar results were obtained with the inlet flow rates of 20.3 mm/sec (0.8 in/sec) and 38.1 mm/sec (1.5 in/sec). Results are not shown in detail for these two cases but it is interesting to calculate the range of Re number in this range of flooding rate. Figures 9-16, 9-17 and 9-18 show the vapor Re number for respectively 20.3, 25.4, and 38.1 mm/sec (0.8, 1.0 and 1.5 in/sec)

cases. These figures indicate that the vapor Reynolds number can be within the laminar and transition regimes, as well as turbulent flow.

The droplet *Weber* number was calculated for the 1.0 in/sec flooding rate at 425 seconds into the transient when the flow conditions present a smooth, quasi-steady state behavior. The *We* number is based on:

where the droplet diameter is calculated from the equation

The *We* is calculated just above the quench front and at the bundle outlet using the following variable values obtained from the code output:

**Table 9-1:
Weber number parameter at 425 seconds**

	Description	Value just above the quench front	Value at the top of the bundle
	Entrainment phase void fraction	0.0029	0.0003
	Vapor density (lbm/ft ³)	0.0610	0.0397
	Surface tension (lbf/ft)	0.00366	0.00366
	Vapor velocity (ft/s)	19.49	54.69
	Entrainment phase (droplets) velocity (ft/s)	3.64	37.51
	Interface area (ft ² /ft ³)	9.79	1.48

The calculated value of the *Weber* number ranges from 7.4 just above the quench front to 3.9 at the top of the bundle.

9.3 Individual Sub-Channel Model

9.3.1 Input deck description

A detailed COBRA-TF sub-channel model of the Rod Bundle Heat Transfer test section was developed to examine the effects of rod-to-rod and rod-to-housing radiation as well as the sub-channel flow behavior during reflood. The RBHT test section is assumed to have 1/8 symmetry which enables COBRA-TF to model the bundle with 10 rods, 10 channels, 12 gaps, and 4 wall sections, as seen in Figure 9-19. Each rod is divided into four (4) surfaces with each surface oriented towards a channel. The heater rod surfaces are connected thermally by azimuthal conduction heat flow paths. Partial rods have less than four surfaces, with the number dependent upon rod orientation. The composition and noding of the rods and housing are identical to the description of the two-channel model in section 9.2.

The sub-channel model uses the same power profile and linear power densities as the two-channel model, the peak linear power being at 108 inches and 0.7 kW/ft. The axial noding of the test section is identical to the two-channel model described in Section 9.2 with 22 nodes and 8 spacer grids except the test section contains 10, not 2 channels. The plenum are modeled at the top and bottom of the test section to provide inlet and exit boundary conditions. An intermediate section with three channels is used to link the test section to the plenums (COBRA-TF does not allow more than six channels to be directly linked to one channel). Figure 9-20 shows the axial nodal diagram for the sub-channel model.

Each rod is modeled with four separate surfaces. The COBRA-TF radiation model exchanges radiation between surfaces of the rods and surfaces in the four adjoining channels, and the channel walls through the rod gaps. Because of the symmetry planes (1/8 symmetry) the net radiation across a line of symmetry is zero. The azimuthal conduction model allows heat to be conducted around the rods from hot surfaces oriented toward the center of the bundle to the cold surfaces nearer the bundle housing.

Initial temperature distributions in the test section are taken from a COBRA run from which the bundle is initially at saturation, 130° C (267 °F), and heated about 110 seconds until the peak rod temperature is 870 °C (1600 °F). This procedure is the prescribed pre-test heatup phase.

9.3.2 Results of Sub-Channel Model

To determine the effect of the housing on the bundle temperature distribution, the sub-channel model was run with and without the ten radiation channels. The inlet conditions were set to zero such that the bundle was heated in an adiabatic manner in a stagnant steam environment. However, as the bundle was heated, steam convective currents developed and steam was released from the top pressure boundary to maintain the system pressure at 40 psia. Also, the bundle underwent convective heat transfer from the hot rods to the unheated surfaces because natural circulation paths were set in motion between grid spans.

The bundle was heated for 50 seconds to obtain the peak rod temperature at 870°C (1600 °F).

The results presented in Figure 9-21 are taken at the peak power location at the end of the 50 second heat-up. All temperature information on Figure 9-21 is in Celsius. Initial temperatures at the peak location were:

Heated Rods:	870 °C (1600 °F)
Corner Rod:	340 °C (645 °F)
Housing:	250 °C (482 °F)

These results confirm the assumption that the central 5x5 array of rods can be assumed to be at the same temperature. For the central rods the maximum temperature difference is 39 °C (70 °F). The outer most row of rods is quite effective in shielding the remainder of the rods.

The detailed sub-channel model will be used to selectively analyze the test facility to establish the exact test facility test conditions.

9.4 Conclusions

Two COBRA-TF models were developed for the RBHT facility. A two-channel model represents the 7x7 rod bundle by splitting the bundle into two channels. One channel describes the inner, hotter rods and another describes the peripheral rods. The peripheral (in this case) rods are colder due to the presence of the housing, which provides a heat sink because of convective heat transfer. The two-channel model does not include radiation heat transfer. This was modeled with a more detailed sub-channel model.

The detailed sub-channel model was developed. The adiabatic heat-up phase for the RBHT facility was simulated. Results show that radiation heat transfer is especially important for the rods facing the housing. The central 5x5 array of rods have practically uniform temperature with a maximum temperature difference of 39 °C (70 °F). The outer most row of rods is quite effective in shielding the remainder of the rods.

These preliminary results show the values of parameters to be expected during reflood of the RBHT bundle and provide the range of fluid Re and We number in those conditions which should be compared with those expected in PWR and/or BWR reflood.

9.5 References

- 9-1 C.Y. Paik et al., "Analysis of FLECHT SEASET 163-Rod Blocked Bundle Data Using COBRA-TF," NUREG/CR-4166, 1985.
- 9-2 Thurgood, M. J., et al., "COBRA-TRAC: A Thermal-Hydraulic Code for Transient Analysis of Nuclear Reactor Vessels and Primary Coolant Systems," NUREG/CR-3046 (PNL 4385), Volumes 1-5, 1982.
- 9-3 Wheeler, C. L., et al., "COBRA-IV-I: An Interim Version of COBRA for Thermal Hydraulic Analysis of Rod Bundle Nuclear Fuel Elements and Cores", BNWL-1962, 1973.

Fig. 9-1

RBHT - PARTITIONING OF SECTIONS, CHANNELS & GAPS

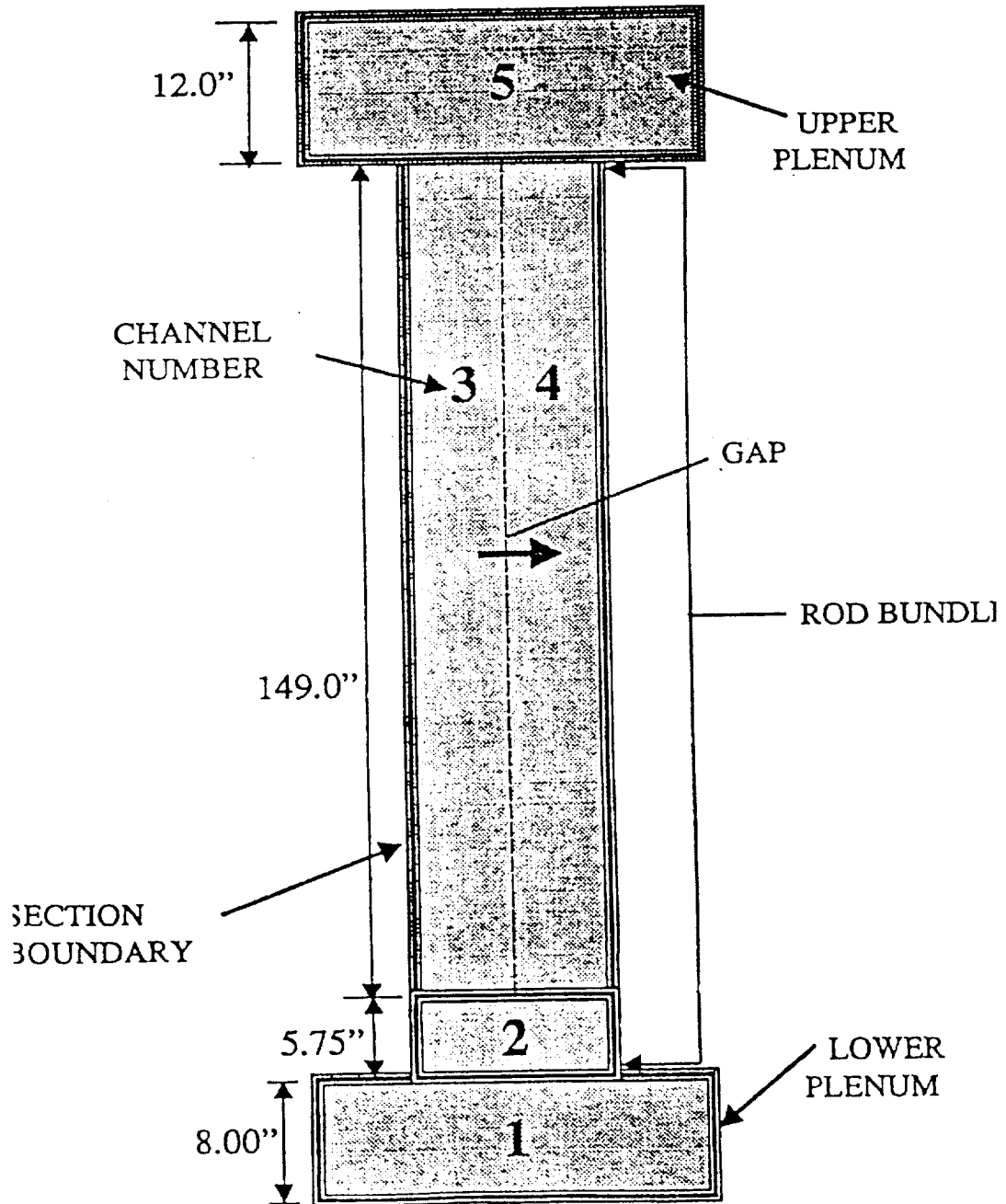


Fig. 9-3

RBHT HEATER ROD - RADIAL DIMENSIONS, MATERIALS & NODING SCHEME

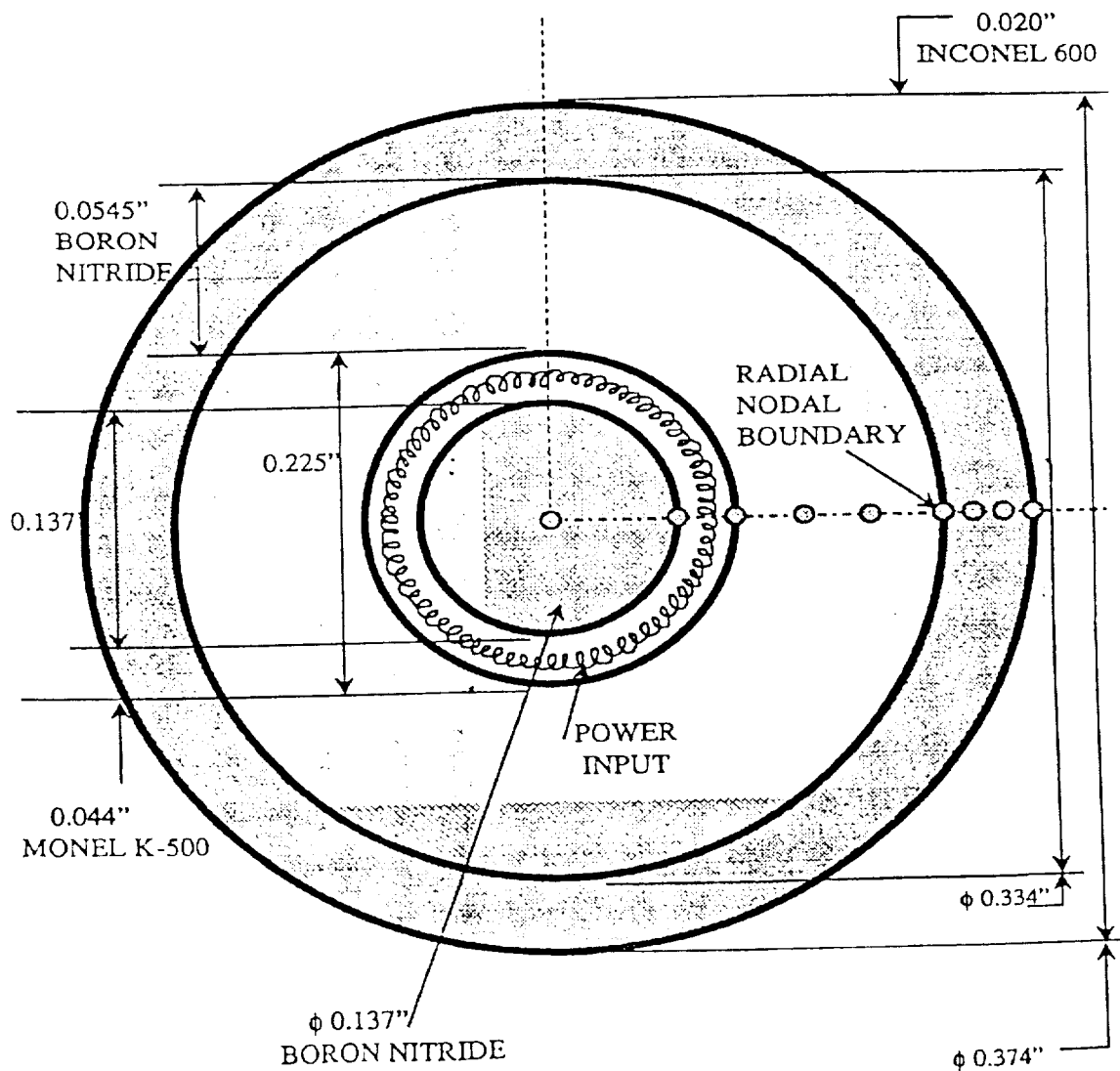


Fig. 9-4

RBHT - RADIAL DIMENSIONS, MATERIALS & NODING SCHEME

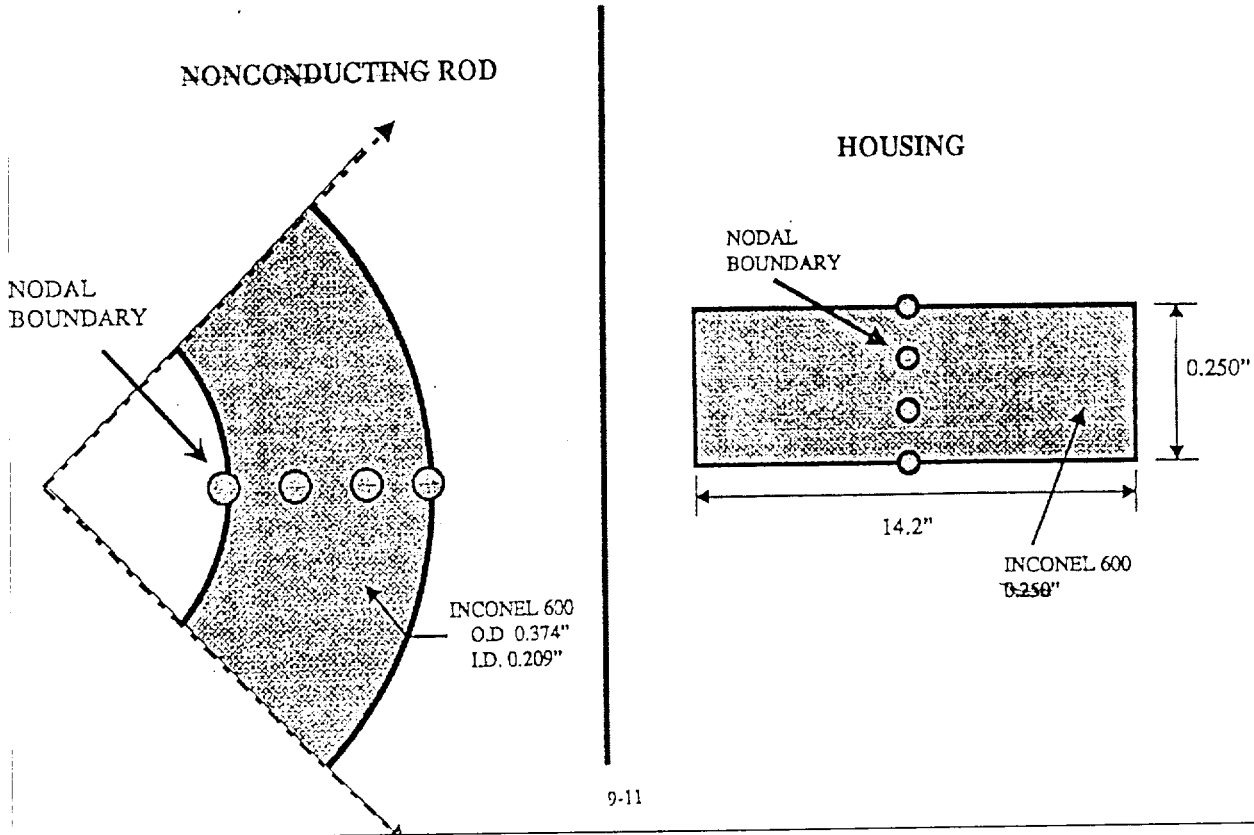


Fig. 9-5

RBHT - AXIAL DIMENSIONS & NODAL SCHEME

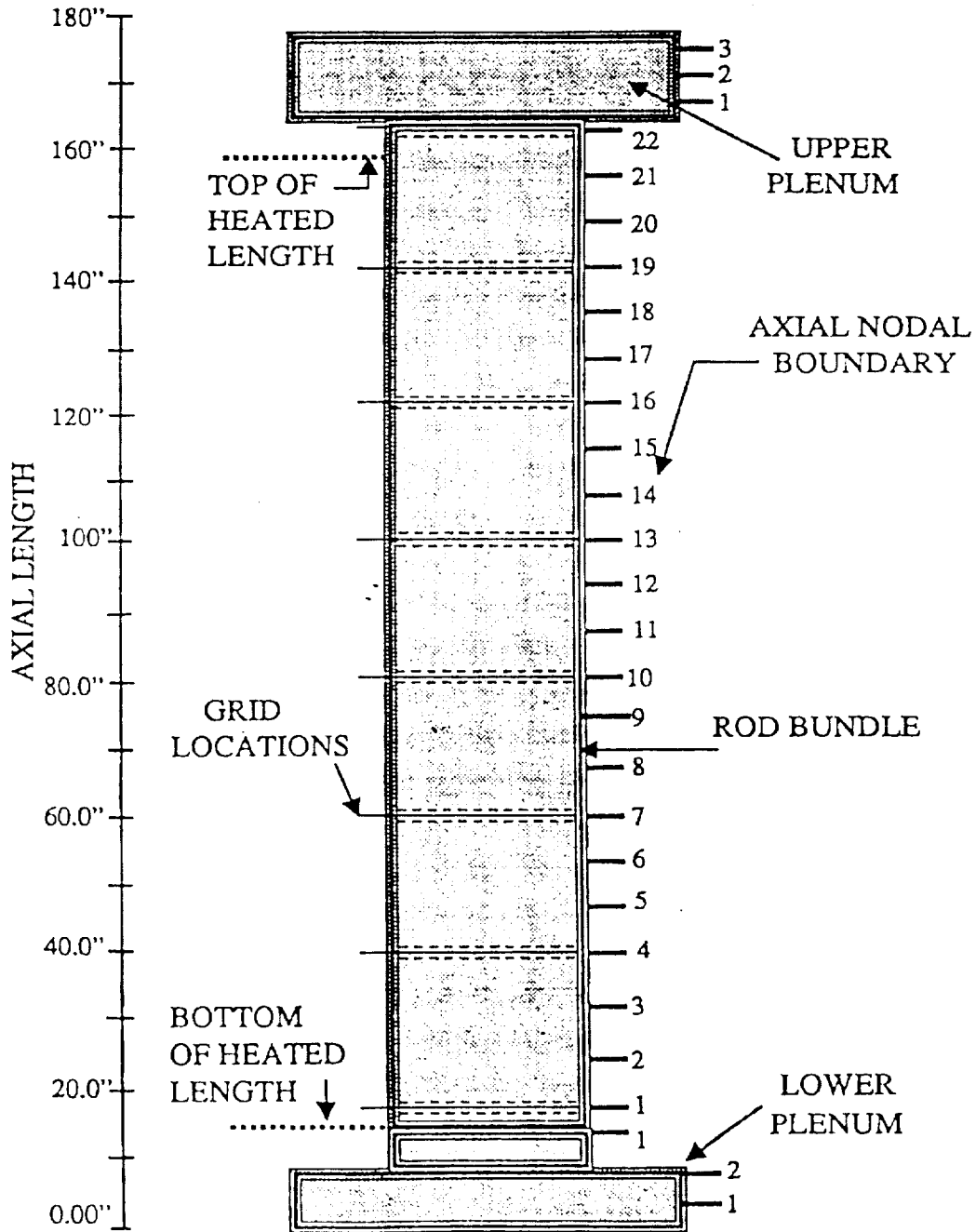


Figure 9-13
Vapor Flow Rate at Outlet of Rod Bundle
2.54 cm/sec (1.0 in/sec) Reflooding Rate

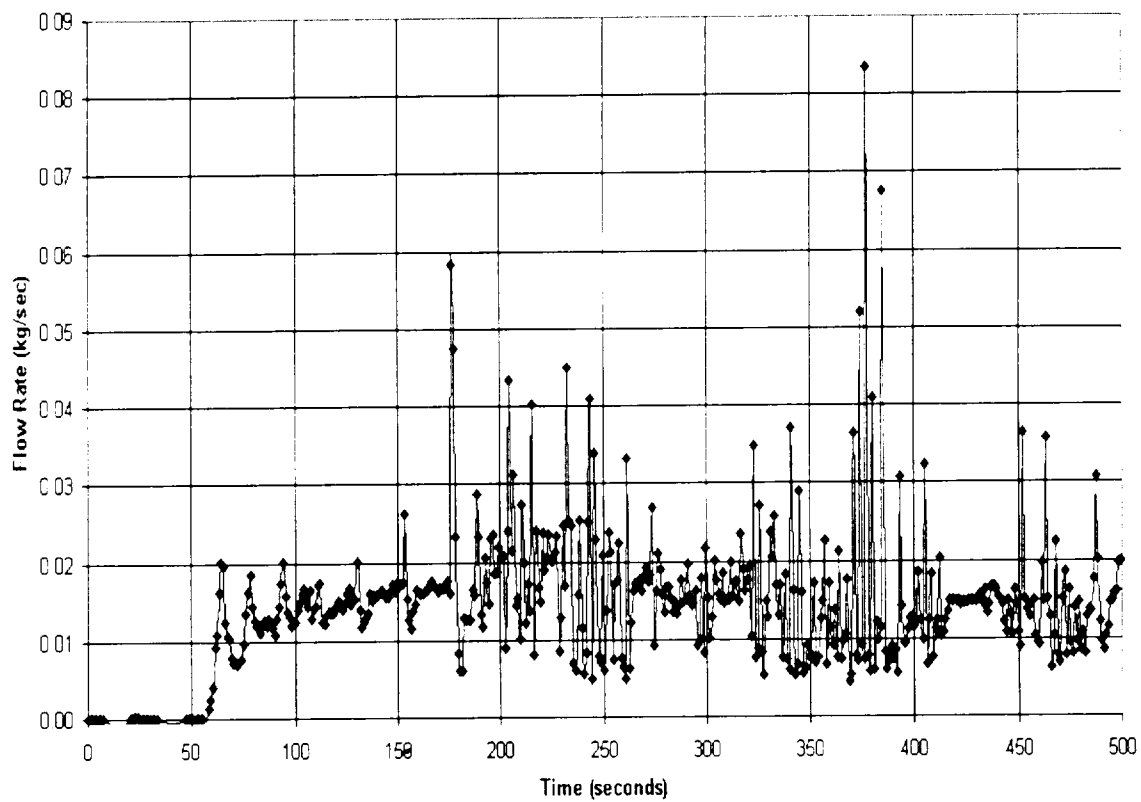


Figure 9-14
Entrainment Flow Rate at Outlet of Rod Bundle
2.54 cm/sec (1.0 in/sec) Reflooding Rate

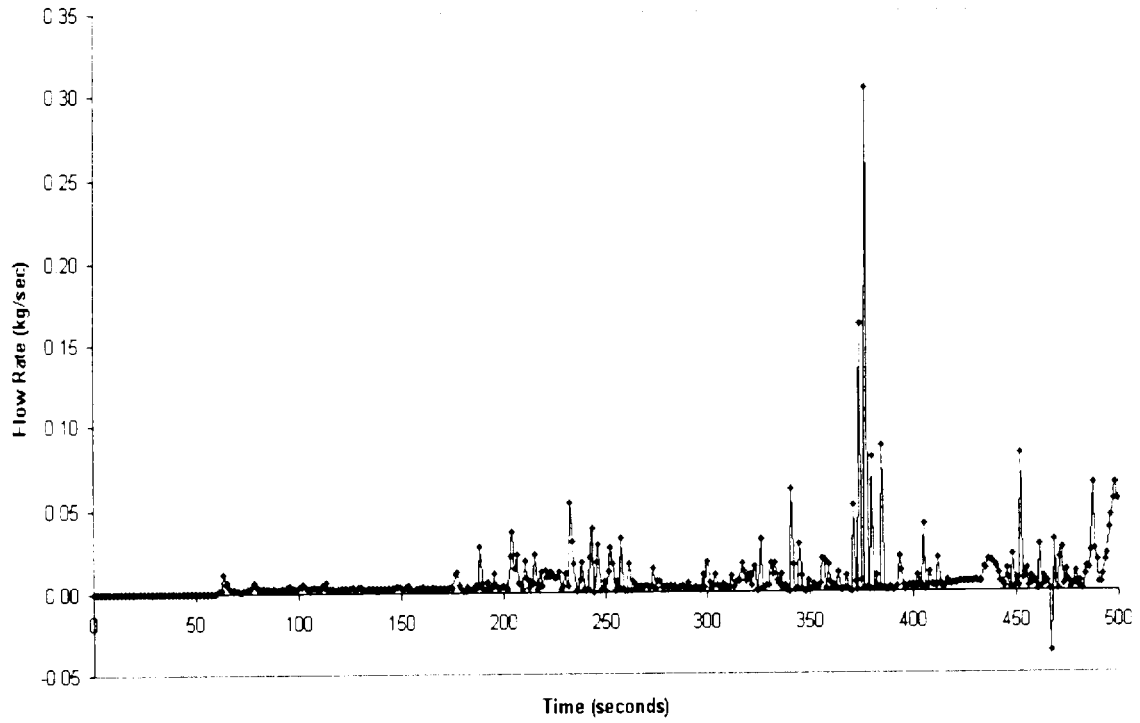


Figure 9-15
Pressure at Inlet of Rod Bundle
1.0 in/sec Reflooding Rate

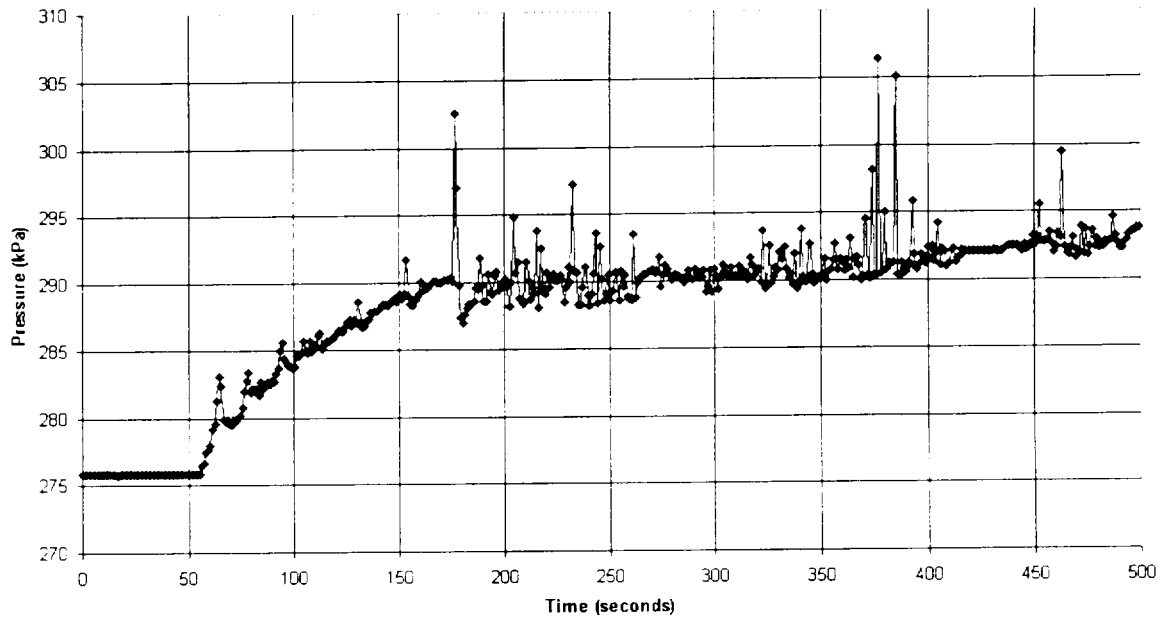
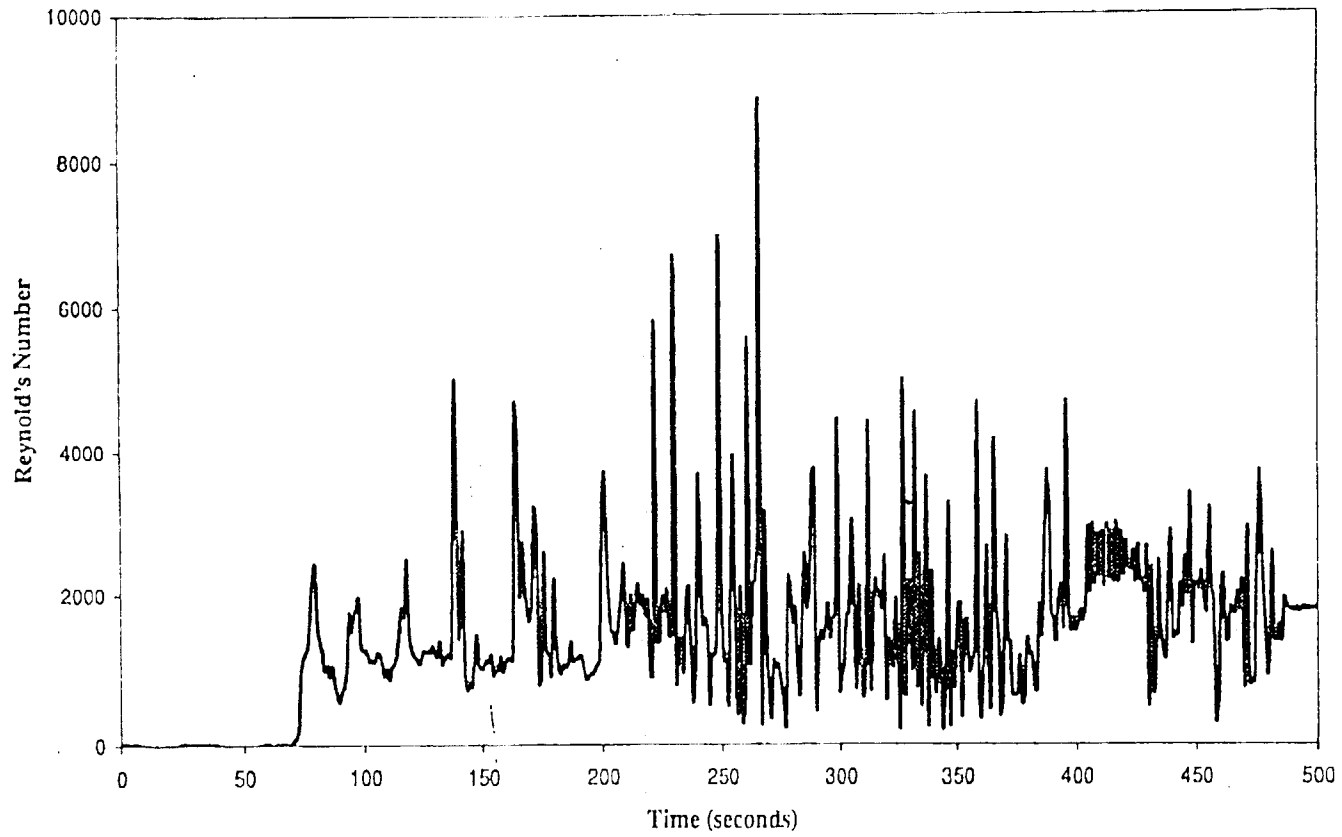


Fig 9-16

Vapor Reynold's Number
2.032 cm/sec (0.8 in/sec) Reflooding Rate



9-16

Figure 9-17
Vapor Reynold's Number
2.54 cm/sec (1.0 in/sec) Reflooding Rate

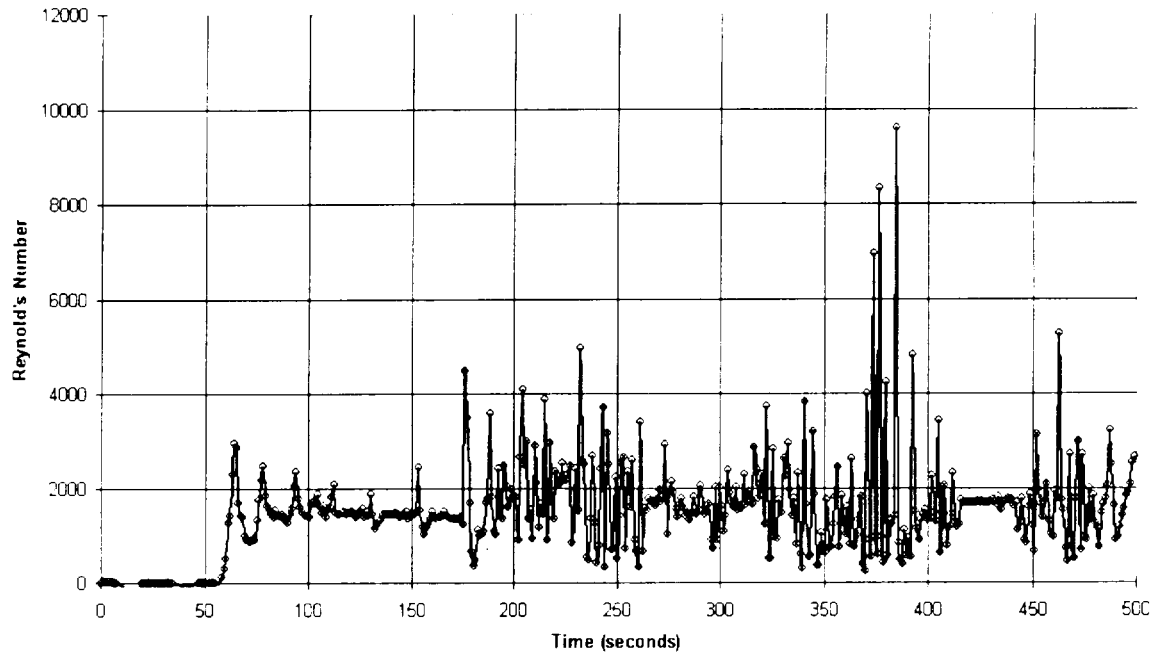
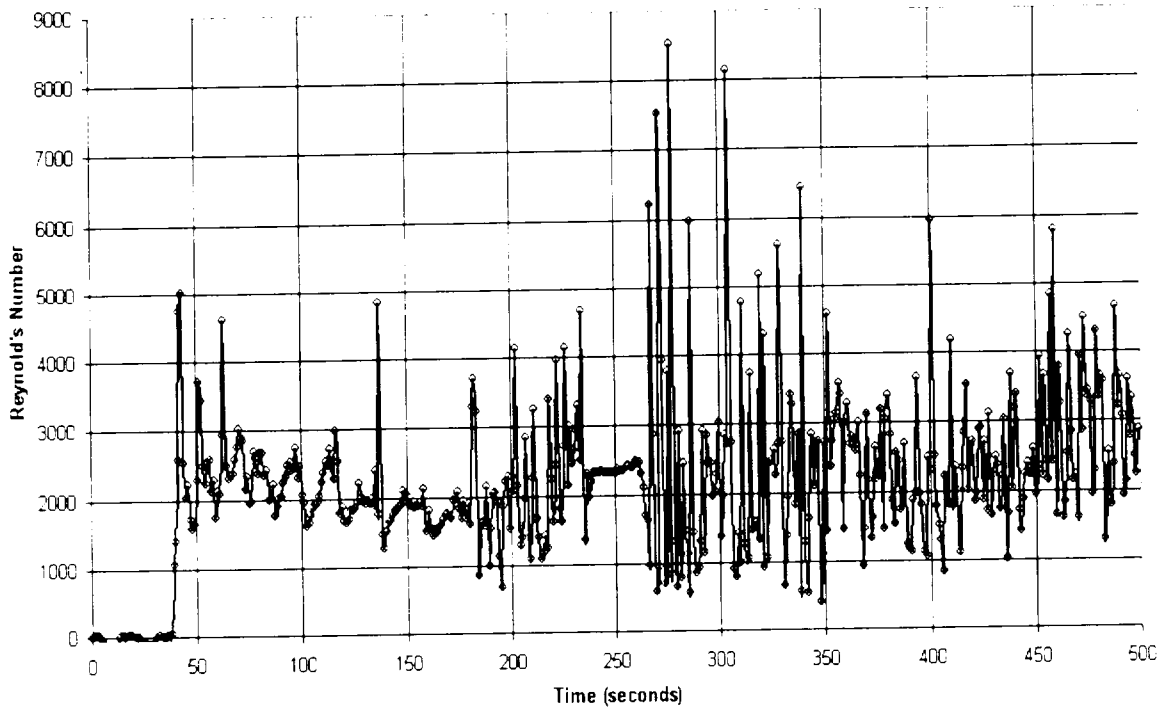


Figure 9-18
Vapor Reynold's Number
3.81 cm/sec (1.5 in/sec) Reflooding Rate



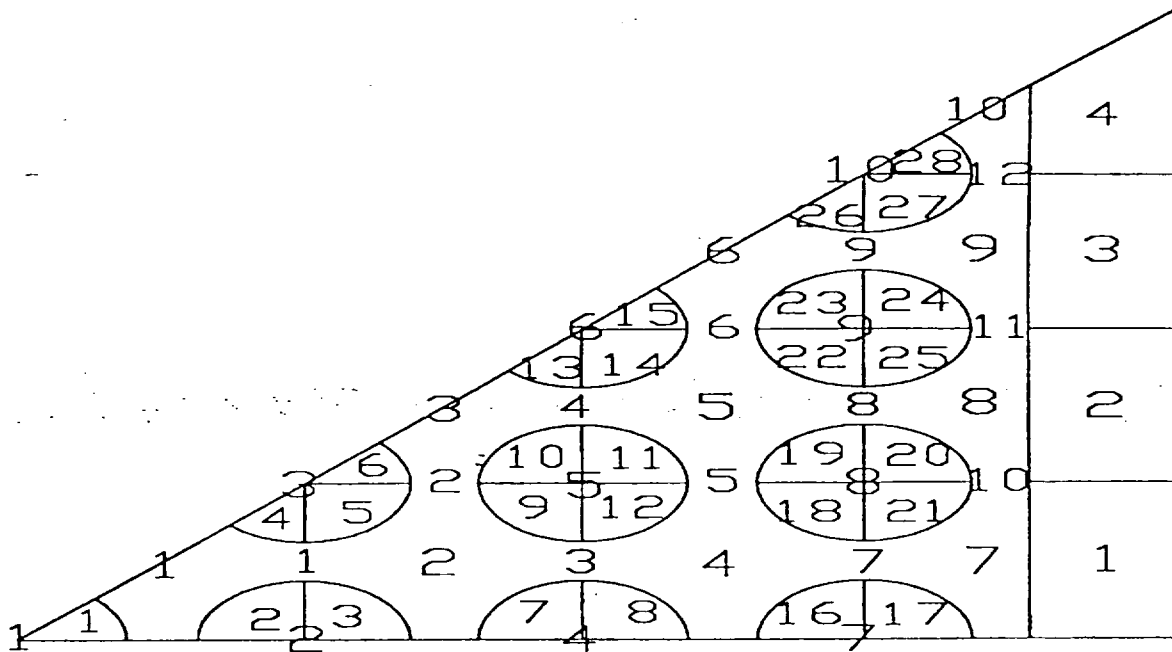


Figure 9-19
Nodal Diagram for Sub-Channel Model

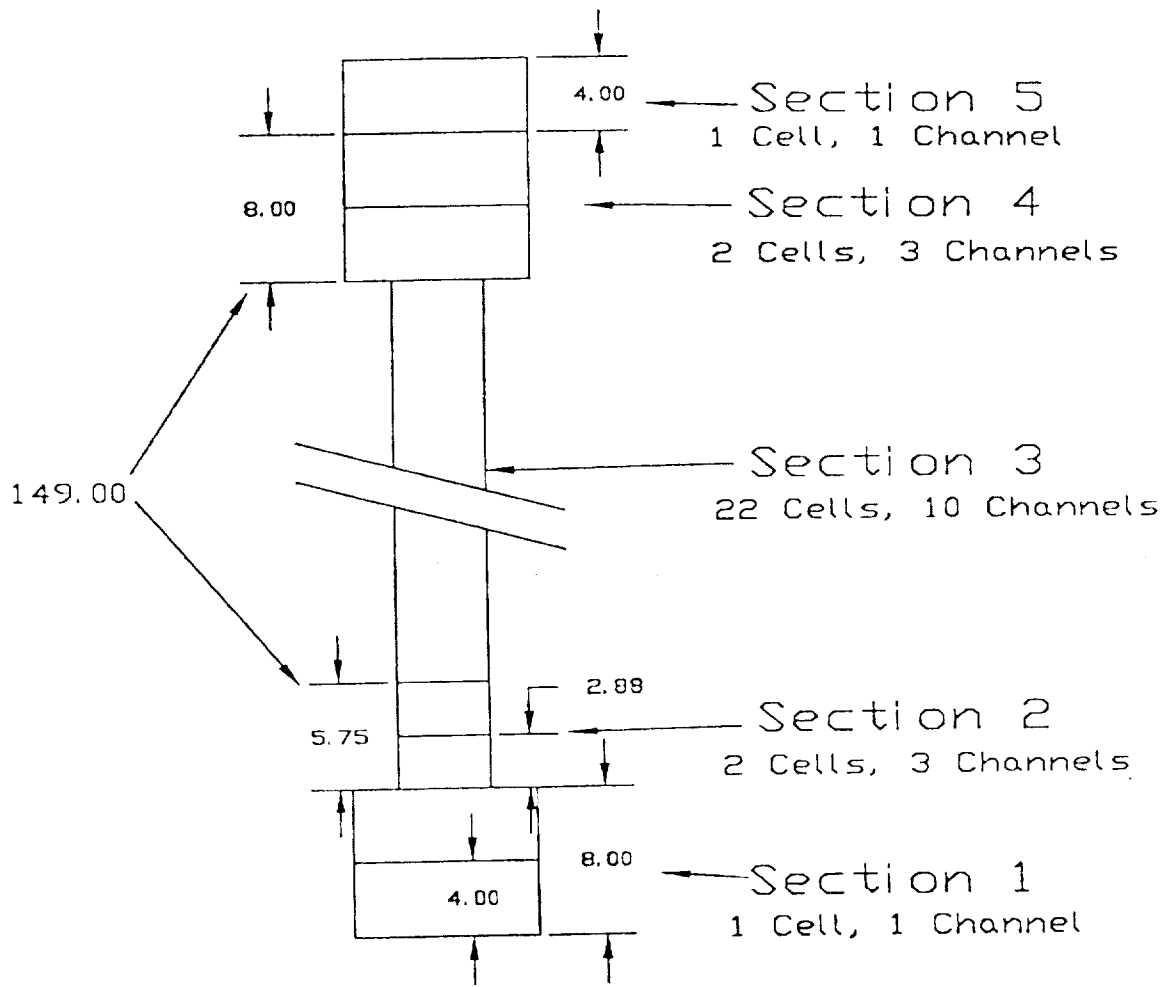
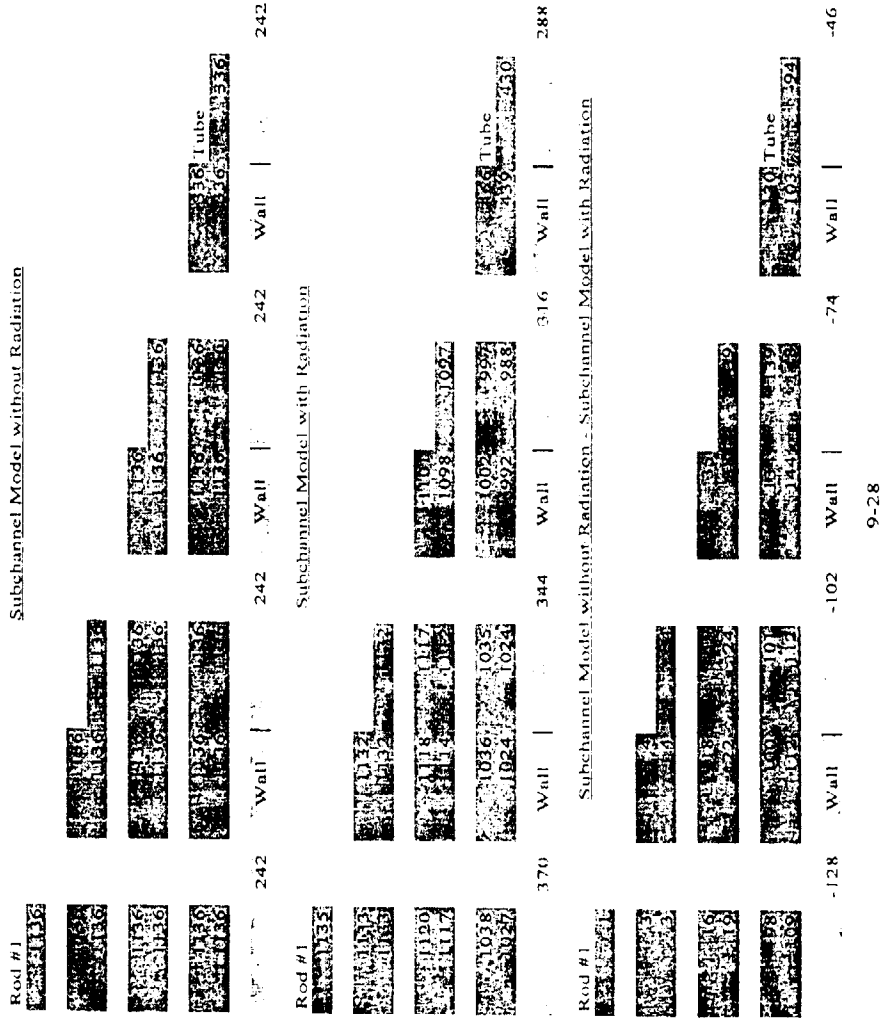


Figure 9-20
Axial Nodal Diagram for Sub-Channel Model

Fig. 9-21

Temperature Distributions after 50 sec Heatup (in °C)



10. Rod Bundle Heat Transfer Test Matrix

10.1 Introduction

A test matrix for the Rod Bundle Heat Transfer tests was developed. The range of conditions are given and the objectives for the proposed tests are described. Some of the proposed tests were compared to the conditions and types of tests described in Section 3 to show how the proposed tests overlap and complement the existing database. The strategy in developing the test matrix was to use a "building block" approach in which simpler experiments are performed first to quantify a particular heat transfer mechanism. Additional complications of two-phase flow film boiling behavior are added in later experiments. The proposed test conditions bracket those expected in postulated LOCA.

10.2 Types of Tests Which are Proposed

The types of tests proposed include:

1. Steady-state liquid flow characterization tests to determine the rod bundle frictional pressure drop and the spacer grid loss coefficients. These tests will provide the bundle-specific hydraulic information to be used in the TRAC and COBRA-TF models.
2. Heat loss experiments to characterize the facility heat loss to the environment. These tests will provide the heat loss boundary information to be modeled in the COBRA-TF model, and to verify the scaling calculations for heat losses.
3. Radiation-only tests with an evacuated rod bundle. These tests will be performed over a range of rod bundle powers to achieve a wide range of heater rod surface temperatures, characteristic of those expected for dispersed flow film boiling. The bundle will be evacuated such that heat transfer will be by radiation only with no convective currents within the bundle. These tests will characterize the rod-to-rod and rod-to-housing radiation heat transfer. The objective will be to confirm the emissivities to be used to characterize the rod bundle and housing surfaces such that the radiation heat transfer component can be subtracted from the total dispersed flow film boiling transfer as well as to verify that the outer row of heater rods effectively shields the inner 5x5 rows of rods. These tests will provide the data for the rod-to-rod and rod-to-surface radiation heat transfer models in TRAC and COBRA-TF. Modeling of this type of tests has been successfully performed using COBRA-TF in the past^(10-1,10-2).

4. Subcooled and saturated boiling experiments at low flows and low pressure. The objectives will be to provide data which can be utilized to validate the boiling models and correlations currently used. The experiments will be conducted in a steady-state manner and the heat transfer and void distributions will be measured along the rod bundle.
5. Convective steam cooling tests over a wide range of Reynolds numbers to determine the single-phase convective heat transfer in superheated steam. The analysis of the FLECHT-SEASET 161 rod bundle data⁽¹⁰⁻³⁾ indicates that for low flooding rates where the vapor becomes highly superheated, the vapor Reynolds numbers can decrease sufficiently to the laminar flow or transition flow regions. Therefore, these tests will characterize single-phase convective heat transfer cooling without the complications of a dispersed droplet field. Data from these tests will be compared to rod bundle steam cooling data from the ORNL tests⁽¹⁰⁻⁴⁾ and the FLECHT-SEASET tests⁽¹⁰⁻⁵⁾, and other data sets for consistency.
6. Steam cooling tests with injected droplets at the entrance of the test bundle. A droplet injection system will be designed to inject drops of a known initial size and velocity into the heated rod bundle subchannels over a range of liquid flows such that quasi-steady state dispersed flow film boiling experiments can be conducted. An estimate of the droplet flow can be made from the FLECHT-SEASET 161 rod bundle tests as well as calculations from COBRA-TF. The objective of these experiments will be to examine the effects of a highly dispersed phase of entrained liquid droplets on convective heat transfer within the rod bundle.

These tests will be simpler to analyze since the additional effects of the rod quench front movement, quench heat release and generation of the entrainment will be minimized. Since these tests will be quasi-steady, the Laser-Illuminated Digital Camera Systems (LIDCS) can be used at selected elevations to track the droplets and measure their size and velocity distributions, such that the change of the droplet interfacial area can be measured and compared to predictions.

The LIDCS System can be positioned upstream and downstream of spacer grids to determine the grid effects on the drop field. Also, local vapor temperature will be measured from steam probes, as well as the exit liquid and vapor temperature flow. From this, a mass and energy balance can be written for the bundle to calculate the quality change along the bundle, and therefore the axial steam flow. Radiation heat transfer can be calculated using the measured rod and surface temperatures, and this value can be subtracted from the measured total heater rod wall heat flux, resulting in the dispersed flow film boiling contribution to the total wall heat flux. The convective heat flux can then be compared to the single-phase convective heat flux based on the steam cooling tests to determine under

what conditions convective heat transfer enhancement is enhanced by the evaporating droplets in the flow. A similar approach was used in the analysis of the FLECHT-SEASET 161 rod bundle experiments, but the lack of separate radiation only tests and good single-phase steam cooling tests resulted in significant data scatter. The inclusion of the radiation only and the steam cooling tests will reduce the uncertainties in the data analysis as well as the modeling uncertainties to avoid compensating errors as much as possible. These tests represent a unique contribution to the rod bundle dispersed flow film boiling literature.

7. Forced reflooding experiments will be performed to compliment the existing data, as determined from Task 2. The forced reflooding tests will also overlap the steam cooling and the droplet injection two-phase experiments. The forced reflooding experiments will contain all the elements of the experiments performed earlier with the additional complications of the heater rod quench front movement, quench heat release, and entrainment expected for reactor conditions, for a prescribed set of initial and boundary conditions.

The focus of these experiments is to examine entrainment at the quench front within the froth region. Laser-Illuminated Digital Camera Systems and gamma densitometers will be used to determine the flow regime and the behavior of the entrained phase over a range of pressure, inlet flow, inlet subcooling, heater rod power, and heater rod initial temperatures. In addition, the data above the quench front can be analyzed in the same fashion as the FLECHT-SEASET 161 rod bundle data and the steam cooling tests with droplet injection to determine the wall heat flux components due to radiation heat transfer and film boiling.

These tests will serve as validation experiments for the models to be developed from the simpler component tests described above. Some of the data for selected tests can be designed as "blind" test data to be released to only the NRC for blind test predictions for the merged TRAC computer code. The COBRA-TF model developed in Task 8 will be used for pre-test calculations to determine the test matrix conditions for these experiments.

8. Gravity reflood experiments or variable inlet injection experiments will also be performed. These experiments will examine the system response on the inlet-flooding rate into the test bundle and the resulting heat transfer within the bundle. In the experiments described above, inlet flow conditions are prescribed boundary conditions. Actual inlet flow in a reactor system is a dependent parameter which depends upon the steam generation rate within the core, driving head in the downcomer, and pressure losses in the reactor piping, steam generators and pumps. The resistances for the generator, pump, and associated piping will be simulated using an orifice at the test section outlet. The parameters of interest are

the orifice resistance, injection flow rate into the downcomer, initial rod bundle temperature, inlet subcooling, and rod bundle power levels. There will be a Laser-Illuminated Digital Camera System and gamma densitometer data to examine the gravity flow behavior within the bundle, effects of the spacer grids, and resulting entrainment. The tests will be modeled using COBRA-TF, which will have been improved as part of the program effort.

10.3 Range of Conditions Considered for the Experiments

The range of conditions used to establish the test matrix covers the postulated calculated reflood transit. Typical calculated reflood conditions were obtained from Westinghouse⁽¹⁰⁻⁵⁾, Framatome⁽¹⁰⁻⁶⁾, and Siemens⁽¹⁰⁻⁷⁾. Westinghouse compared the ranges of existing data to their model to show that it had been tested over the range of model application.

The composite table of all the predicted conditions from the reactor vendor calculations is given in Table 10-1. The table is subdivided into each of the different heat transfer regimes and the range of the calculated plant conditions is given for each. As can be seen, there is a large variation in parameters such as liquid and vapor Reynolds number, liquid subcooling and vapor superheat. The range of pressures is small since all plants reflood at low pressures. The Westinghouse plant parameters were extracted from best-estimate WCOBRA/TRAC calculations, while the plant parameters from Framatome and Siemens were taken from their Appendix K evaluation model calculations.

The liquid Reynolds number was based on the inlet flow and the bottom cell in the bundle which was single phase liquid. The vapor Reynolds number was based on the local vapor superheat, and the calculated vapor flow rate in the dispersed flow film-boiling region of the bundle. The wall superheat is from the calculated peak cladding temperature for the calculation. The liquid subcooling and the vapor superheat are also given.

Using Table 10-1 as a guide, a test matrix was developed to capture most of the range of conditions which the vendor and NRC safety analysis computer codes are required to calculate. Not all the heater rod temperature conditions will be directly simulated in the Rod Bundle Heat Transfer test program since many of the test conditions are at very high heater rod temperatures (>2000 °F>1093°C) which can limit the lifetime of the heater rods. Since the RBHT program strategy is to reuse the expensive heater rods in two bundle builds, the very high temperature tests will be conducted in the second bundle build. Also, data are available from the FLECHT-SEASET program in which several tests were run at very high temperatures, near or at the licensing limit, which can be used with the Rod Bundle Heat Transfer data to cover the full range of calculated conditions for reflood heat transfer model development.

The other source for the test conditions are those conditions obtained from the analysis of the FLECHT-SEASET test data and the earlier FLECHT Cosine⁽¹⁰⁻⁸⁾ and the FLECHT Skewed⁽¹⁰⁻⁹⁾

reports. In these tests, a mass and energy balance was used to calculate the axial quality behavior along the test bundle at different times using the non-equilibrium steam vapor temperature measurements. The vapor Reynolds number, void fraction, calculated quality, and rod temperatures are shown in Figures 10-1 to 10-3 for FLECHT-SEASET test 31504, which is a 25.4 mm/sec (1-inch/sec) flooding rate test at 2.76 bars (40 psia), 66.7°C (120 °F) inlet subcooling, peak power of 2.3 kW/m (0.7 kw/ft) and an initial cladding temperature of 871°C (1600 °F). As the figures indicate, the high vapor temperatures result in very low vapor Reynolds numbers, well within the laminar region. The vapor Reynolds number is approximately proportional to $1/T_v^2$ such that as the vapor superheats, the Reynolds number decreases, even for relatively high vapor velocities⁽¹⁰⁻³⁾.

10.4 Proposed Preliminary Test Matrix

A preliminary test matrix for the Rod Bundle Heat Transfer test facility is given in this section. A sufficient number of COBRA-TF calculations have been performed to specify the range of conditions for the tests as an envelope for the test facility design. Therefore, parameters such as flows, temperature limits, pressures, and powers have been broadly specified for the facility design to specify thermal-hydraulic conditions which provide data.

The Tests are divided into the same classifications as given in Section 10.2 and reflect the building-block approach for characterizing the test facility as well as minimizing the duty on the heater rods.

1. Steady-state flow characterization of the test facility, designed to provide the detailed pressure drop and loss coefficient information of the test facility so the facility can be modeled accurately. The Reynolds number range of interest covers laminar, transition, and fully turbulent ranges; therefore the grid loss coefficients will be a strong function of the Reynolds number. The tests will be performed with the rod bundle unpowered, at approximately 2.68 bars (40 psia), and using subcooled water. The Reynolds number range that will be investigated is 1500 - 25000. Several tests and repeat tests, approximately 25 total valid tests, will be performed to characterize the grid loss coefficients, rod bundle frictional losses and the total bundle pressure loss.
2. Heat loss experiments to determine the heat loss characteristics of the facility. These tests will be performed in two steps. The first series of tests will be with the rod bundle unpowered using the hot water from the accumulator tank at 1.34 bars ($T_{sat} = 108.9^\circ\text{C}$) [20 psia ($T_{sat} = 228^\circ\text{F}$)], and 4.02 bars ($T_{sat} = 145^\circ\text{C}$) [60 psia ($T_{sat} = 293^\circ\text{F}$)]. The bundle will be filled with hot water and the temperature distribution, as a function of time will be measured. The heat losses will be calculated from the data. Approximately three valid tests will be performed with an additional repeat test. The higher temperature heat loss data will be obtained as

part of the radiation only and steam cooling tests. It should be noted that all heated tests will have sufficient instrumentation to characterize the heat losses.

3. Radiation only tests with the facility evacuated to minimize free convection currents within the rod bundle. These tests will be used to characterize the rod-to-rod and rod-to-housing heat transfer within the bundle, and to verify the radiation heat losses given in Sections 6 and 7. These tests will be performed using a constant power calculated to give maximum temperatures of 260, 538, and 816°C at 2.76 bars (500, 1000, and 1500 °F at 40 psia) in a quasi-steady fashion. The tests will provide data for heat loss calculations. Heat loss should equal the bundle power if the temperature is constant. Pre-test calculations using both MOXY and COBRA-TF will be performed to estimate the target power level for the given peak temperature. Approximately 6 tests with repeat tests will be performed.
4. Subcooled and saturated steady-state boiling experiments. The experiments will be performed over a range of inlet subcooling, from approximately -17-27°C (1 - 80°F), with a pressure range of 1.34 to 4.02 bars (20 to 60 psia). The liquid flow rate and temperature will be varied to cover the liquid Reynolds range from approximately 4000 to 30000. The heater rods will be powered and the test section total power needed to develop boiling will be calculated using COBRA-IV or VIPRE-II subchannel codes. Simpler calculations will also be performed as a check. The heater rods should not exceed critical heat flux since the objective is to investigate stable nucleate and saturated boiling. Approximately 30 tests will be performed including repeat tests. The specific test matrix will be completed after the pre-test calculations have been performed for the range of conditions.
5. Convective steam cooling steady-state tests over a wide range of vapor Reynolds numbers from 1500 to 30000 with pressure variations from 1.34 to 4.02 bars (20 to 60 psia). As with the boiling tests in part 4 above, pre-test predictions of the steam cooling tests will be made using COBRA-IV and/or VIPRE-II subchannel codes to help determine the test power. Simpler calculations will also be performed as a check. The bundle will be heated to a maximum temperature of 538 °C (1000 °F) to determine the consequence of temperature on the steam physical properties, i.e., the local Reynolds number. The tests will also be analyzed using the subchannel vapor temperature measurements with COBRA-IV and/or VIPRE-II. The data will be reduced to obtain local heat transfer and Reynolds numbers. Approximately 30 tests will be performed after the pre-test predictions have been performed.
6. Steady-state dispersed flow film boiling tests in which droplets, of known size and velocity, are injected into the steam flow for the same conditions as the steam only convective cooling tests. The test conditions will be preserved between these

two different experiments to determine the effects of the droplets on the flow and resulting heat transfer behavior. The amount of the liquid flow will be estimated from the FLECHT-SEASET data and scaled appropriately for the Rod Bundle Heat Transfer facility. The same scaling logic will have already been used for the 3x3 heated bench test. The heated bench test will have already been performed to qualify the Laser Illuminated Digital Camera System, which will measure the drop size and velocity.

The range of vapor Reynolds numbers is the same as the steam cooling tests, from 1500 - 30000. The pressure will be varied from 1.34 to 4.02 bars (20 to 60 psia), and the initial drop size will be varied from approximately 0.5 to 1.52 mm (0.02 to 0.06-inches). The initial drop velocity will be estimated from COBRA-TF pre-test calculations and from FLECHT-SEASET data. The initial drop velocity is a function of the inlet quality to be simulated. The rod bundle will be heated and the maximum temperature will be kept below 816 °C (1500 °F), with most tests temperatures peaking at 538 °C (1000 °F) to prolong the bundle life.

7. Forced reflood experiments over a range of inlet flooding rates, which will correspond to liquid Reynolds of approximately 4000 to 25000 and vapor Reynolds numbers from 1500 to 30000. The tests will be performed over the pressure range of 1.34 to 4.02 bars (20 to 60 psia) with inlet subcoolings of approximately 2.78 to 66.7 °C (5 to 120 °F), and peak rod powers chosen not to exceed 1000 °C (1800 °F). The initial temperatures and powers will be determined by pre-test predictions using COBRA-TF. The code calculations will also be used to verify the range of Reynolds numbers within the bundle. There will be approximately 20 forced reflood.
8. Gravity reflood and or variable reflood tests. The purpose is to examine the effect of variable inlet flow on entrained liquid which is carried to upper regions of the bundle. In a PWR, the inlet flow initially surges into the core as the downcomer fills and its head increases. The two-phase froth front and liquid continuous flow regime can penetrate further into the bundle than the quench front to produce inverted annular film boiling. However, the head in the core region quickly comes in equilibrium with the downcomer head and the flow into the bundle decreases. The water in the bundle quickly heats and boils and entrainment from the bundle increases. Water above the quench front tends to be entrained and carried through the bundle, providing improved cooling at the upper elevations.

These tests will use a stepped variable inlet flooding rate and will vary the flooding rate time history, inlet subcooling and the system pressure. The variable flooding rate tests will be integrated into the forced flooding experiments so that the final low flooding rate period will overlap with the forced flooding rate tests. Approximately 5 tests are planned.

10.5 Conclusions

Eight (8) different types of experiments have been planned for the Rod Bundle Test Facility to characterize the facility as well as to obtain data on dispersed flow film boiling. The experiments cover the ranges of conditions which best estimate and Appendix K reflood models are required to calculate. Hydraulic heat loss characterization experiments will be conducted. Single phase liquid boiling experiments, radiation only experiments, and single phase steam convection heat transfer experiments will also be performed to characterize the facility. In this fashion, the modeling uncertainties of the test facility are reduced.

The tests are structured in a building block approach to separate and understand the components of dispersed flow film boiling, so there is less of a chance of compensating error being applied in a specific heat transfer mode.

The precise test conditions will be developed. There is a need to perform further pre-test predictions to select the range of rod powers and initial temperatures to provide the data needed while at the same time, to minimize the duty on the heater rods. The facility design envelope is sufficiently broad to be able to perform tests over a wide range of initial and boundary conditions.

Table 10-1
Range of PWR Reflood Conditions

Heat Transfer Regime	PWR Range of Conditions.	
<u>Single Phase Liquid</u>		
Re_l	5500 - 25000	
P (bar) [psia]	1.38 - 3.10	[20 - 45]
$T_{sub} = T_{sat} - T_l$ ($^{\circ}C$) [$^{\circ}F$]	< 44	[<80]
<u>Single Phase Vapor</u>		
Re_v	2500 - 9500	
P (bar) [psia]	1.38 - 3.10	[20 - 45]
$T_{sat} = T_v - T_{sat}$ ($^{\circ}C$) [$^{\circ}F$]	333 - 778	[600 - 1400]
<u>Subcooled Boiling</u>		
Re_l	5500 - 25000	
P (bar) [psia]	1.38 - 3.10	[20 - 45]
$T_{sub} = T_{sat} - T_l$ ($^{\circ}C$) [$^{\circ}F$]	< 44	[<80]
<u>Saturated Nucleate Boiling</u>		
Re_l	5500 - 25000	
P (bar) [psia]	1.38 - 3.10	[20 - 45]
$T_{sat} = T_w - T_{sat}$ ($^{\circ}C$) [$^{\circ}F$]	2.78 - 16.7	[5 - 30]
<u>Transition Boiling</u>		
Re_l	5500 - 25000	
Re_v	2500 - 9500	
P (bar) [psia]	1.38 - 3.10	[20 - 45]
$T_{sub} = T_{sat} - T_l$ ($^{\circ}C$) [$^{\circ}F$]	0 - 44	[0 - 80]
<u>Inverted Annular Film Boiling</u>		
P (bar) [psia]	1.38 - 3.10	[20 - 45]
$T_{sat} = T_v - T_{sat}$ ($^{\circ}C$) [$^{\circ}F$]	222 - 333	[400 - 600]
$T_{sub} = T_{sat} - T_l$ ($^{\circ}C$) [$^{\circ}F$]	0 - 11.1	[0 - 20]
<u>Dispersed Flow Film Boiling</u>		
Re_v	2500 - 9500	
P (bar) [psia]	1.38 - 3.10	[20 - 45]
$T = T_w - T_{sat}$ ($^{\circ}C$) [$^{\circ}F$]	222 - 1056	[400 - 1900]
$T_{sub} = T_{sat} - T_l$ ($^{\circ}C$) [$^{\circ}F$]	0	[0]
$T_v = T_w - T_v$ ($^{\circ}C$) [$^{\circ}F$]	< 1000	[<1800]

10.6 References

- 10-1 Chiou, J. S. and L. E. Hochreiter, "Combined Radiation and Dispersed Flow Film Boiling in a BWR Rod Bundle with Top Spray," Proceedings of 26th National Heat Transfer Conference, Philadelphia, PA, 1989.
- 10-2 Hochreiter, L.E. and J. S. Chiou, "COBRA-TF Analysis of SVEA Spray Cooling Experiments," Proceedings of 26th National Heat Transfer Conference, Philadelphia, PA, 1989.
- 10-3 Lee, N., S. Wong, H. C. Yeh, and L. E. Hochreiter, "PWR FLECHT-SEASET Unblocked Bundle, Forced and Gravity Reflood Test Data Evaluation and Analysis Report," NUREG/CR-2256, 1981.
- 10-4 Yoder, G., et al, "Dispersed Flow Film Boiling in Rod Bundle Geometry, Steady-State Heat Transfer Data and Correlation Comparisons," NUREG/CR-2435, 1982.
- 10-5 Bajorek, S. M. , Letter to L.E. Hochreiter on "Calculated Range of Conditions for PWR Reflood Transients," June 1998.
- 10-6 Nithianandan, C.K., Framatome Technologies, Letter to L.E. Hochreiter on "Calculated Range of Conditions for PWR Reflood Transients," September 1998.
- 10-7 O'Dell, L., Siemens, Letter to L.E. Hochreiter on "Calculated Range of Conditions for PWR Reflood Transients," September 1998.
- 10-8 Lilly, G.P., H. C. Yen, L. E. Hochreiter, and N. Yamaguchi, "PWR FLECHT Cosine Low Flooding Rate Test Series Evaluation Report", WCAP-8838, 1977.
- 10-9 Lilly, G.P., H. C. Yeh, L. E. Hochreiter, and N. Yamaguchi, "PWR FLECHT Skewed Profile Low Flooding Rate Test Series Evaluation Report," WCAP-9183, 1977.

11. TEST FACILITY DESIGN (TASK 10)

11.1 Introduction

The Rod Bundle Heat Transfer (RBHT) test facility is designed to conduct systematic separate-effects tests under well-controlled conditions in order to generate fundamental rod bundle heat transfer data including single phase steam cooling tests, low flow boiling tests, steam flow tests with injected droplets and inverted annular film boiling and dispersed flow film boiling heat transfer. The facility is capable of operating in both forced and variable flow reflood modes covering wide ranges of flow and heat transfer conditions at pressures from 1.34 to 4.02 bars (20 psig to 60 psig).

11.2 General Design Description

The test facility consists of the following major components, shown schematically in Figure 11-1:

- A test section consisting of a lower plenum, a low-mass housing containing the heater rod bundle, and an upper plenum
- Coolant injection and steam injection systems
- Closely coupled phase separation and liquid collection systems
- An injection system
- A pressure fluctuation damping tank and steam exhaust piping

11.3 Detailed Component Design Description

The various components of the RBHT test facility are described in the following paragraphs. All components are well insulated to minimize heat losses to the environment.

11.3.1 Test Section

The test section consists of the heater rod bundle, the flow housing, and the lower and upper plenums, as shown in Figure 11-2.

The heater rod bundle simulates a small portion of a 17x17 reactor fuel assembly. The electrically powered heater rods have a diameter of 9.5 mm (0.374 inches) arranged in a 7x7 array with a 12.5984 mm (0.496 inch) pitch, as shown in Figure 11-3. The heater rod

specifications are listed in Table 11-1. The bundle has 45 heater rods and four unheated corner rods. The corner rods are used to support the bundle grids and the grid and fluid thermocouple leads. The support rods are made from Inconel 600 tubing having a diameter of 9.525 mm (0.375 inches), a wall thickness of 2.108 mm (0.083 inches), and form a length of 3.96 m (156 inches). The heater rods are single ended and consist of a Monel 500 electrical resistance element filled and surrounded by hot pressed boron nitride (BN) insulation, and enclosed in an Inconel 600 cladding, as shown in Figure 11-4. This material was chosen for its high strength and low thermal expansion coefficient at high temperatures, which minimizes rod bowing and failure at high temperature operating conditions since it was desired to reuse the heater rods for a second bundle build. The heater rods have a 3.657 m (12 foot) heated length with a skewed axial power profile, as shown in Figure 11-5, with the peak power located at the 2.74 m (9 foot) elevation. The maximum-to-average power ratio (P_{min}/P_{avg}) is 1.5 and the minimum-to-average power ratio (P_{min}/P_{avg}) is 0.5 at both ends of the heated length. The bundle has a uniform radial power distribution.

Power to each rod is provided by a 60 volt, 12,600 amp, 750 kW DC power supply. Each rod is rated for 10 kW, and designed to operate at 13.8 bars (200 psig) at a maximum temperature of 1204°C (2200°F), but because of its solid construction can be operated at up to 103.4 bars (1500 psig). Each rod is instrumented with eight (8) 0.508 mm (20 mil) diameter ungrounded thermocouples attached to the inside surface of the Inconel sheath at various locations. All of the thermocouple leads exit at the heater rod bottom end. Thermocouple specifications are shown in Table 11-2. The Inconel 600 thermocouple sheath is compatible with the heater rod cladding and housing material to reduce thermal expansion and minimize the possibility of missing thermocouple failure during the thermocycling operations.

The rod bundle has eight (8) grids located 0.522 m (20.55 inches) apart except for the spacing between the first and second grids, which are 588.26 mm (23.16 inches) apart. The first grid is located 101.854 mm (4.01 inches) above the bottom of the heated length. The grid elevations are similar to the ones found in a 17x17 fuel assembly. The grids in conjunction with the corner support rods form the heater rod bundle support structure. The heater rod top extensions are attached to the 2.4 cm (1 inch) thick nickel ground plate by means of a Morse taper that provides a good electrical contact. The heater rod bottom extension and copper electrode extend through the lower plenum-O ring pressure seal plate. The copper electrodes, which are 5.842 mm (0.230 inches) in diameter and 203 mm (8 inches) long, extend through holes drilled in the low-melt reservoir shown in Figure 11-6. This reservoir serves as the electrical power supply positive side connection. It contains a low temperature melting alloy (at about 71.11°C (160°F)) which is an excellent conductor, thus providing a good electrical contact to each heater rod.

The flow housing provides the pressure and flow boundary for the heater rod bundle. It has a square geometry. Its nominal inside dimensions are 90.17 mm sq. (3.55 x 3.55 inches), and wall thickness 6.35 mm (0.25 inches), as shown in figure 11-7. The housing is made out of Inconel 600 the same material used for the heater rod cladding and thermocouple sheaths. As pointed out previously, the high strength of Inconel 600 at elevated temperatures will minimize housing distortion during testing. The 6.35 mm (0.25 inch) wall thickness is the minimum allowable for

operating at 4.02 bars (60 psig) and 537.77°C (1000°F), taking into consideration the cutouts to accommodate the large windows and the numerous pressure and temperature penetrations through the walls. The empty housing has a flow area of 81.29 sq. cm (12.60 square inches). With the rod bundle in place the flow area is 45.80 sq. cm (7.1 square inches). This area is 8.2% larger than the ideal flow area of a 7x7 rod bundle configuration. The excess flow area is due to the flow housing inside dimensional tolerance and the space needed to insert the rod bundle in the housing. The gap between the outer rods and the flow housing inner wall is 2.54 mm (0.100 inches) wide.

The flow housing has six pairs of windows. Each window provides a 50.8 mm x 292.1 mm (2x11.5 inch) viewing area. Each pair of windows is placed 180° apart and located axially at elevations overlapping rod bundle spacer grids, thus providing a viewing area about 88.9 mm (3.5 inches) below and 152.4 mm (6 inches) above the corresponding spacer grids. The windows will facilitate the measurement of droplet size and velocity using a Laser Illuminated Digital Camera System. The two-phase void fraction will be measured using a X-ray densitometer, as well as, sensitive differential pressure cells. In addition, high speed movies using diffused back lighting can be taken during the experiments for visualization and flow regime information. The windows are made out of optical grade fused quartz and are mounted on the housing by means of a bolted flange and Thermiculite high temperature gasketing material, as shown in Figure 11-8.

The flow housing has twenty-two (22) pressure taps located at various elevations, as shown in Figure 11-7. The pressure taps are connected to sensitive differential pressure cells, providing measurements to calculate single-phase friction losses for determining bare rod bundle and grid loss coefficients. Nine (9) of these pressure taps are located about 76.2 mm (3 inches) apart to provide detailed void fraction measurements in the froth region above the quench front. The flow housing is supported from the nickel plate and upper plenum, allowing it to freely expand downward, thus minimizing thermal buckling and distortion.

11.3.2 Lower Plenum

The lower plenum is attached to the bottom of the flow housing. The lower plenum is made out of nominal 203.2 mm (8 inch) sch. 40, 304 S.S. pipe with an inside diameter of 201.6 mm (7.937 inches), a height of 203.2 mm (8 inches), and a volume of 6569.5 cm³ (0.232 cubic feet), as shown in Figure 11-9. The lower plenum is used as a reservoir for the coolant prior to injection into the rod bundle during reflood. It connects to the injection water line and steam cooling line. It has two penetrations for thermocouples monitoring the coolant temperature prior and during reflood, and a pressure tap for static and differential pressure measurements.

The lower plenum also has four Conax fittings with multiple probes sealing glands for the bundle grid, steam probes, and support rod wall thermocouple extensions that are routed through the bottom of the rod bundle. It contains a flow baffle, which is attached to the flow housing bottom flange. The flow baffle has a square geometry, similar to the flow housing, as shown in Figure

11-10. The flow baffle wall has numerous small diameter holes that act as a flow distributor and flow straightener to provide an even flow distribution into the rod bundle.

11.3.3 Upper Plenum

The upper plenum serves as the first stage for phase separation and liquid collection of the two-phase effluent exiting the rod bundle. The liquid phase separates due to the sudden expansion from the bundle to the larger plenum flow area. The de-entrained liquid is collected around the flow housing extension in the upper plenum. The extension acts as a weir preventing the separated liquid from falling back into the heater rod bundle. The upper plenum vessel configuration is shown in Figure 11-11. The vessel is made from a 203.2 mm (8 inch) 304 S.S pipe with an inside diameter of 201.6 mm (7.937 inches) and a height of 304.8 mm (12 inches). It has a volume of 9825.95 cm³ (0.347 cubic feet). The plenum has a 76.2 mm (3 inch) pipe flanged connection to the steam separator and two penetrations for fluid thermocouples. It is covered with a 203.2 mm (8 inch) 304 S.S. blind flange. This flange has a 25.4 mm (1 inch) penetration for steam injection, venting, and connecting the safety relief valve and rupture disc assembly. It also has a pressure tap penetration for static and differential pressure measurements. In addition, the upper plenum contains an exhaust line baffle, shown in Figure 11-12. The baffle is used to further de-entrain water from the steam, and prevents water dripping from the upper plenum cover flange to be carried out by the exhaust steam. The baffle has a 76.2 mm (3 inch) flange connection at one end. It is inserted through the upper plenum exit nozzle, and it is bolted between the nozzle flange and the flange of the pipe going to the steam separator.

11.3.4 Carryover Tanks

The de-entrained liquid from the upper plenum drains into the top of a 25.6 mm (1 inch) tube which extends inside a small carryover tank to detect and measure the carryover liquid as soon as possible. This tank, shown in Figure 11-14, is connected close coupled in series with a larger carryover tank, shown in Figure 11-13, which collects and measures the amount of liquid overflow from the smaller carryover tank. The small carryover tank has a volume of about 4247.53 mm³ (0.15 cubic feet) to more accurately measure the water being collected as a function of time. This tank is made from a 76.2 mm (3 inch) schedule 40 pipes having an overall length of 0.9144 m (36 inches) including the end caps. The large carryover tank is made from a 101.6 mm (4 inch) schedule 40 pipes with a bottom end cap and top flanges having an overall length of 152.4 mm (6 feet) and a capacity of 15007.9 mm³ (0.53 cubic feet). Each tank is connected with 25.4 mm (1 inch) flexible hose, and has a one (1) inch drain tube, and 9.525 mm (3/8 inch) tubes with wall penetrations for installing fluid and level meters.

11.3.5 Steam Separator and Collection Tanks

The wet steam exhausted from the upper plenum flows through a steam separator (or dryer), shown in Figure 11-15, where carryover liquid droplets are further separated from the steam and collected in a small collection tank, shown in Figure 11-16, attached to the bottom of the steam separator. The steam separator relies on centrifugal force action to provide 99% dry steam. The separated liquid is drained into a collection tank where a differential pressure cell is used as a level meter to measure the liquid accumulation. The steam separator is fabricated from a 355.6 mm (14 inch) diameter 316 S.S. pipes and is 914.4 mm (36 inch) long. It has 50.8 mm (2 inch) connecting nozzles, a 25.4 mm (1 inch) drain, and a 12.7 mm (0.5 inch) top vent. It also has two pressure taps for liquid level measurements and two 38.1 mm (1.5 inch) side nozzle connections.

The drain tank is a small vessel with a capacity of 0.0113 cubic meters (0.4 cubic feet). It is made from a 101.6 mm (4 inch) schedule 10, 304 S.S. pipe with an overall length of 121.9 mm (48 inch), including both end caps. It has a 25.4 mm (1 inch) drain nozzle, a 25.4 mm (1 inch) pipe top connection to the steam separator, pressure taps and fluid thermocouple connections.

11.3.6 Pressure Oscillation Damping Tank

The dry steam from the steam separator flows into a pressure oscillation-damping tank. As its name implies, it is used to dampen pressure oscillations at the upper plenum caused by rapidly oscillating steam generation rates in the heater rod bundle during reflood. This effect is coupled to the characteristics of the pressure control valve, which is located downstream in the steam exhaust line. It is desirable to have a smooth pressure control in order to minimize uncertainties when calculating mass balances, steam generation rates, and heat transfer coefficients in the heater rod bundle, and avoid the pressure control valve causing oscillations in the bundle as it cycles. The tank has a volume of 0.227 m³ (8 cubic feet), which is approximately equal to the total volume of the rest of the test facility. This design criterion was used successfully in the ACHILLES reflood test facility^(11-1 to 11-6). The pressure tank is fabricated from a 355.6 mm (14 inch), 304 S.S. standard schedule pipe by 2.59 m (102 inch) long, as shown in Figure 11-17. Inside the tank is a 76.2 mm (3 inch), schedule 40, 304 S.S. pipe that provides a tortuous path for the steam flow to expand into a large volume, thus damping pressure oscillations. The inlet and outlet nozzles are 76.2 mm (3 inch) in diameter with flanges. The vent and drain lines are made of 25.4 mm (1 inch) pipe. There are 9.53 mm (3/8 inch) tube penetrations for a fluid thermocouple and two static pressure taps. The tank walls are heated with clamp-on strip heaters up to about 10° above saturation temperatures to prevent steam condensation.

11.3.7 Exhaust Piping

The steam flowing out of the pressure oscillation-damping tank is exhausted through a 76.2 mm (3 inch) schedule 40, 304S.S. pipes, shown schematically in Figure 11-20. The exhaust line has a Vortex flowmeter, a 76.2 mm (3 inch) V-Ball pressure control valve, and a muffler at the exit to minimize the noise caused by steam blowing into the atmosphere. The pressure control valve is

activated by a signal from a static pressure transmitter located on the upper plenum. The line is also instrumented with a static pressure transmitter, fluid thermocouples, and outer wall thermocouples. The 76.2 mm (3 inch) line has flow-straightening vanes which reduce the pipe length requirements upstream of the Vortex meter in order to obtain accurate flow measurements. This line has strapped-on electrical heaters to keep the wall temperature about 11.11°C (20 °F) above saturation to insure that single-phase steam flow measurements are made by the Vortex flowmeter.

11.3.8 Injection Water Supply Tank

The injection water system consists of a water supply tank, a circulating pump, and interconnecting lines to the test section lower plenum. The water supply tank, shown in Figure 11-18, has a capacity of 200 gallons. It is designed for 4.14 bars (60 psig) and 154.44°C (310 °F). The tank is equipped with a submersible electrical heater to heat the injection water to specified test temperatures. The tank is pressurized by a nitrogen supply system, which regulates the over-pressure needed for the forced flooding injection tests. The tank has inlet and outlet nozzles, pressure taps for level measurements, fluid and wall thermocouples. Water from the tank can be circulated through the test section by a centrifugal pump with a capacity up to two hundred and fifty (250) gallons per minute which is needed to perform liquid single-phase flow tests.

11.3.9 Water Injection Line

The water injection line, shown schematically on Figure 11-20, consists of a 50.8 mm (2 inch) diameter 304 S.S. tubing with a 2.7686 mm (0.109 inch) wall. It is rated for 60 psi (4.14 bars) and 154.44°C (310 °F) service. This line has a Coriolis Effect type flowmeter, a V-ball control valve, a quick opening solenoid valve, and appropriate shut-off and drain valves. It also has penetrations for static pressure and fluid thermocouples, and outside wall thermocouples. The line has tracer electrical cable type heater to maintain the water being injected at the proper test inlet temperatures. The water injection line can also be extended to the downcomer during gravity reflood tests.

11.3.10 Steam Supply

A boiler with a capacity of 2613 kg (5760 pounds) per hour at 10.3 bars (150 psig) provides steam for the single phase steam cooling , pressure drop and water droplet injection tests. It also provides steam for preheating the test components prior to testing. The boiler is connected to the lower plenum by means of a 50.8 mm (2 inch), 304 S.S. tube. It is equipped with a Vortex flowmeter to measure steam flows, fluid and wall thermocouples, a V-ball control valve, and a quick acting solenoid valve. The boiler is also connected to the upper plenum to provide steam for preheating the test components prior to testing.

11.3.11 Droplet Injection System

A system to inject water droplets into the test section has been included in the RBHT design. The droplet injection system consists of six (6) 2.38 mm (3/32 inch) OD stainless steel tubes entering through the test section at the 1.295 m (51 inch) elevation. The tubes run perpendicular to the heater rods and penetrate through both sides of the housing as seen in Figure 11-19. The tubes can be easily removed when not needed so they do not interfere with other types of tests. Water is supplied to the injector tubes from the injection water supply tank as described in Section 11.3.8 and a series of small holes are drilled in the tubes to inject water directly into each of the 36 sub-channels.

11.4 Test Facility Instrumentation

The test facility instrumentation is designed to measure temperatures, power, flows, liquid levels, pressures, void fractions, and droplet sizes, distribution, and drop velocities. The vapor velocity cannot be directly measured in a two-phase dispersed flow, but it can be calculated at different axial positions from the data. Overall and transient mass and energy balances, mass inventories, carryover liquid and steam flows as a function of time can be calculated. Heater rod power, temperature, and fluid temperature are used to calculate heat fluxes and heat transfer coefficients, quench times, rod bundle energy losses, convective and radiation heat transfer to steam, droplets, grids, support rods, and housing. Effects of grids, support rods and housing behavior during reflood can be determined. Void fraction measurements below the quench front and in the froth level above the quench front, in conjunction with the laser illuminated digital camera measurements are used to determine droplet entrainment behavior droplet effects on heat transfer, and steam desuperheating. The laser illuminated digital camera system measurements provide droplet size distribution and velocities during reflood.

11.4.1 Loop Instrumentation and Controls

Loop instrumentation is shown schematically in Figure 11-20, and listed in the instrumentation and data acquisition channels shown in Table 11-3. Sixty-one (61) instrumentation channels are assigned to the collection of electrical power, fluid and wall temperatures, levels, flows, differential pressures, and static pressure measurements. The injection water supply tank has three fluid and three wall thermocouples to monitor water and wall temperatures during heat-up prior to testing. It has a differential pressure transmitter used as a level meter to determine water mass in the tank and mass depletion during reflood testing. It also has a static pressure transmitter which monitors the nitrogen overpressure and controls the nitrogen flow needed to maintain a constant pressure during forced injection reflood tests.

The water injection line is equipped with a Coriolis Effect Micromotion flowmeter that directly measures mass flows up to 454 kg/min (1000 lbs/min) with an accuracy of plus or minus eleven hundredths of a percent ($\pm 0.11\%$) of rate. The steam line has a Rosemount Vortex shedding

flowmeter to measure flow up to 7.08 m³/min (250 ft³/min) with an accuracy of plus or minus sixty-five hundredths of a percent ($\pm 0.65\%$) of rate. Each flowmeter is connected through a pneumatic controller to a V-ball flow control valve. Each line has a fluid thermocouple to measure water or steam temperature during heat-up and forced injection testing. The injection line has three wall thermocouples to monitor wall temperatures during heat-up and during testing. One of these thermocouples in conjunction with a temperature controller regulates the power to an electrical heating cable wrapped around the injection line. The heating cable is used to heat-up the injection line wall and to maintain the injection water at the required injection temperature.

The carryover tank instrumentation consists of one (1) fluid thermocouple, three (3) wall thermocouples, and a liquid level meter which measures the amount of carryover liquid being collected during testing. In addition, a differential pressure transmitter is connected from the top of the carryover tank to the upper plenum to determine the static pressure in the carryover tank.

The steam separator and drain tank are instrumented with two (2) wall thermocouples to monitor wall temperatures during heat-up. The drain tank has a fluid thermocouple to measure temperatures of de-entrained liquid being collected during testing. The volume of de-entrained water is measured with a level meter connected across the drain tank. A differential pressure transmitter is connected between the steam separator and upper plenum.

The pressure oscillation damping tank has three (3) wall thermocouples which are used to monitor vessel walls during heat-up, and to insure that the vessel wall is at a temperature above saturation to prevent condensation. One wall thermocouple in conjunction with a temperature controller monitors the power applied to clamp-on heaters that heat up the tank to the desired wall temperature.

The exhaust line is equipped with a Rosemount Vortex shedding flowmeter which, in conjunction with a static pressure transmitter and a fluid thermocouple measurements are used to calculate steam volumetric flows up to 7.08 m³/min (250 ft³/min). The flowmeter has an accuracy of plus or minus sixty-five hundredths of a percent ($\pm 0.65\%$) of the rate. The exhaust line also has wall thermocouples to measure pipe wall temperatures. One wall thermocouple in conjunction with a temperature control regulates the power going to clamp-on heaters which are used for heating the pipe walls up to a temperature well above saturation ($\sim 11^{\circ}\text{C}$ [$\sim 20^{\circ}\text{F}$]) preventing steam condensation and to insure accurate single phase steam flow measurements. The exhaust line has a V-ball pressure control valve this valve is controlled by a static pressure transmitter through a pneumatic controller connected to the top of the upper plenum in order to maintain constant test section pressure during testing.

11.4.2 Test Section Instrumentation

The test section is heavily instrumented to obtain data described at the beginning of Section 11-4 Test Facility instrumentation.

The test section instrumentation consists of the heater rod bundle and flow housing, the lower plenum, and the upper plenum groups. The heater rod bundle and flow housing instrumentation is shown schematically in Figure 11-21 and listed in Table 11-3. This figure shows the instrumentation axial locations in relation to heater rod heated length, heater axial power profile, grids, housing pressure taps, and windows.

Five grids have thermocouples attached to their surfaces in order to determine quenching behavior during reflood. Eight groups of heater rods have thermocouples at different elevations to cover, as much as possible, the entire rod bundle heated length. The radial location of each heater rod group is shown in Figure 11-22. The radial locations of instrumentation rods were chosen in order to be able to characterize heat transfer of hot rods simulated by the center rods, rod-to-rod and rod-to-housing radiation heat transfer. For this purpose, heater rod thermocouples, steam probes, and housing wall thermocouples are located at the same elevations. In addition, symmetrical location of the same group of instrumented heater rods will help in the data analysis and will determine any anomalies in the radial flow distribution through the rod bundle. Rod thermocouples are also placed at varying distances downstream from a grid to determine the decreasing heat transfer gradient between grid spans. The steam probe or fluid thermocouples are located at short distances upstream and downstream of a grid to determine the effect of water droplets being shattered by the grids on droplet size and distribution, and the desuperheating effect on steam temperatures in the disperse flow regime.

The vapor or steam temperature will be measured using miniature thermocouples which are attached to the spacer grids or are used for traversing. These are very small bare thermocouples that have a fast response time such that they can follow the vapor temperature accurately in a dispersed, non-equilibrium, two-phase flow. As the froth front approaches, the number and sizes of the droplets increase which can lead to wetting of these thermocouples. Experiments performed as part of the FLECHT-SEASET program indicated that very small bare thermocouples would provide reliable vapor superheat ready for the longest time period until they quench as the froth region approached. While the Lehigh vapor probe was considered, it is too large and causes a flow distribution effect which is not typical of the bundle. The Lehigh probe would block 68% of the gap between adjacent heat rods. The effect of the probe would be to distort the data downstream of the sensing location. Such flow distribution effects were observed in the Lehigh data as well as the INEL single tube data which used these probes. In addition, there will be traversing vapor temperature measurement probes mounted on rakes with multiple thermocouples.

The traversing steam probe rakes will be installed at the mid span between grids at the upper rod bundle elevations. The steam probes will measure steam temperatures in the rod bundle flow

subchannels and the gap between the heater rods during the dispersed flow regime. The conceptual design of a transversing steam probe rake is shown in Figure 11-23. Each rake consists of three 0.381 mm (15 mil) diameter ungrounded thermocouples mounted on a 0.356 mm (14 mil) thick by 6.35 mm (¼ inch) wide inconel strip. The thermocouples are spaced 12.6 mm (0.496 inch) apart which correspond to the heater rod spacing in the bundle. The thermocouple tips are located facing the steam flow. A 2.39 mm (94 mil) diameter tube attached to the strip is used to traverse the steam probe rake across the rod bundle. This tube also carries the thermocouples leads outside the flow housing through an extension tube and a pressure seal arrangement. This instrument is now in the development phase and will be tested in the nine (9) rod bundle bench test prior to installing it on the large rod bundle.

Two fluid thermocouples are placed 24.5 mm (1 inch) below the bottom of the bundle heated length such that injection water temperatures are monitored prior and when reflood is started. Twenty two (22) differential pressure transmitters are connected to the housing wall pressure taps providing measurements to calculate single phase bare bundle and grid friction losses, bundle mass inventory and void fraction during reflood. Nine (9) differential pressure cells are connected to pressure taps located 76.2 mm (3 inch) apart to provide detail mass inventory, and void fraction data in the froth region above the quench front. In addition, heater rod and housing wall thermocouples are placed at these pressure tap mid spans locations to determine convective and radiant heat transfer coefficients in the froth region where the differential pressure cells will give the average void fraction.

As described on section 11.3.1 the flow housing has six pairs of windows at the following elevations: 685.8, 1193.8, 1752.6, 2260.6, 2768.6, 3302.0, and 3962.4 mm (twenty seven (27), forty seven (47), sixty nine (69), eighty nine (89), one hundred nine (109), one hundred thirty (130) inches and on hundred fifty six (156) inch). Each pair of windows are one hundred eighty degrees (180°) apart. The window lenses are made from optical grade fused quartz and provide a 50.8 mm (2 inch) by 292.1 mm (11.5 inch) viewing area. The windows are positioned about 88.9 mm (3.5 inch) below and 152.4 mm (6 inch) above grid numbers 2, 3, 4, 5, 6, and 7. The windows will be preheated to prevent wetting during the time when dispersed flow is occurring and LCDS measurements are being made. The windows will be heated using infrared heaters on each window and by pulsing the rod bundle for preheating the flow housing walls. The infrared heaters will be removed just before a test is started. Two significant measurements above and below the grid can be made through the windows: Void fraction measurements with a gamma Densitometer, and entrained water droplet size, velocity, and distribution with a Laser Illuminated Digital Camera System. High speed movies can also be shot through this window to observe the different two-phase flow regimes during testing.

We will have three densitometers or an x-ray detector which will be located at different elevations during testing. The bottom densitometer will measure void fractions as the quench front approaches this location, while the other densitometers will measure void fraction in the dispersed flow regimes.

The Densitometer system is shown schematically in Figure 11-24. There are three (3) systems each at different elevations consisting of an AM 241, 120 mCi, 59.5 KeV gamma ray source, a Reuter-Stokes gas proportional counter, a preamplifier and an amplifier, high voltage power supply, a single channel analyzer, and a rate meter. The radiation beam intensity is measured across the center gap among the bundle heater rods. The beam is passed through a small beryllium window fabricated from an S 200F alloy sheet. These windows are mounted on a metal plate that replaces the glass window lenses. The Densitometer provides an average cordial void fraction across the bundle. The three Densitometers are located at various elevations during a test.

A droplet imaging system known as VisiSizer has been developed in conjunction with Oxford Lasers of Acton, Massachusetts to measure the size and velocity of water droplets entrained in the steam flow of the RBHT test section. VisiSizer uses a pulsed infrared laser to image water droplets on a 1000 x 1000 pixel high-resolution black and white digital camera through a set of windows in the bundle housing.

A digital system such as VisiSizer was chosen over conventional high-speed cameras because of issues with reliability and speed of data acquisition. A high-speed camera is capable of only a few seconds of imaging and is a tedious process that does not give instantaneous results. Each frame of a standard imaging technique would need to be analyzed by hand. The VisiSizer system is capable of analyzing 12 to 13 frames per second for an indefinite period of time. Film from the FLECHT-SEASET tests show much less image quality than images taken with VisiSizer in the experiments performed so far. However, VisiSizer is incapable of measuring anything other than complete droplets. This makes it an inadequate tool for gathering information about the entrainment front where there are ligaments and other unusual water behavior. Therefore, it is still a possibility that a high-speed camera will be used in tandem with VisiSizer for preliminary RBHT tests.

An infrared laser is used with the system because it is capable of passing through the quartz viewing windows and being absorbed by the water droplets entrained in the steam flow. Because the infrared rays are absorbed by the water droplets, the resulting droplet shadows can be recorded by the digital camera. So far, there has been no effect of laser light scattering from rods to droplets. Pictures taken in and out of the rod bundle have the same imaging characteristics, droplet analyzing capability, and clarity. A band pass laser light filter is placed in front of the digital camera to eliminate non-infrared light from other sources and an anti-glare attachment is used to eliminate any illumination interference from outside the viewing area. In addition, rod bundle geometry has little effect in the measurement of droplet distributions and velocities.

The frames captured by the camera are fed back to a PC at approximately 12 to 13 frames per second. The software can analyze each frame for droplet size and velocity and write the recorded data to a size and velocity data array. The software program determines droplet sizes by determining the area of black vs. white pixels in each droplet image. Once the droplet area is determined, the program calculates the perimeter of the droplet image to determine the sphericity of the droplet. The VisiSizer system is capable of determining the surface area based

on diameter of any and all droplets. At any droplet concentration that is measurable with the system, an accurate measure of the total droplet surface area can be obtained. So far, number fluxes of up to 6 droplets per frame in velocity mode (12 droplet images) have been analyzed successfully with the droplets in a very narrow viewing area. There is the capability to increase this droplet number flux by several times using larger and multiple viewing areas.

Operating the laser in a double pulse mode enables the VisiSizer system to measure both droplet diameter and velocity for a particular probe volume. The laser pulses twice with a known pulse delay (on the order of one (1) millisecond) while the camera shutter remains open, creating two images in the same frame of each droplet. The distance between images is then determined and the velocity calculated. These velocity characteristics are enough to characterize the behavior of the flow despite the fact that the droplets are only captured in a single frame.

The local distribution of droplets will be determined for a known probe volume governed by the software settings. Droplets that lie out of this probe volume on either side of the line of sight will be rejected based on focus. The opposite sides of the probe volume will be set by the spacing of the rods in the bundle. Each droplet is recorded in a two-dimensional array according to size and velocity. The droplet sizes are recorded in lognormal bins while the velocity bin size is user defined. Data for the transient reflood experiments is recorded in user defined quasi-steady state time periods. At the end of each time period the data is saved and a new array is opened. Arrays characterized by similar droplets populations can then be combined for better statistical results.

The VisiSizer will enable the experimenters to collect a vast amount of information about the droplet flow in the test section. The information will be collected in an easy to handle data array and all information will be written to a CD-ROM to ensure the information will be available for later use.

The droplet injection system described in Section 11.3.12 has been constructed so that RBHT can collect steady state information on droplet behavior. The injection system creates droplets of a known size and flow rate in the test section. The injection tubes are easily removed and replaced. This enables multiple injection sizes to be used as needed. The flow rate of the injection is controlled through a series of valves and flow meters. These factors should allow for the production of various droplet sizes. VisiSizer can study the droplet flow and distribution before a grid and then the system can be moved to image droplets immediately after the grid with the same conditions. In this way the effects of a spacer grid on the droplet diameter distribution can be determined.

The four corner support rods are unheated, they are used to support the bundle grids and to support grid and steam probes thermocouple leads going out of the bundle. These rods are instrumented with eight (8) thermocouples attached at various elevations corresponding to heater rods and housing wall thermocouples. The purpose of this arrangement is to quantify radiation heat transfer losses to unheated surfaces and determine their behavior during reflood.

The DC power supply can be controlled by regulating the voltage, current, or total power output.

The voltage drop across the heater rod bundle is measured by a voltmeter connected to voltage taps at the Low-Melt pot and the Nickel Ground Plate. The electrical current is measured by a copper shunt calibrated for 15,000 amps proportional to an output signal of 0-50 milli volts.

The Lower Plenum is instrumented with two (2) fluid and two (2) wall thermocouples. The fluid thermocouples monitor the injection water temperature prior and during testing. The wall thermocouples measure the vessel wall during heat-up and testing. One of the wall thermocouples in conjunction with a temperature controller regulates electrical power to clamp-on heater rods to maintain the vessel wall at inlet temperatures.

The Upper Plenum is also instrumented with two (2) fluid thermocouples and two (2) wall thermocouples. The fluid thermocouples measure steam and carryover liquid during testing. The wall thermocouples monitor vessel wall temperatures during heat-up and testing. The Upper Plenum is also instrumented with a static pressure transmitter which measures and controls the test section pressure during testing.

11.4.3 Data Acquisition System

The control and data acquisition system provides control functions and data collection functions for the RBHT Test Facility. This system consists of two parts, the computer and display terminals residing in the control room, and the VXI mainframe and terminal panels residing in the test facility. The two parts are connected via an industry standard IEEE 1394 (Firewire) serial control and data interface.

The computer provides the display, control, and data storage functions. It has the capability of displaying control function setpoints and process variables, and critical operating parameters during tests, along with selected variables such as various rod temperatures displayed in real-time during the experiment. This system will provide dial, meter, and strip-chart functions as required. The computer collects and saves data from the various instruments, such as voltage, current, pressure, level, flow, and temperature; and provides control functions such as heater rod power, injection water pressure, upper and lower plenum temperature, etc.

The instrumentation part of this system, residing in the test facility, consists of an industry standard VXI mainframe (Vme bus with extensions for Instrumentation) from Hewlett-Packard (HP E8401A), and a set of terminal panels (HP E1586A). The VXI mainframe contains a firewire controller card (HP E8491A) and several (currently seven) state-of-the-art data acquisition and control cards (HP E1419A). The terminal panels provide the isothermal reference junctions needed for the thermocouples, as well as the voltage and current-loop input/output (i/o) interface to the RBHT Test Facility. These terminal panels are connected to the HP E1419A cards with SCSI cables. Seven cards yield a capability of 448 i/o. The VXI mainframe can hold up to twelve cards, and the firewire interface can support up to sixteen mainframes.

Each E1419A card can support up to eight signal conditioning plug-ons (scp's), conditioning eight channels each. Each E1509A scp contains low-pass antialiasing filters, fixed at 7 Hz. Because of this, the scan rate for each channel must be greater than or equal to the nyquist rate of 14 Hz. The maximum a/d conversion rate on each HP E1419A card is nominally 100kHz, but is controlled to the rate the user requires. The seven cards can be synchronized to perform the scans simultaneously. The theoretical maximum scan rate for each channel (on any individual card) is $100,000/64 = 1,562.5$ Hz, if all 64 channels are scanned. (Note, the actual scan rate would be less because of multiplexer switching, amplifier settling times due to gain changes, etc. There are different scp's available from HP providing different filter values to scan at these rates.) The normal data-scanning rate will be 2 Hz during the majority of the tests, but this rate can be increased to 10 Hz for specific times during testing.

11.5 RBHT Test Facility Improvement

Significant improvements related to other rod bundle testing programs, listed in Section 3.0 Literature Review have been incorporated in the RBHT-Test Facility. These improvements are:

- A low mass square flow housing design which better fits a square rod bundle array and minimizes the housing mass and the excess rod bundle flow area.
- The six pairs of windows which provide large viewing areas below and above grid locations, making it possible to observe and make void fraction and droplet measurements during reflood testing.
- The use of Densitometers or x-ray detectors to obtain void fraction measurements in the subcooled, quench, and froth level regions.
- The use of a laser illuminated Digital Camera system to measure entrained water droplets sizes, distribution, and velocities in the transition and disperse flow regions.
- The use of a transversing steam probe rake to measure simultaneously steam temperatures in the flow subchannel and in the rod-to-rod gap.
- Differential pressure transmitter axially located three (3) inches apart in conjunction with heater rod and flow housing wall thermocouples to obtain detailed void fraction and heat transfer information.
- Water droplets injection system in conjunction steam injection to study the droplet-steam cooling effects on heat transfer and grids.

- Addition of a large pressure oscillation-damping tank to minimize test section oscillations observed in the FLECHT and FLECHT-SEASET tests.
- The incorporation of closely coupled liquid collection tanks and piping to reduce delay times for liquid collection.

11.6 Conclusions

The RBHT test facility has been designed as a flexible rod bundle separate-effects test facility which can be used to perform single-phase and two-phase experiments under well-controlled laboratory conditions to generate fundamental reflood heat transfer data. The facility is capable of operating in both forced and variable reflood modes covering wide ranges of flow and heat transfer conditions at pressures up to 4.02 bars (60 psig). It is heavily instrumented that meets all the instrumentation requirements developed under Task 7. It can be used to conduct all types of the planned experiments according to the test matrix developed under Task 9. It is felt that the RBHT facility with its robust instrumentation represents a unique NRC facility for the in-depth studies of the highly ranked reflood phenomena identified in the PIRT table developed under Task 1, and will produce the data and analysis needed to refine reflood heat transfer models in the current safety analysis computer codes.

11.7 References

1. Denham, M.K., D. Jowitt, and K.G. Pearson, "ACHILLES Unballooned Cluster Experiments, Part 1: Description of the ACHILLES Rig, Test Section, and Experimental Procedures," AEEW-R2336, Winfrith Technology Centre (Commercial in Confidence), Nov. 1989.
2. Denham, M.K. and K.G. Pearson, "ACHILLES Unballooned Cluster Experiments, Part 2: Single Phase Flow Experiments," AEEW-R2337, Winfrith Technology Centre (Commercial in Confidence), May 1989.
3. Pearson, K.G. and M.K. Denham, "ACHILLES Unballooned Cluster Experiments, Part 3: Low Flooding Rate Reflood Experiments," AEEW-R2339, Winfrith Technology Centre (Commercial in Confidence), June 1989.
4. Pearson, K.G. and M.K. Denham, "ACHILLES Unballooned Cluster Experiments, Part 4: Low Pressure Level Swell Experiments," AEEW-R2339, Winfrith Technology Centre (Commercial in Confidence), July 1989.
5. Dore, P. and M.K. Denham, "ACHILLES Unballooned Cluster Experiments, Part 5: Best Estimate Experiments," AEEW-R2412, Winfrith Technology Centre (Commercial in Confidence), July 1990.

6. Dore, P. and D.S. Dhuga, "ACHILLES Unballooned Cluster Experiments, Part 6: Flow Distribution Experiments," AEA-RS-1064, Winfrith Technology Centre (Commercial in Confidence), December 1991.

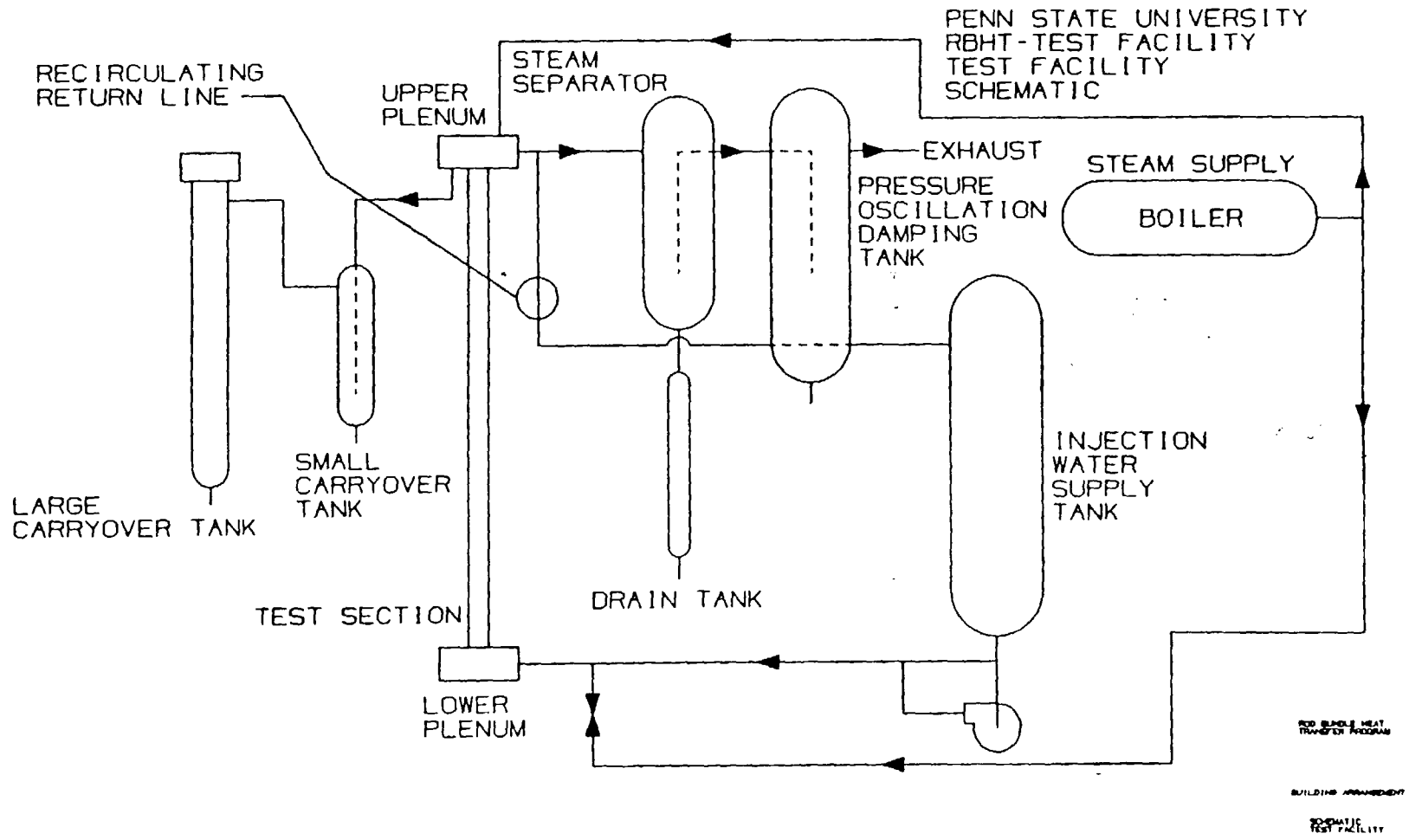


Figure 11-1. RBHT Test Facility Schematic

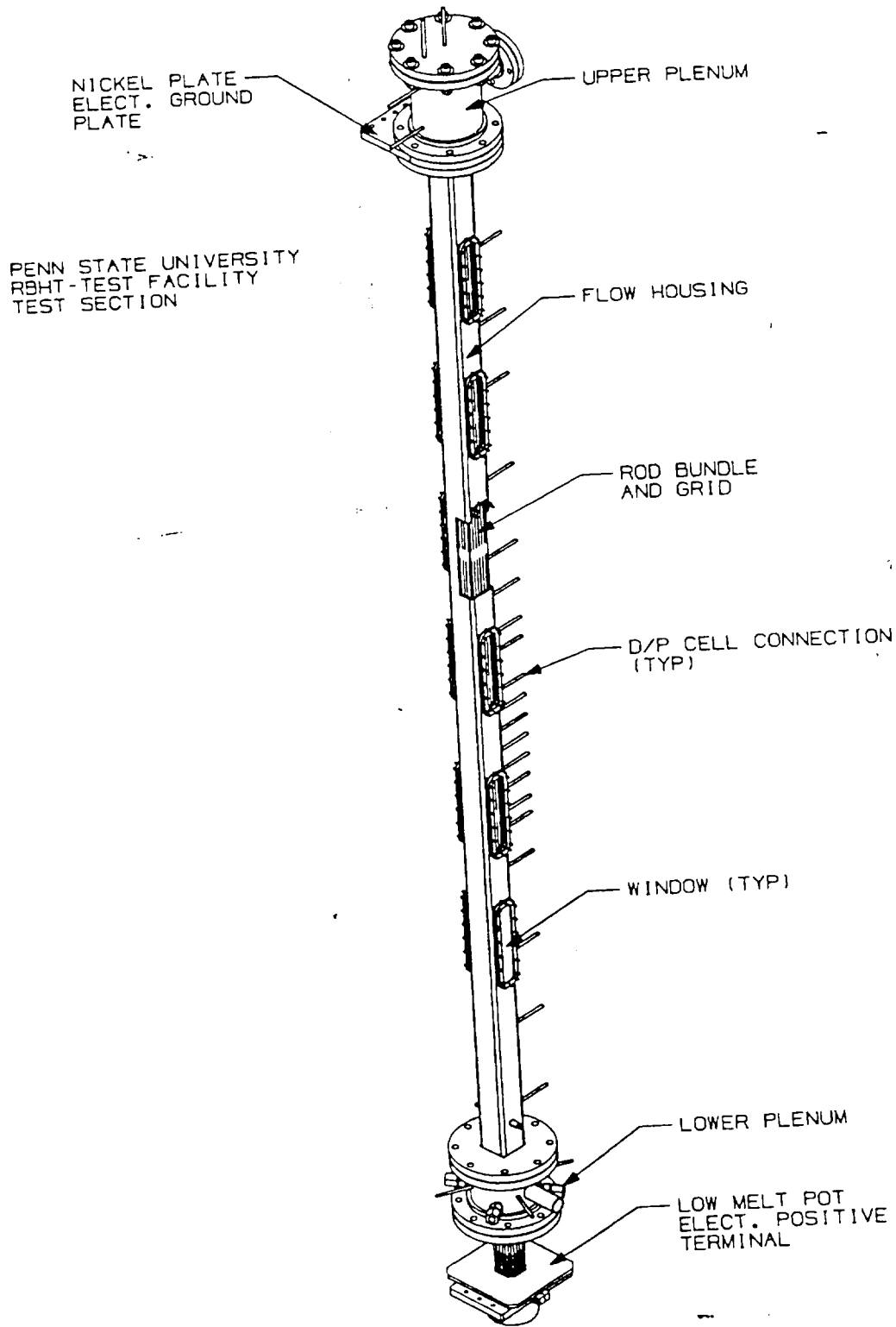


Figure 11-2. Test Section Isometric View

PENN STATE UNIVERSITY
RBHT-TEST SECTION
7X7 ROD BUNDLE ARRAY
CROSS SECTION

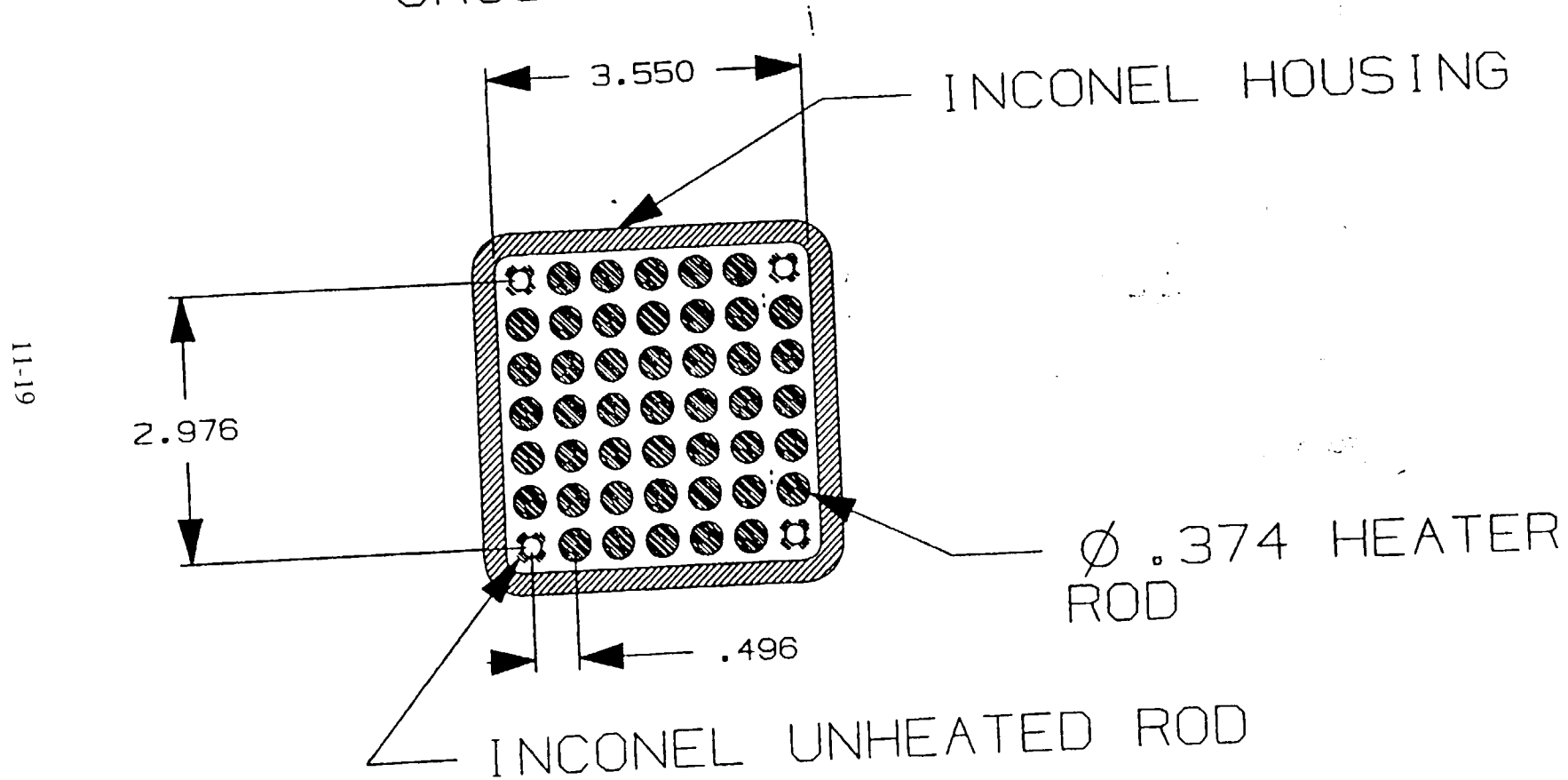
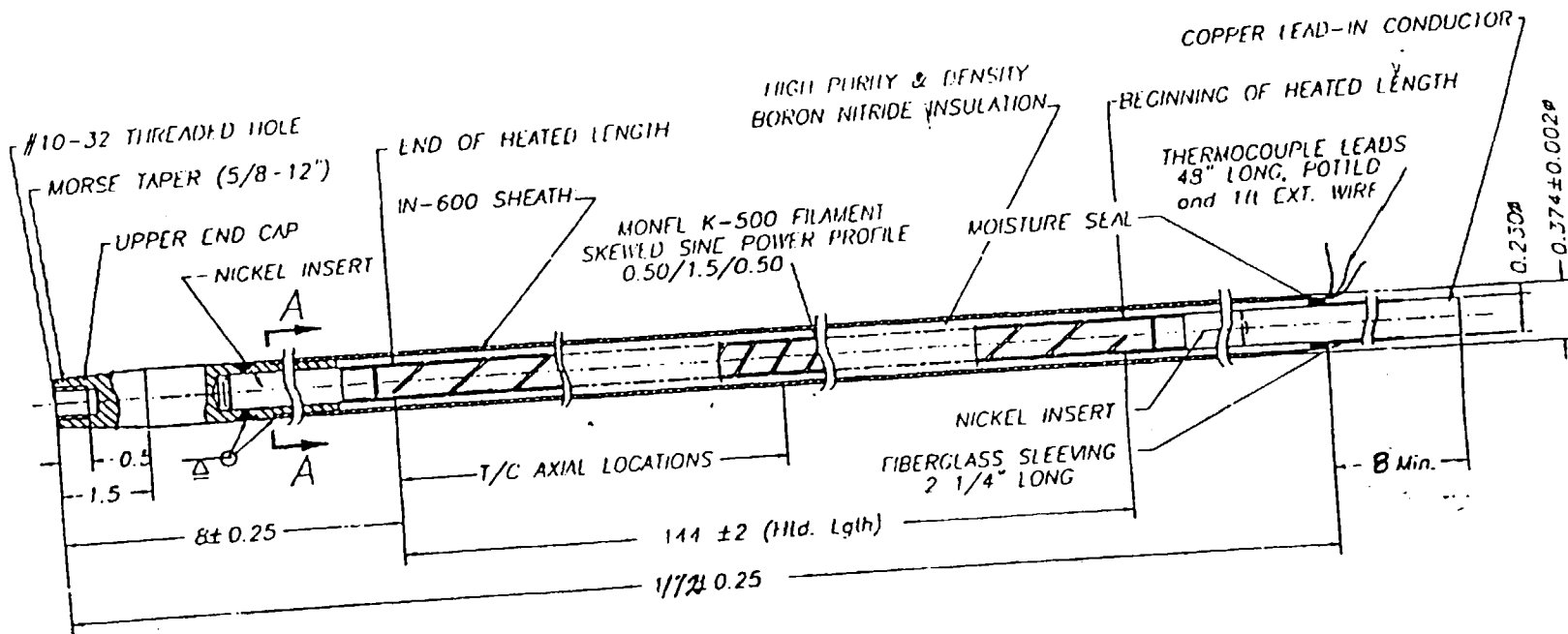
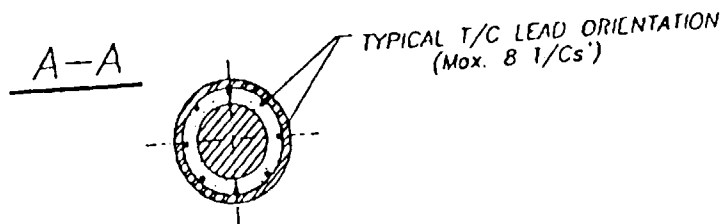


Figure 11-3. Rod Bundle Cross Sectional View



11-20

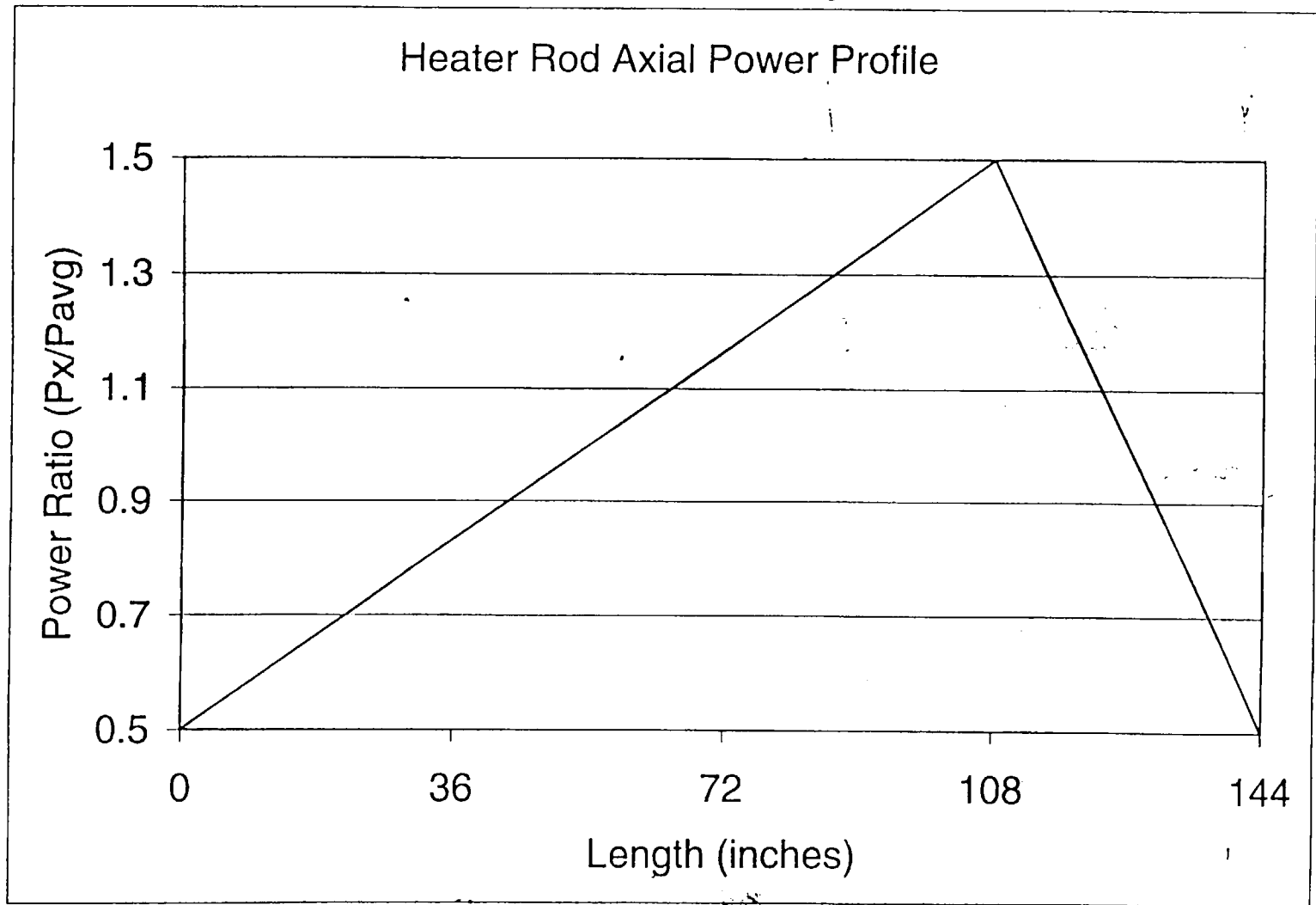


NOTES:

1. All dimensions in inches.

PENN STATE HEATER ROD SCHEMATIC

Figure 11-4. Heater Rod



11-21

Figure 11-5. Heater Rod Axial Power Profile

PENN STATE UNIVERSITY
RBHT-TEST FACILITY
LOW-MELT RESERVOIR AND CLAMP

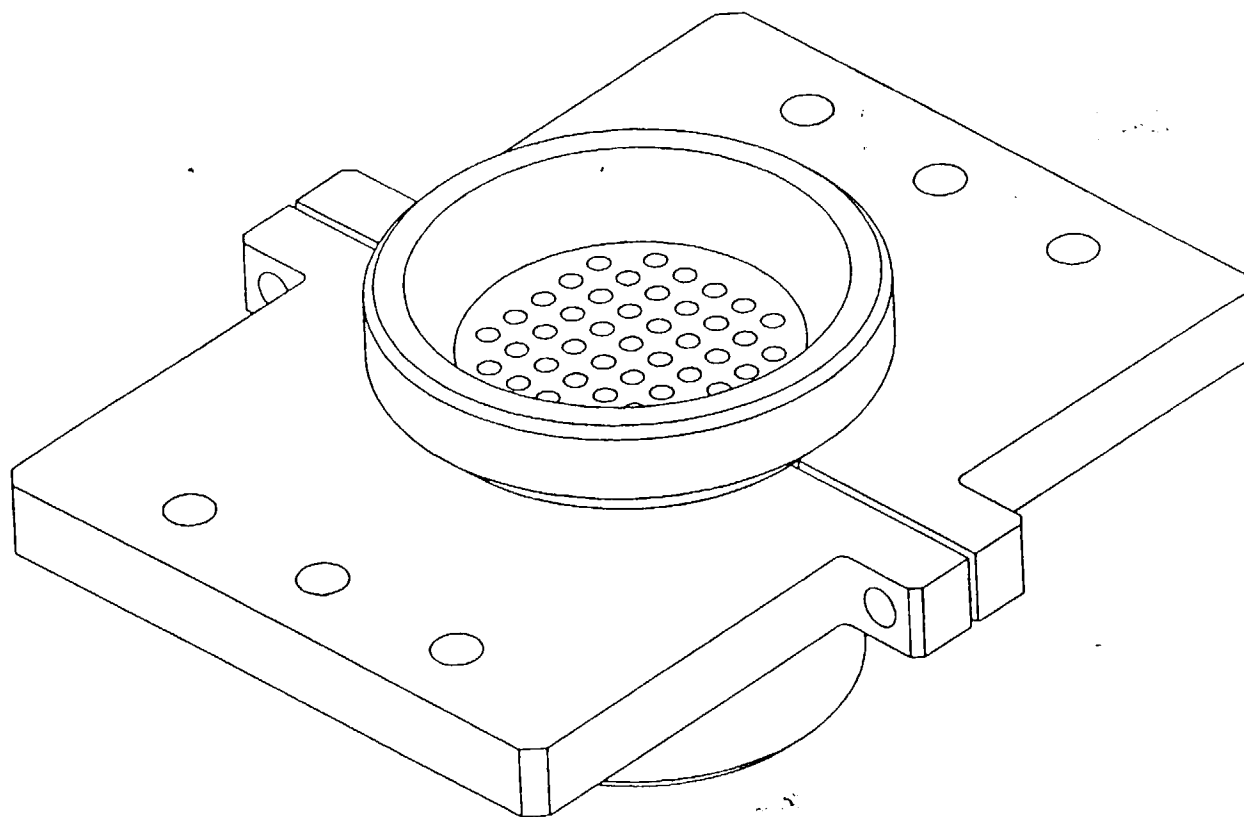


Figure 11-6. Low-Melt Reservoir

PENN STATE UNIVERSITY
RBHT-TEST FACILITY
FLOW HOUSING WELDMENT

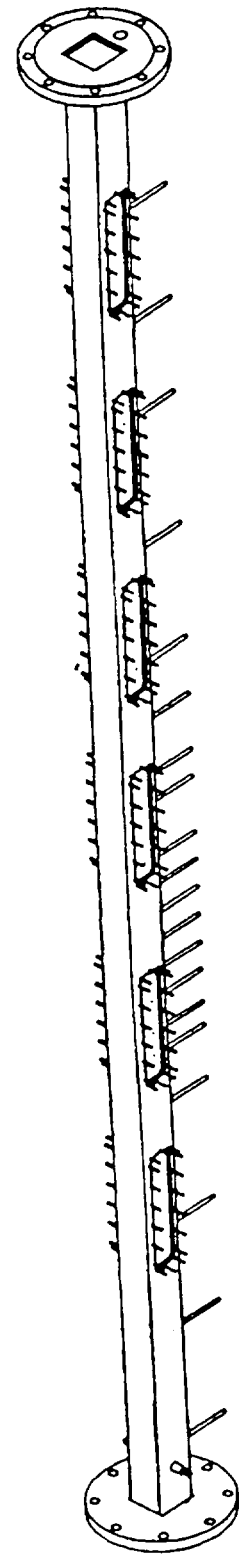
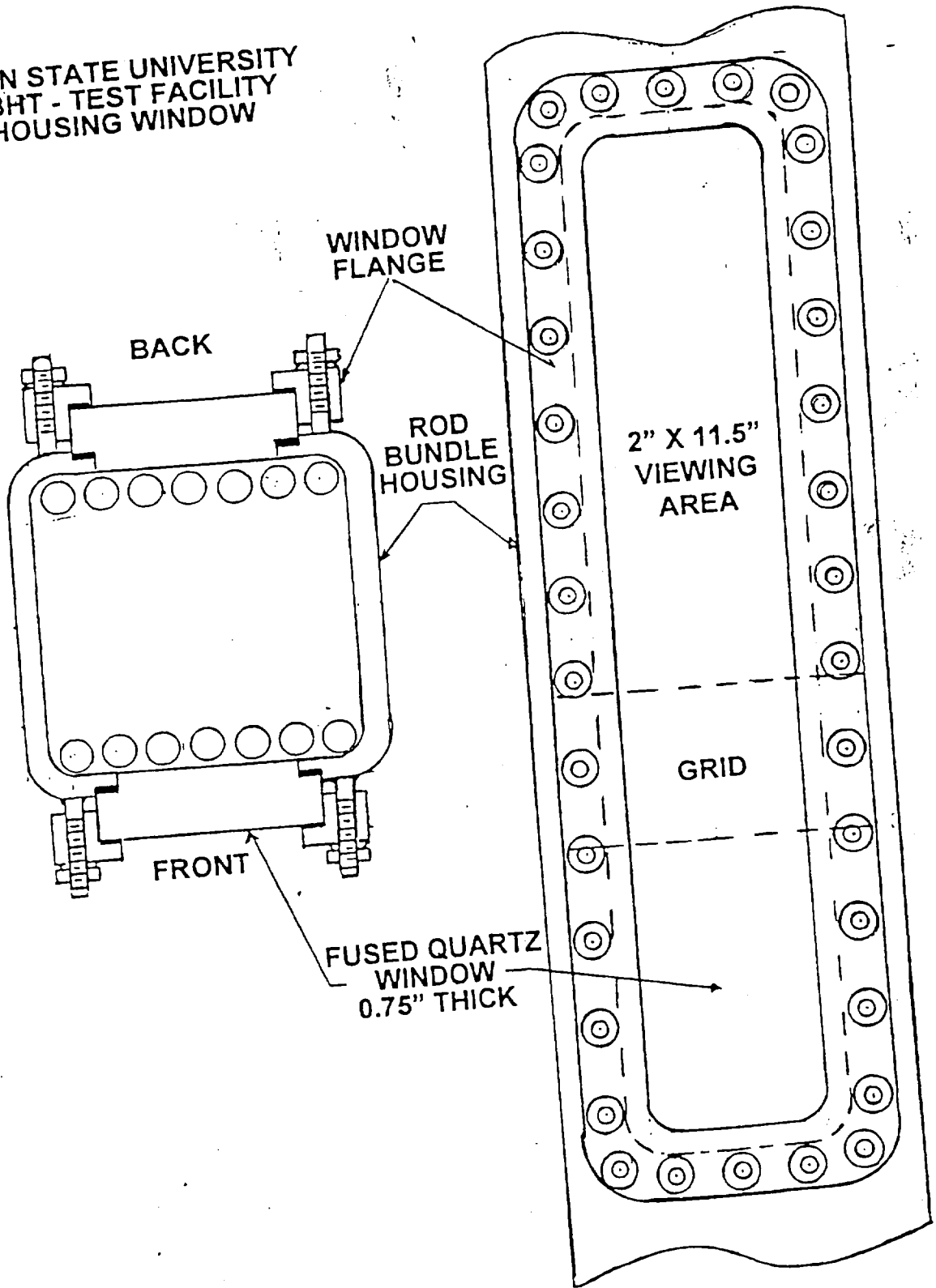


Figure 11-7. Low Mass Flow Housing Assembly

PENN STATE UNIVERSITY
RBHT - TEST FACILITY
HOUSING WINDOW



Rod Bundle - 4/8/88 - Raiph

Figure 11-8. Housing Window

PENN STATE UNIVERSITY
RBHT-TEST FACILITY
LOWER PLENUM

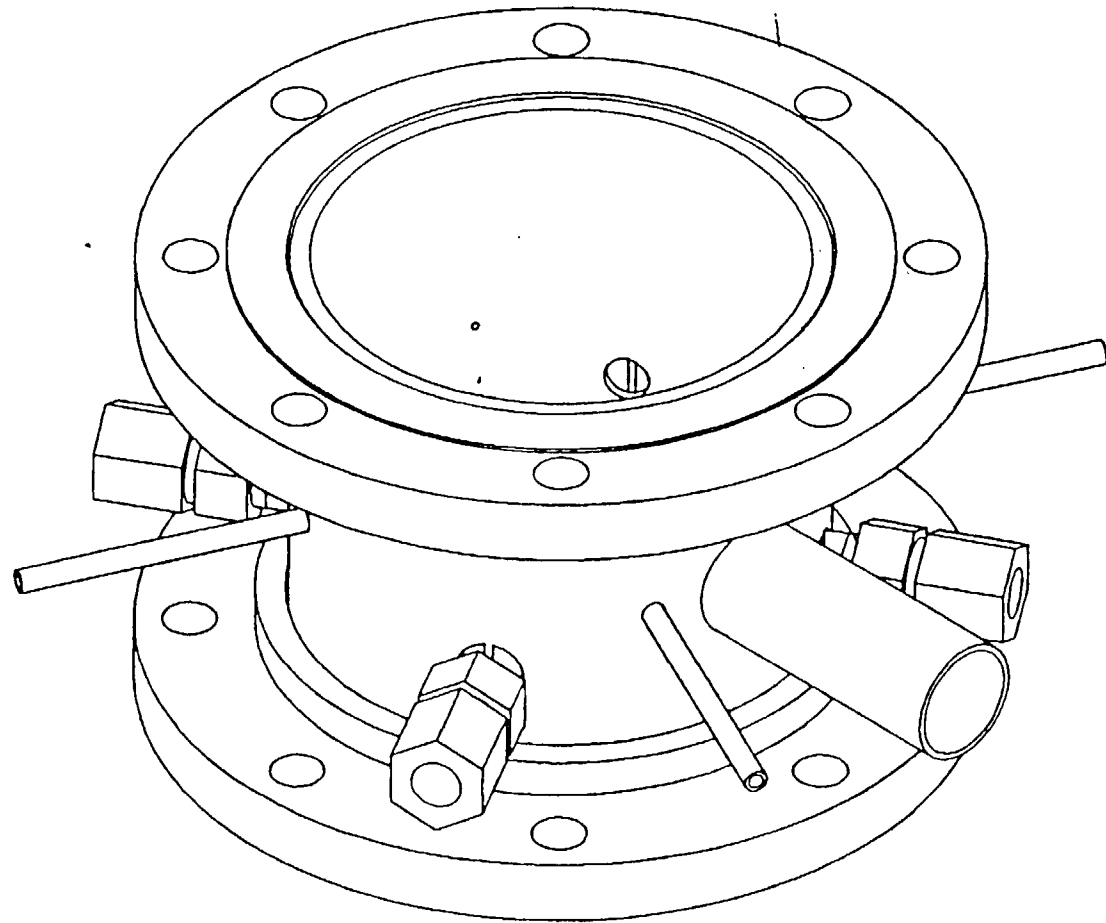


Figure 11-9. Lower Plenum

PENN STATE UNIVERSITY
RBHT-TEST FACILITY
LOWER PLENUM FLOW BAFFLE

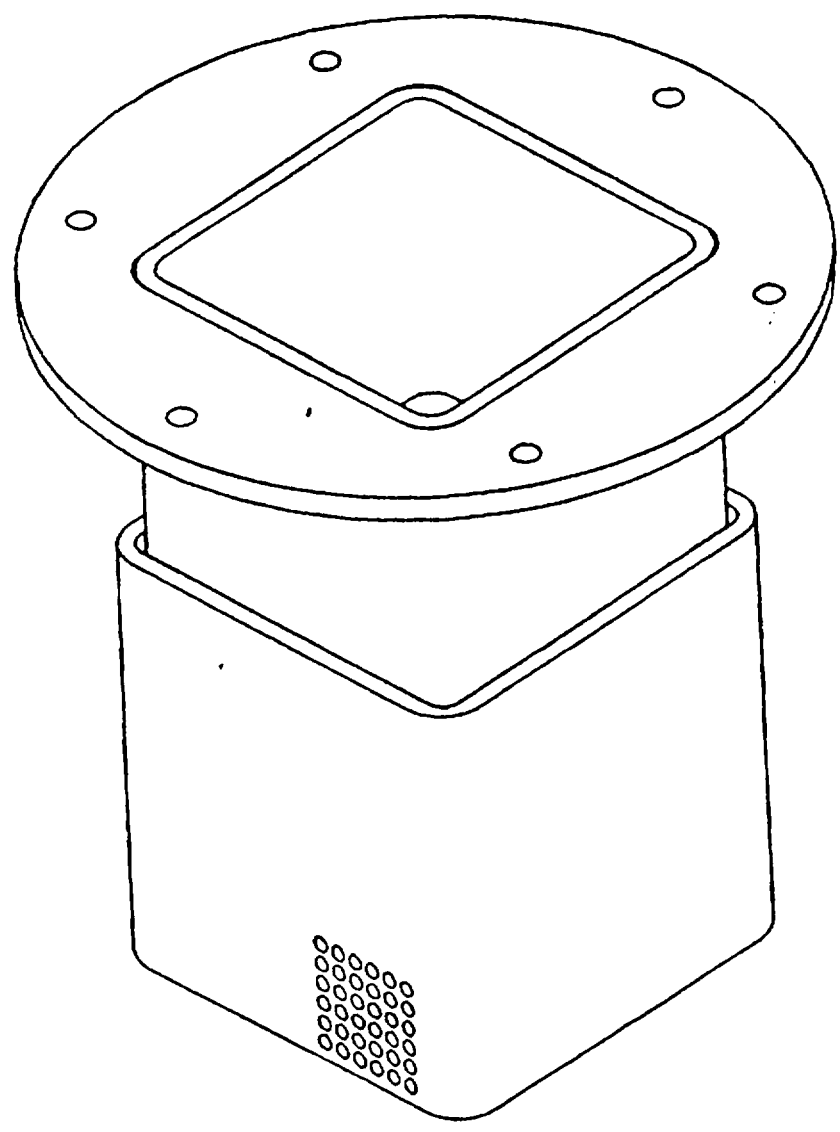


Figure 11-10. Lower Plenum Flow Baffle

PENN STATE UNIVERSITY
RBHT-TEST FACILITY
UPPER PLENUM

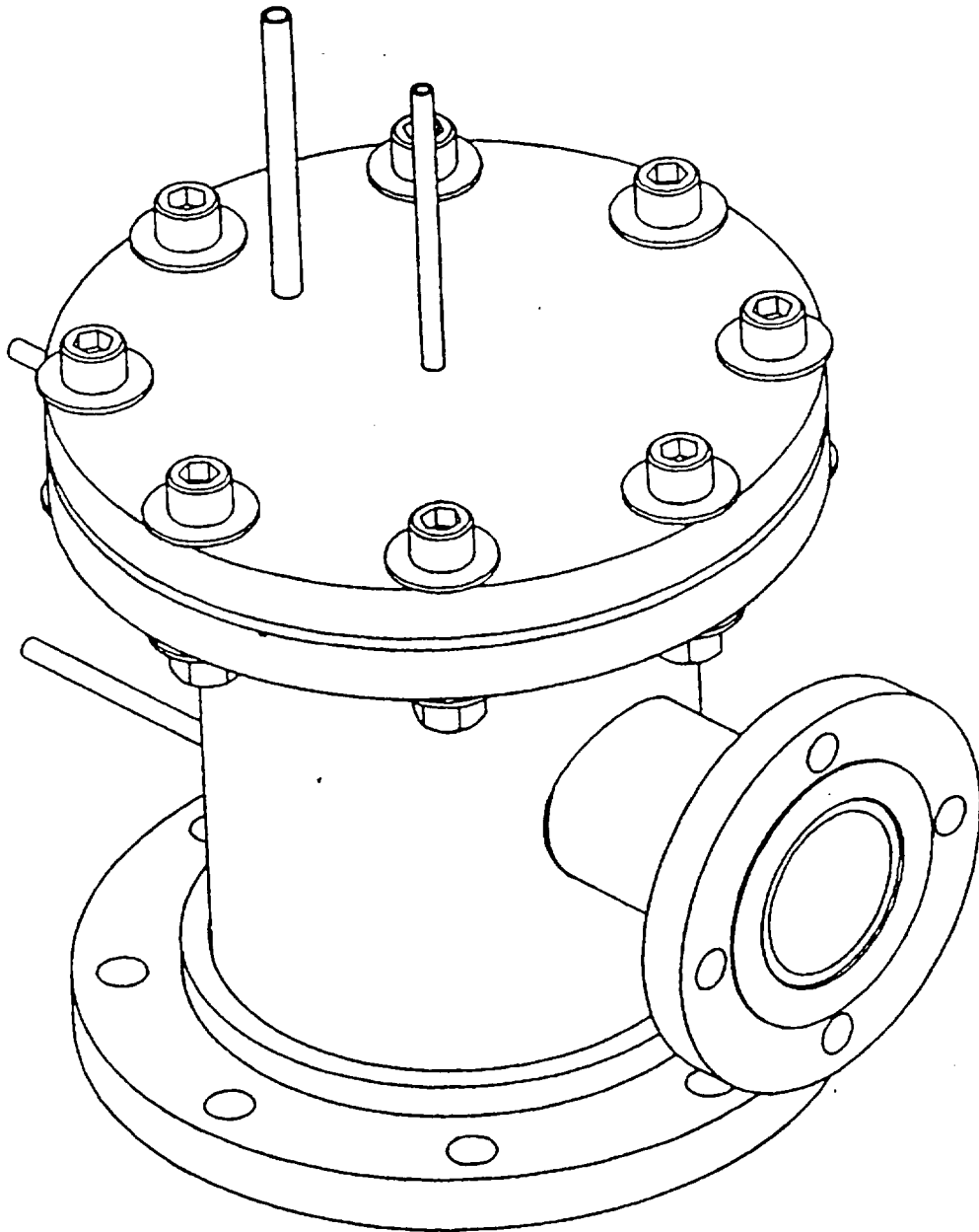


Figure 11-11. Upper Plenum

PENN STATE UNIVERSITY
RBHT-TEST FACILITY
EXHAUST LINE BAFFLE

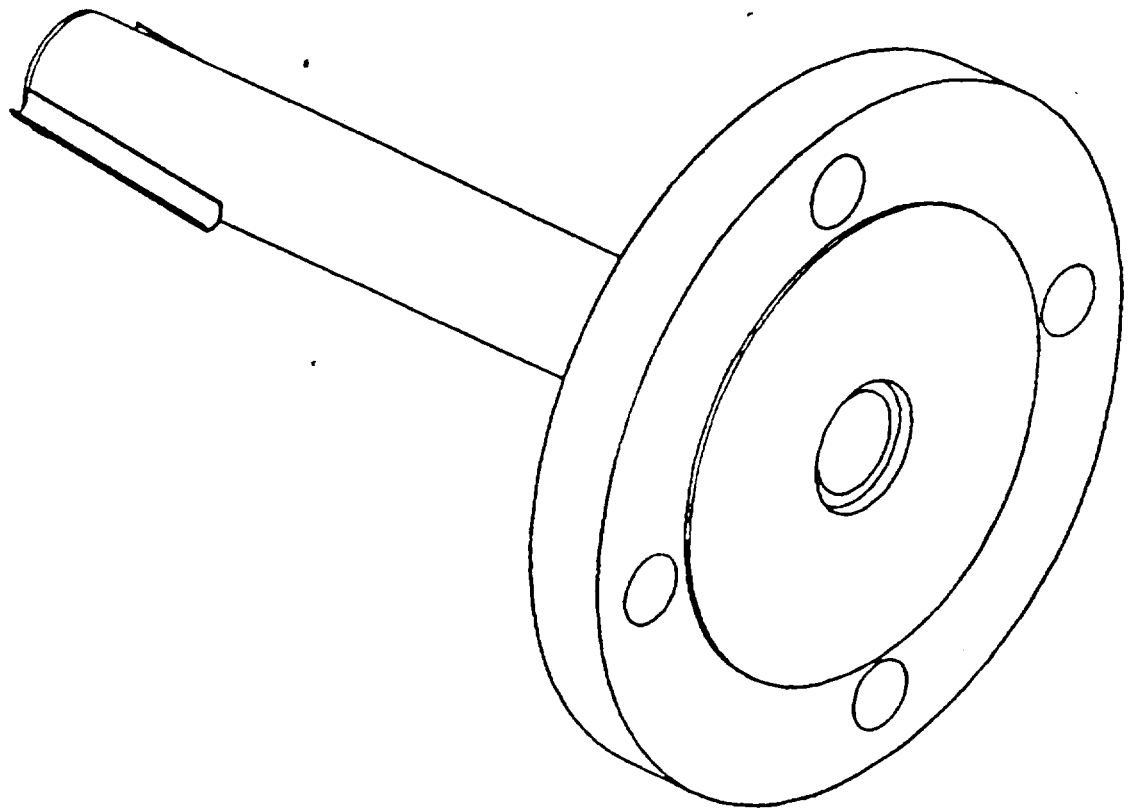


Figure 11-12. Exhaust Line Baffle

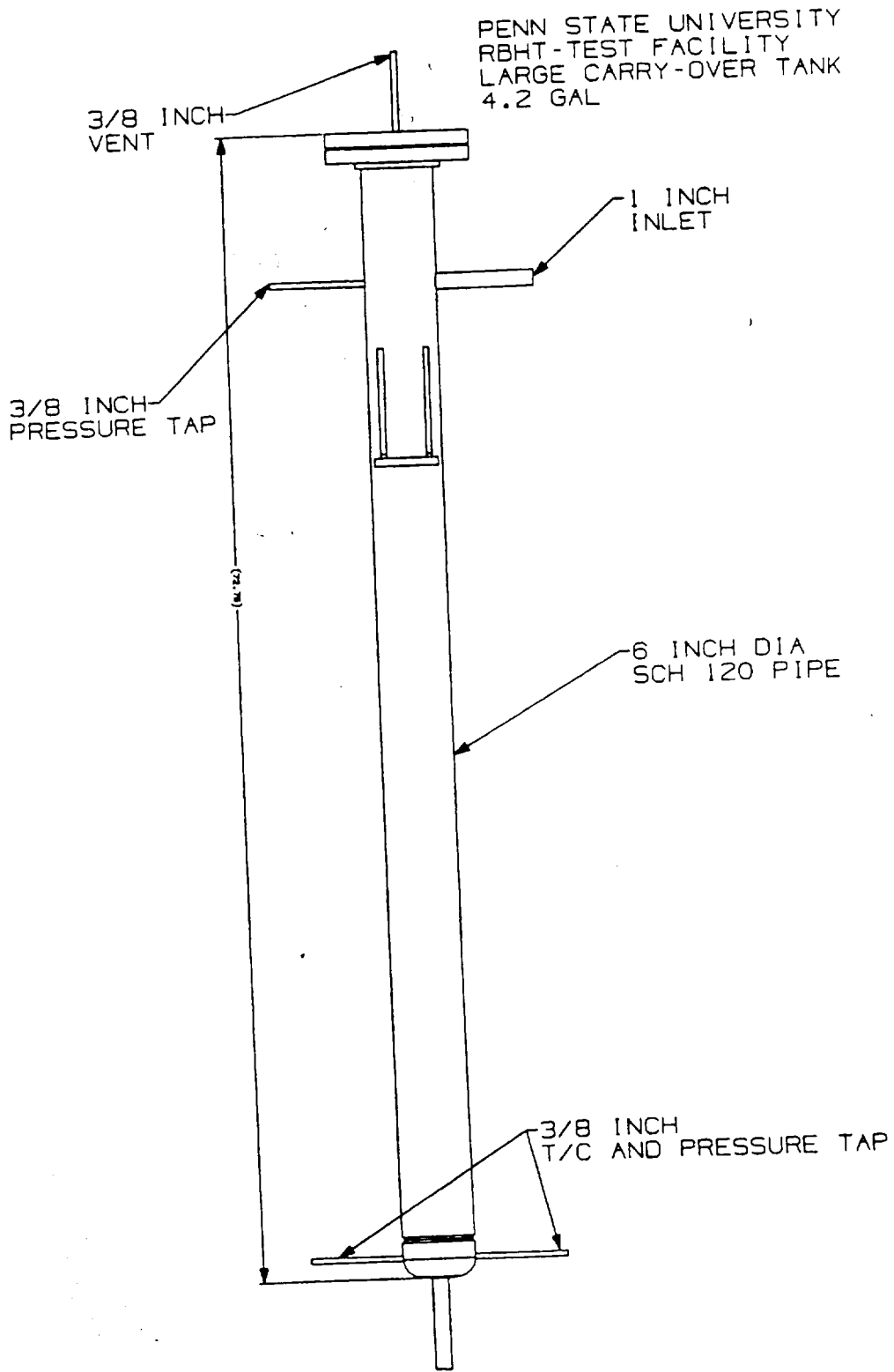


Figure 11-13. Large Carryover Tank

PENN STATE UNIVERSITY
RBHT - TEST FACILITY
STEAM SEPARATOR

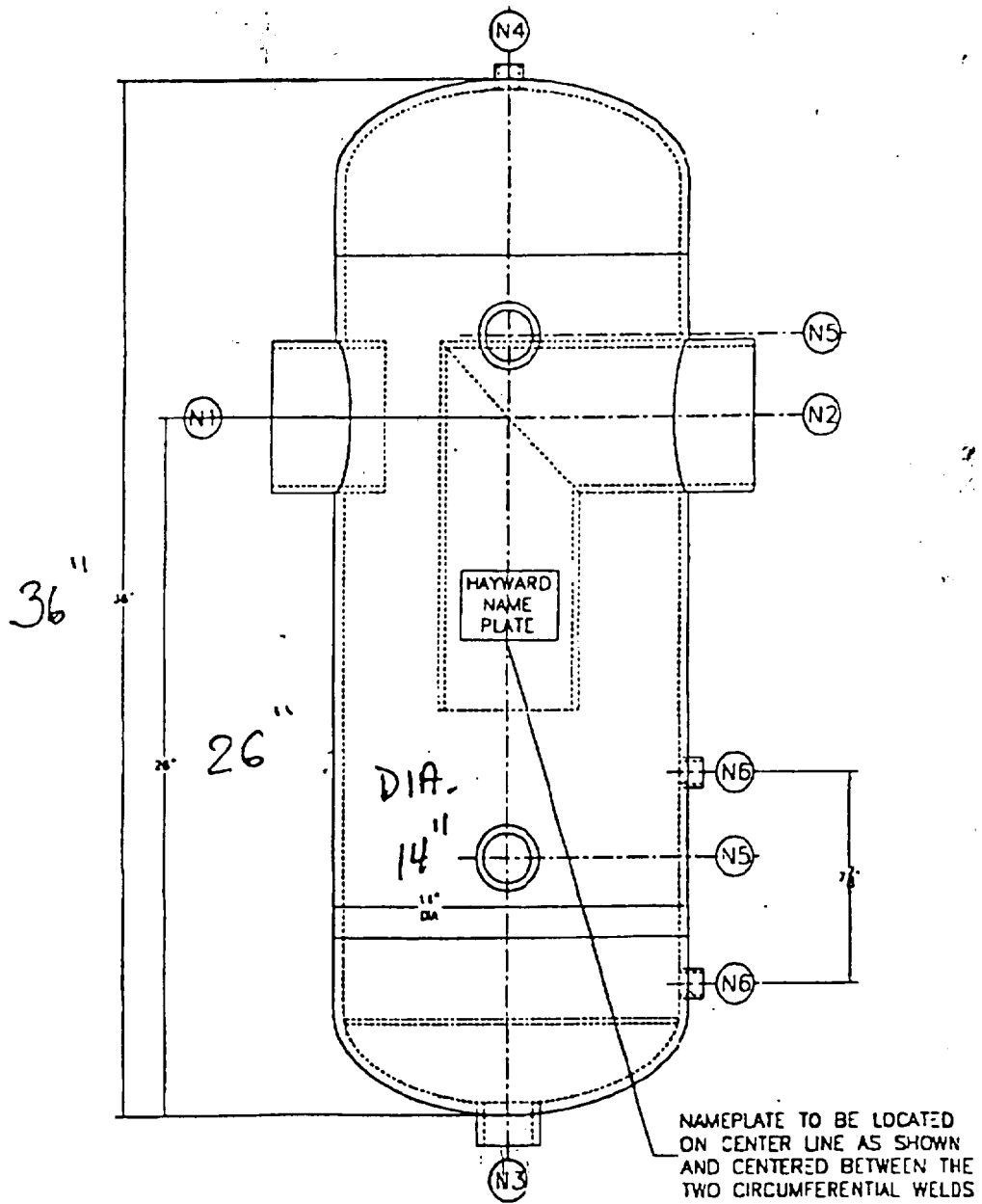
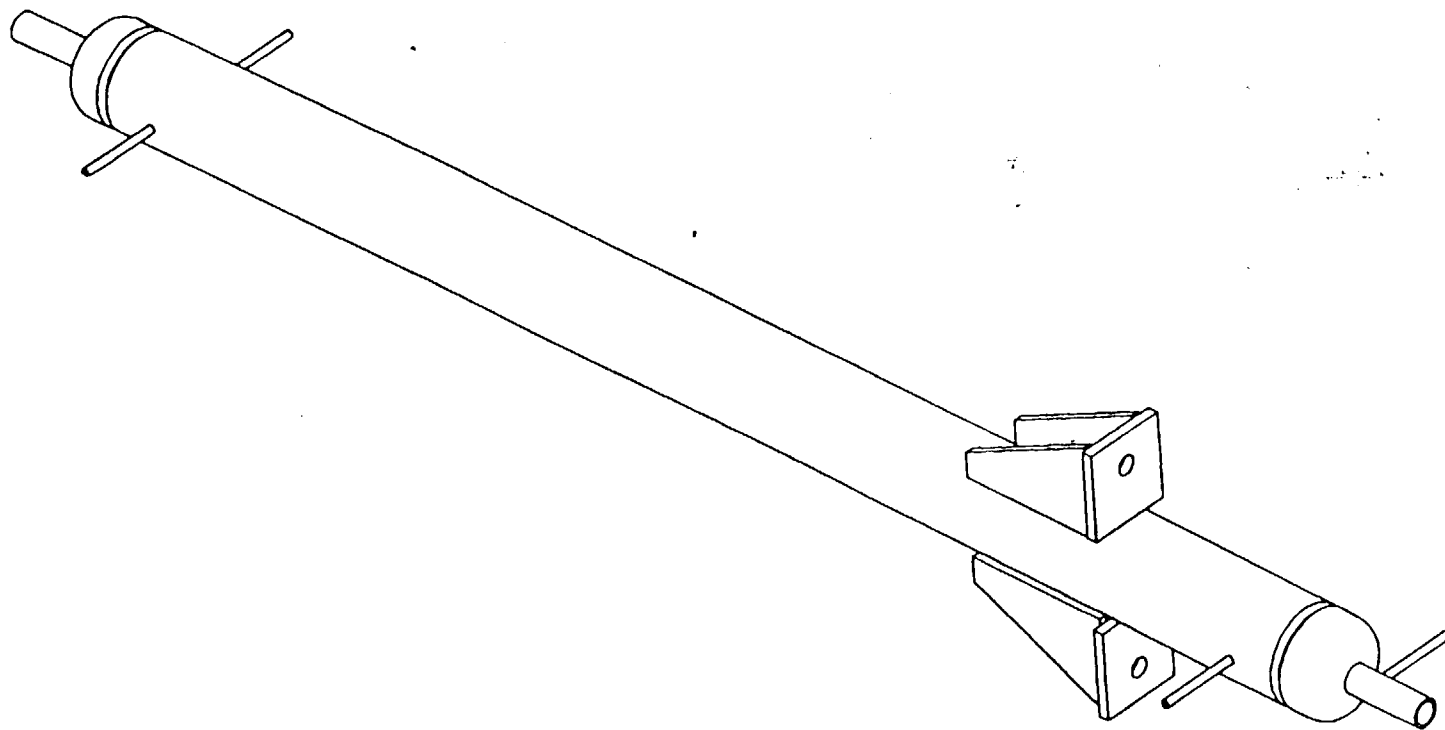


Figure 11-15. Steam Separator

PENN STATE UNIVERSITY
RBHT-TEST FACILITY
STEAM SEPARATOR DRAIN TANK



11-32

Figure 11-16. Steam Separator Collection Tank

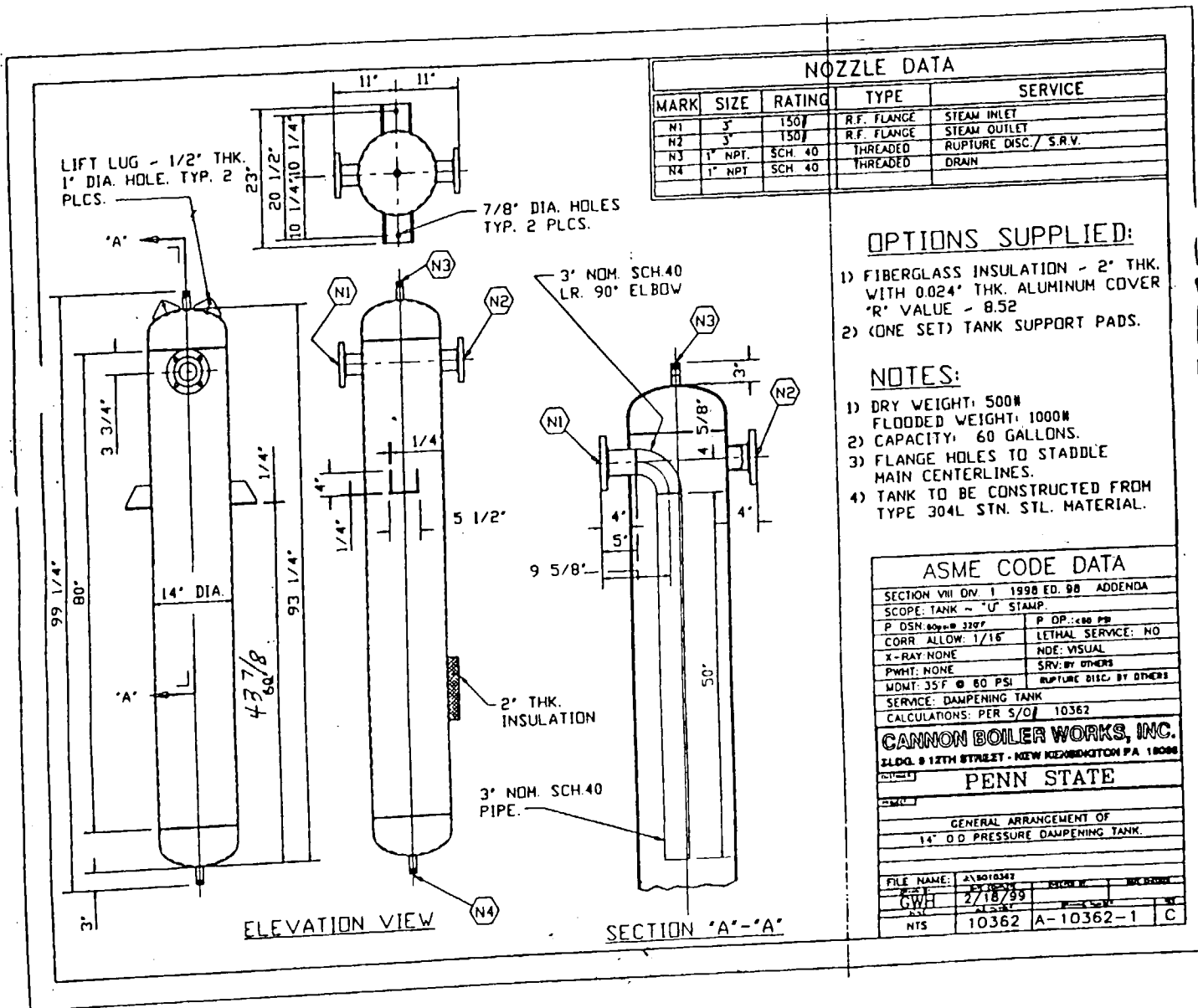


Figure 11-17. Pressure Oscillation Dampening Tank

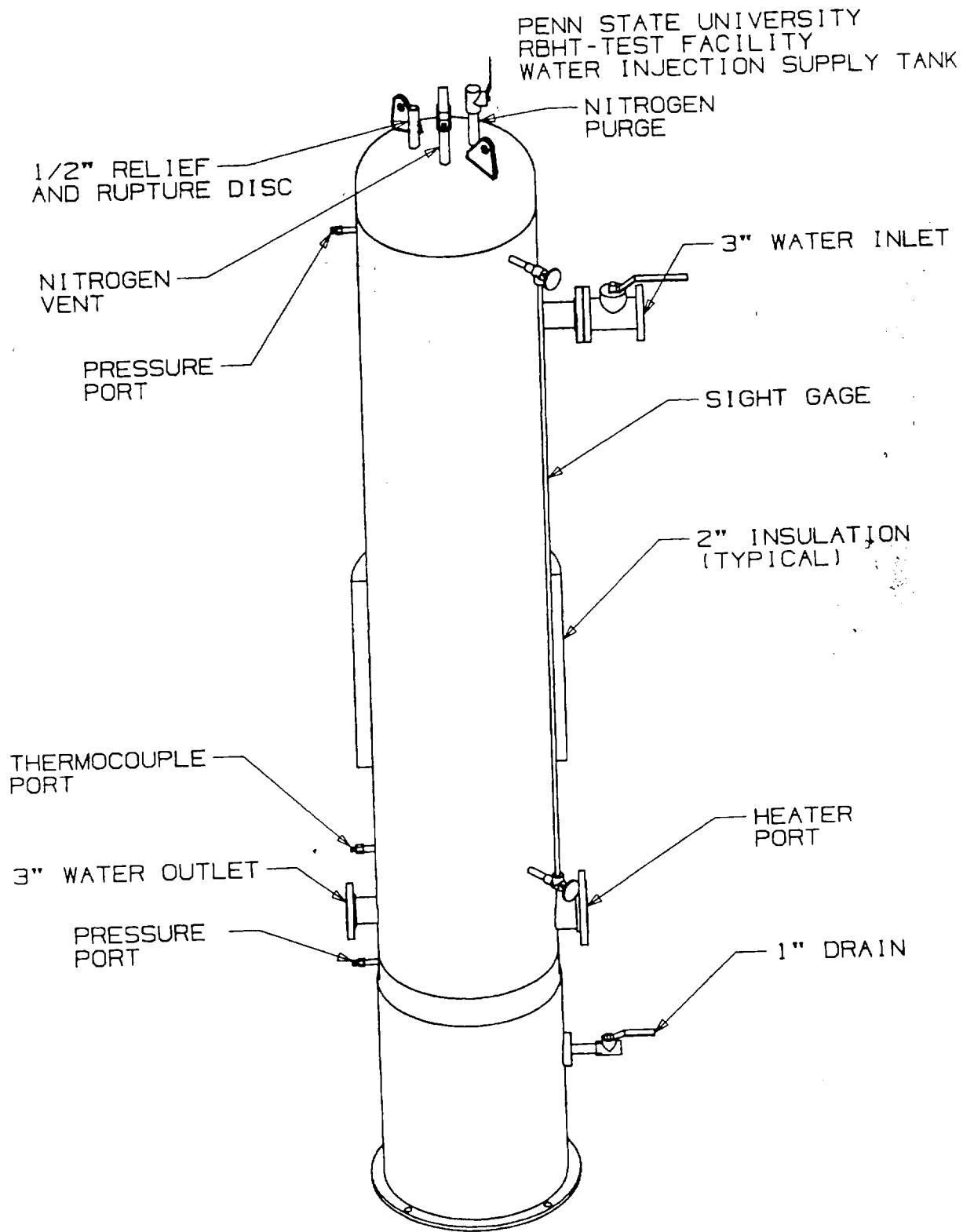
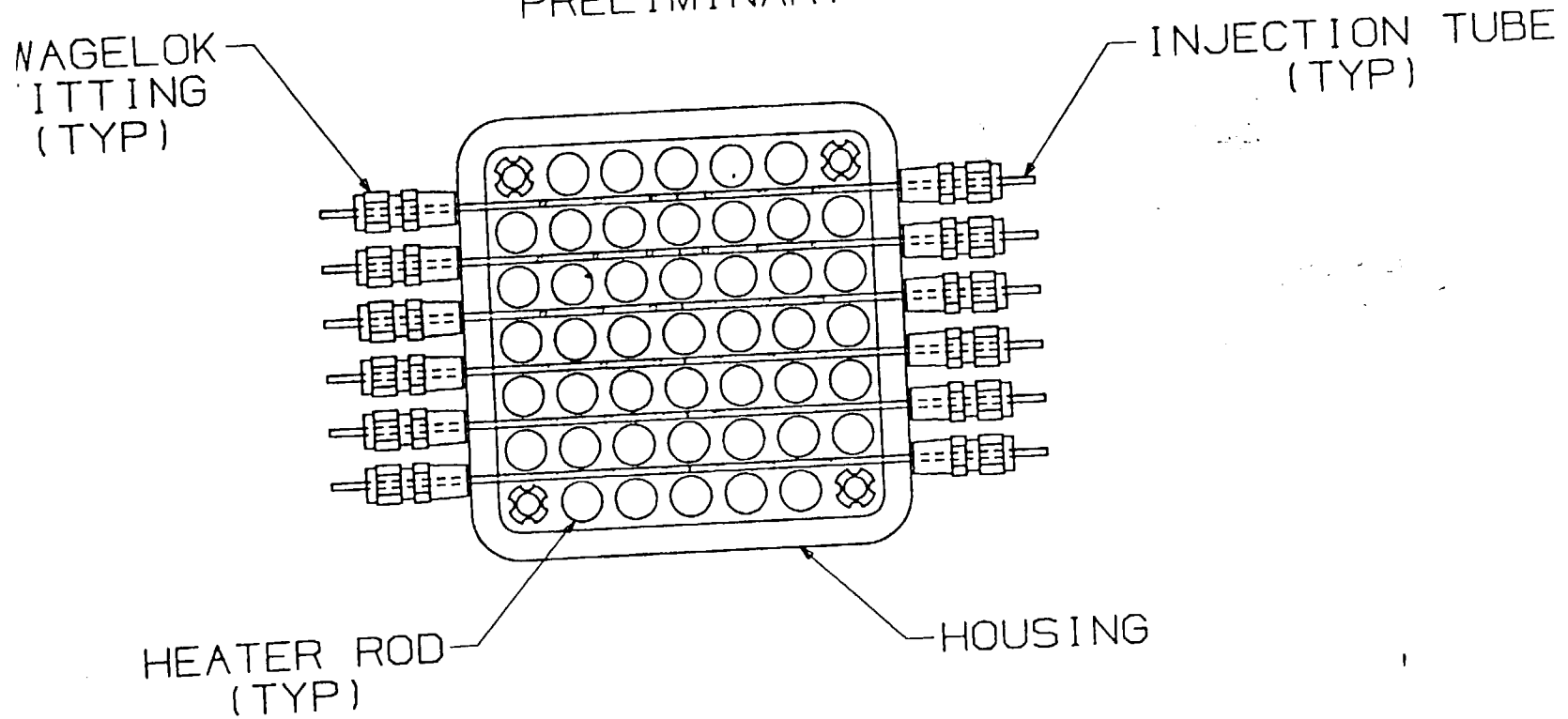


Figure 11-18. Injection Water Supply Tank

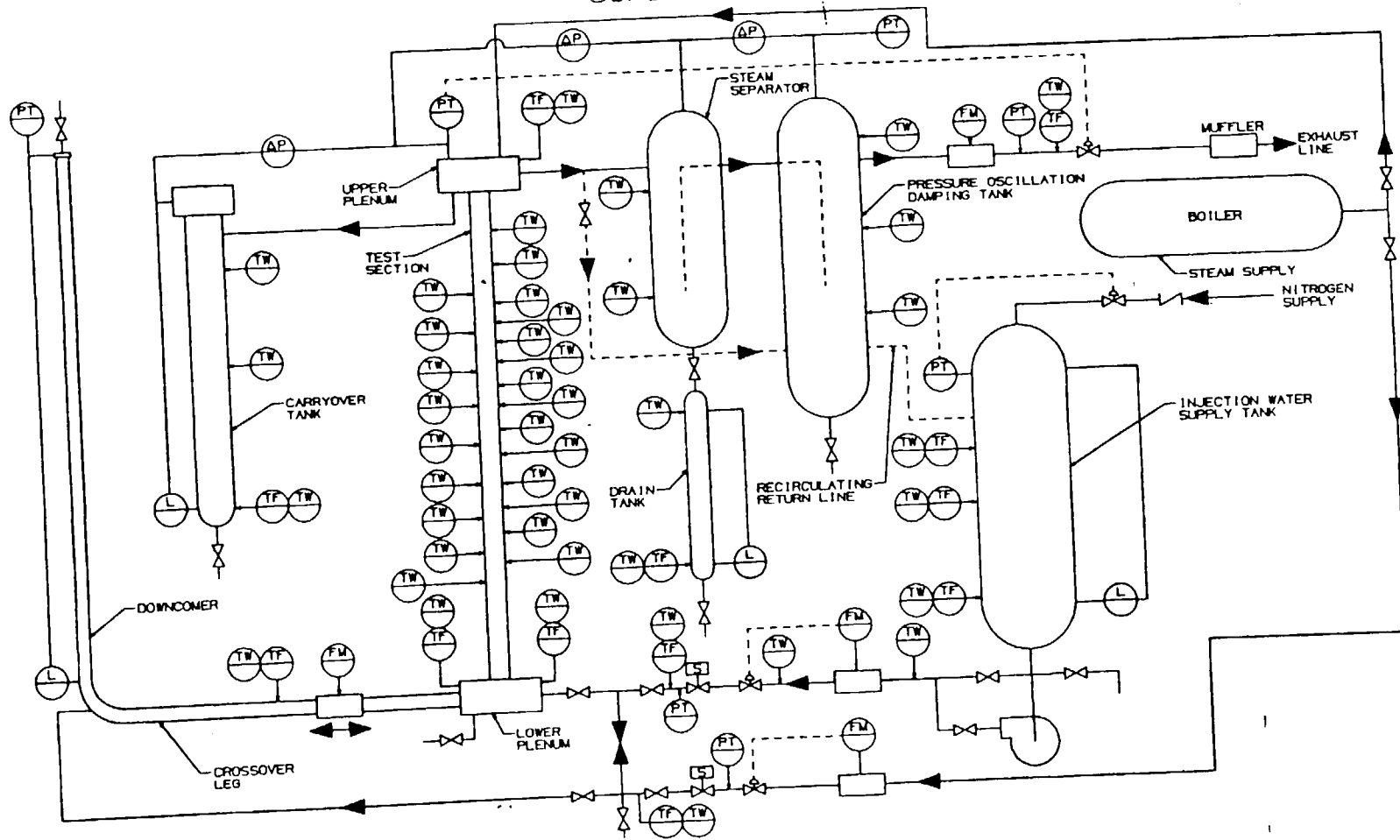
PENN STATE UNIVERSITY
RBHT-TEST FACILITY
DROPLET INJECTION SCHEMATIC
PRELIMINARY



11-35

Figure 11-19. Droplet Injection Schematic

PENN STATE UNIVERSITY
 RBHT-TEST FACILITY
 INSTRUMENTATION
 SCHEMATIC



11-36

Figure 11-20. Loop Instrumentation Schematic

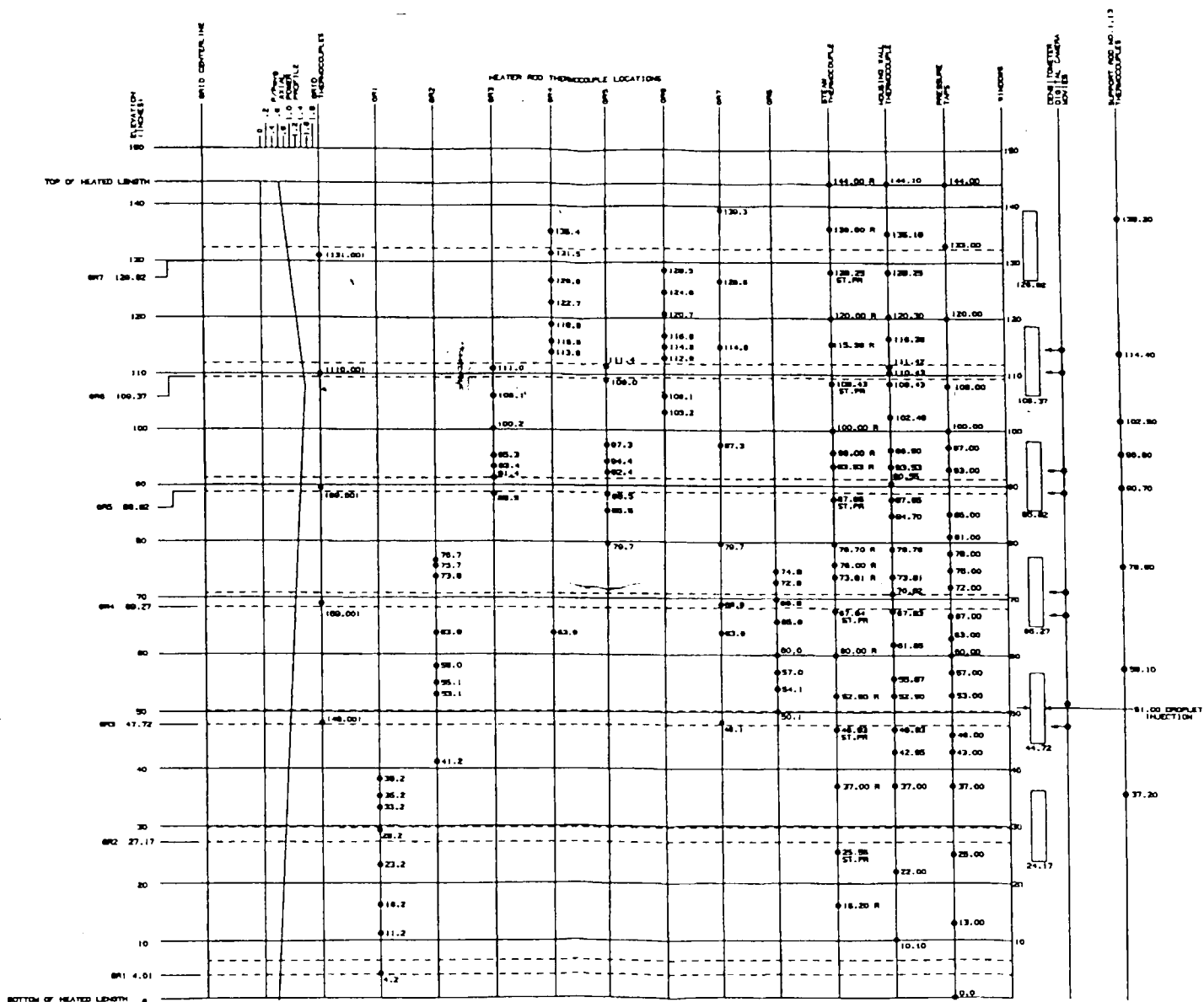
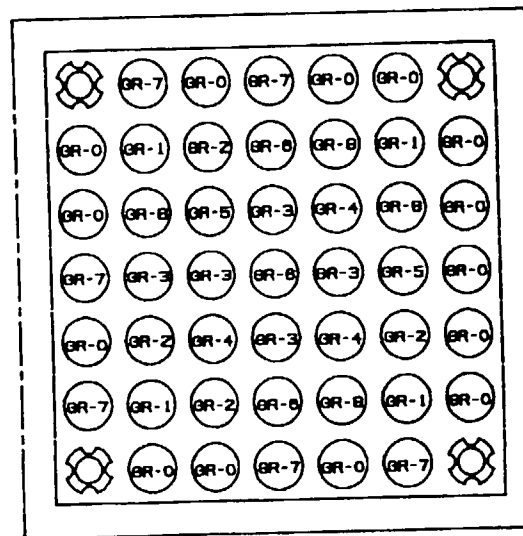


Figure 11-21. Rod Bundle and Housing Instrumentation Axial Locations

PENN STATE UNIVERSITY RBHT-TEST FACILITY INSTRUMENTED HEATER ROD LOCATIONS

11-38

GROUP NO.	QUANTITY	HEATER RODS
GGRR--0	14	
GGRR--1	4	
GGRR--2	4	
GGRR--3	4	
GGRR--4	4	
GGRR--5	4	
GGRR--6	4	
GGRR--7	4	
GGRR--8	4	
TOTAL :	45	



GR-0 UNINSTRUMENTED
GR-1 THRU 8 INSTRUMENTED

Figure 11-22. Instrumented Heater Rod Radial Locations

PENN STATE UNIVERSITY
 RBHT - TEST FACILITY
 TRAVERSING STEAM PROBE

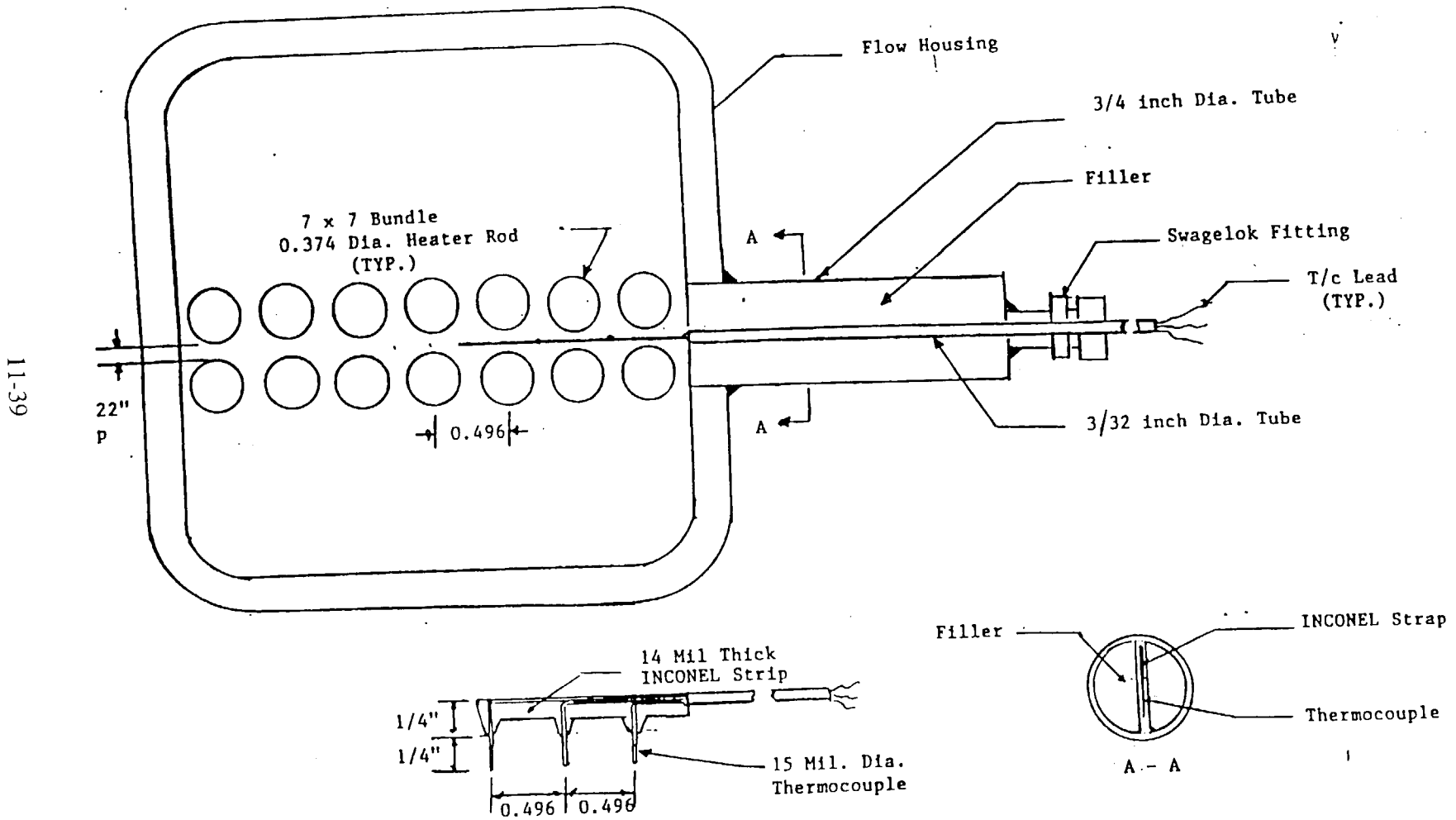
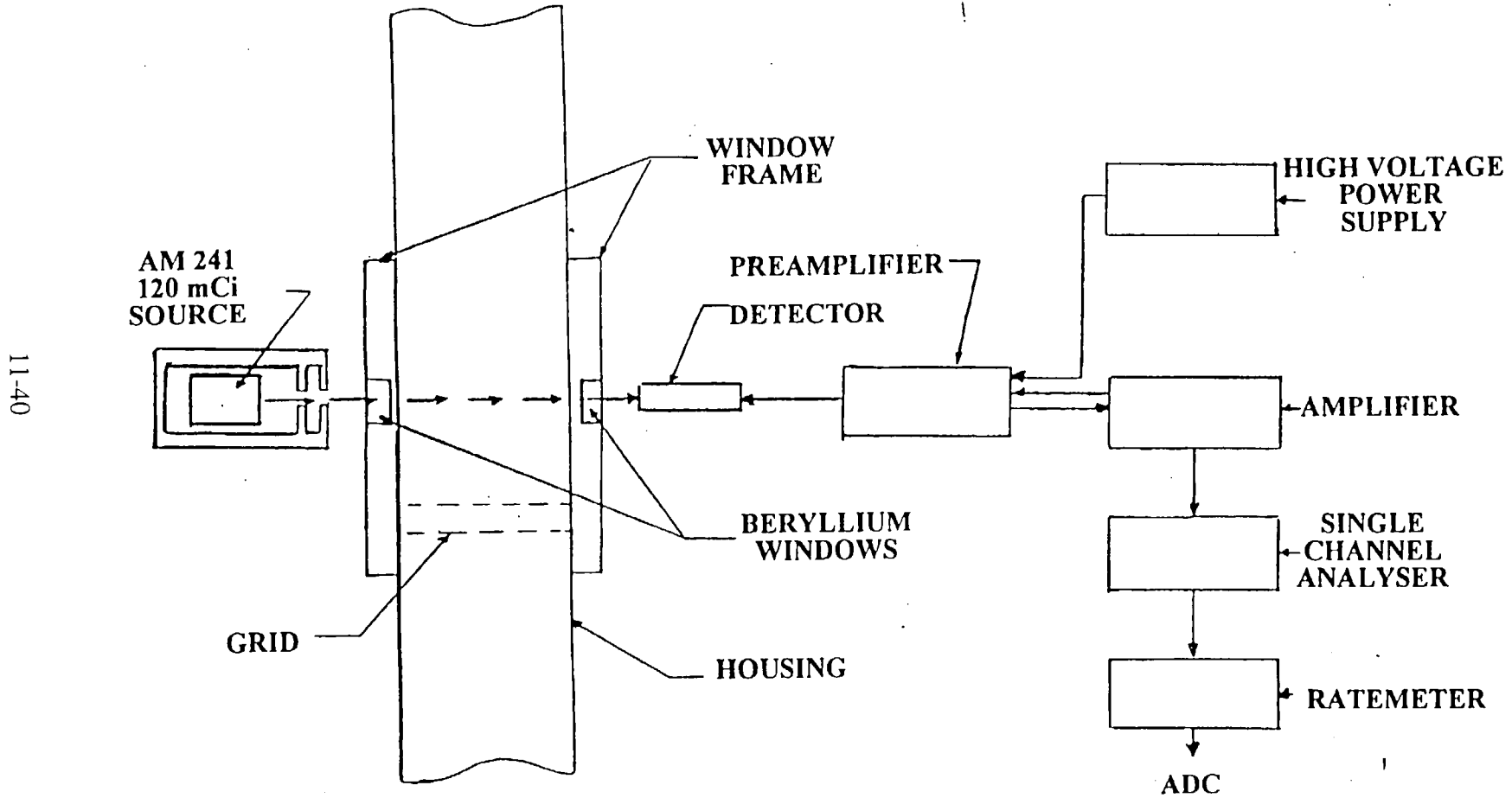


Figure 11-23. Traversing Steam Probe Rake

PENN STATE UNIVERSITY
RBHT - TEST FACILITY
DENSITOMETER SCHEMATIC

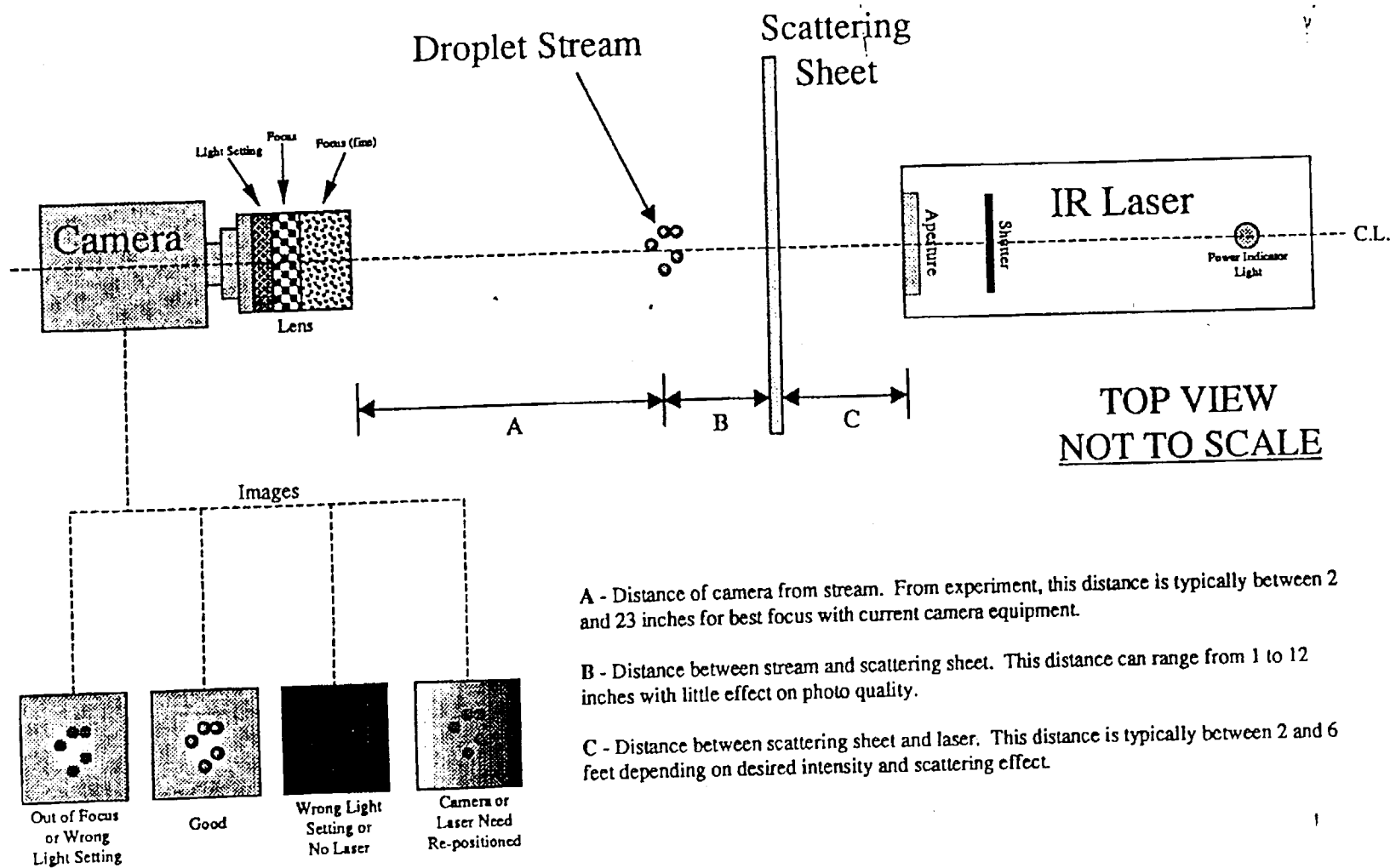


11-40

REVIEW.PPT - 4/2/91 - RALPH

Figure 11-24. Densitometer Schematic

Diagram 1
 Laser Illuminated Digital Camera System Setup
 Figure 11-25



11-41

Figure 11-25. Digital Camera and Laser Instrumentation

Table 11-1

General Specifications

Operating Pressure	200 psi
Maximum Sheath Temperature	2200°F
Heater Rod (Schematic Drawing)	
Design Power	10.0 kW
Design Voltage	57 V
Design Current	175.4 A
Design Resistance (@ 1000°F)	0.325 Ω
Electrical Resistance (@ 70°F)	0.306 Ω ±5%
Axial Power Profile	Linear 0.5/1.5/0.5 (See Figure 11-5)
Heated Length	144 in.
Average Linear Power	0.83 kW/ft
Peak Linear Power	1.25 kW/ft
Outside Diameter	0.374 ±0.002 in.
Overall Sheath Length	172 in.
Electrode Length	8 in.
Electrode Diameter	0.230 ±0.002 in.
Extension Length – Top	8 ±0.25 in.
Sheath Surface Finish	As Swaged (63 μin. or better)

Table 11-2
Thermocouple Specifications

Type	Premium grade ANSI Type K
Diameter	0.020 inches
Sheath	Inconel 600
Insulation	MgO
Junction	Ungrounded, BN backfilled
Length	up to 18 feet
Resistance, Lead to Sheath	$1 \times 10^{11} \Omega$ at 50 volts
Length beyond Heater Sheath	48 inches

Table 11-3. Instrumentation and Data Acquisition Channel List (Page 1 of 8)

SLOT 1			
CHAN	NAME	PANEL/ INPUT #	Slot, SCP & SCP #
497	Pnl1-Therm2S	1-0	1-E1508A-0
418	Lg CT fl	1-1	1-E1508A-0
419	Lg CT wall-t	1-2	1-E1508A-0
420	Lg CT wall-m	1-3	1-E1508A-0
421	Lg CT wall-b	1-4	1-E1508A-0
422	Sm CT fl	1-5	1-E1508A-0
423	Sm CT wall-t	1-6	1-E1508A-0
424	Sm CT wall-b	1-7	1-E1508A-0
1	HR_B1-48.1	1-8	1-E1508A-1
2	HR_B1-63.9	1-9	1-E1508A-1
3	HR_B1-68.9	1-10	1-E1508A-1
4	HR_B1-79.7	1-11	1-E1508A-1
5	HR_B1-97.3	1-12	1-E1508A-1
6	HR_B1-114.9	1-13	1-E1508A-1
7	HR_B1-126.6	1-14	1-E1508A-1
8	HR_B1-139.3	1-15	1-E1508A-1
9	HR_D1-48.1	1-16	1-E1508A-2
10	HR_D1-63.9	1-17	1-E1508A-2
11	HR_D1-68.9	1-18	1-E1508A-2
12	HR_D1-79.7	1-19	1-E1508A-2
13	HR_D1-97.3	1-20	1-E1508A-2
14	HR_D1-114.9	1-21	1-E1508A-2
15	HR_D1-126.6	1-22	1-E1508A-2
16	HR_D1-139.3	1-23	1-E1508A-2
17	HR_F7-48.1	1-24	1-E1508A-3
18	HR_F7-63.9	1-25	1-E1508A-3
19	HR_F7-68.9	1-26	1-E1508A-3
20	HR_F7-79.7	1-27	1-E1508A-3
21	HR_F7-97.3	1-28	1-E1508A-3
22	HR_F7-114.9	1-29	1-E1508A-3
23	HR_F7-126.6	1-30	1-E1508A-3
24	HR_F7-139.3	1-31	1-E1508A-3

SLOT 2			
CHAN	NAME	PANEL/ INPUT #	Slot, SCP & SCP #
499	Pnl3-Therm2S	3-0	2-E1508A-0
392	U Plen wall-b	3-1	2-E1508A-0
399	Sup Tnk fl-t	3-2	2-E1508A-0
400	Sup Tnk fl-m	3-3	2-E1508A-0
401	Sup Tnk fl-b	3-4	2-E1508A-0
402	Sup Tnk wall-t	3-5	2-E1508A-0
403	Sup Tnk wall-m	3-6	2-E1508A-0
404	Sup Tnk wall-b	3-7	2-E1508A-0
49	HR_B2-4.2	3-8	2-E1508A-1
50	HR_B2-11.2	3-9	2-E1508A-1
51	HR_B2-16.2	3-10	2-E1508A-1
52	HR_B2-23.2	3-11	2-E1508A-1
53	HR_B2-29.2	3-12	2-E1508A-1
54	HR_B2-33.2	3-13	2-E1508A-1
55	HR_B2-35.2	3-14	2-E1508A-1
56	HR_B2-38.2	3-15	2-E1508A-1
57	HR_C2-41.2	3-16	2-E1508A-2
58	HR_C2-53.1	3-17	2-E1508A-2
59	HR_C2-55.1	3-18	2-E1508A-2
60	HR_C2-58	3-19	2-E1508A-2
61	HR_C2-63.9	3-20	2-E1508A-2
62	HR_C2-73.8	3-21	2-E1508A-2
63	HR_C2-75.7	3-22	2-E1508A-2
64	HR_C2-76.7	3-23	2-E1508A-2
65	HR_D2-103.2	3-24	2-E1508A-3
66	HR_D2-106.1	3-25	2-E1508A-3
67	HR_D2-112.9	3-26	2-E1508A-3
68	HR_D2-114.9	3-27	2-E1508A-3
69	HR_D2-116.8	3-28	2-E1508A-3
70	HR_D2-120.7	3-29	2-E1508A-3
71	HR_D2-124.6	3-30	2-E1508A-3
72	HR_D2-128.5	3-31	2-E1508A-3

Table 11-3. Instrumentation and Data Acquisition Channel List (Page 2 of 8)

SLOT 1			
CHAN	NAME	PANEL/ INPUT #	Slot, SCP & SCP #
498	Pnl2-Therm2S	2-32	1-E1508A-4
385	L Plen fl-t	2-33	1-E1508A-4
386	L Plen fl-b	2-34	1-E1508A-4
387	L Plen wall-t	2-35	1-E1508A-4
388	L Plen wall-b	2-36	1-E1508A-4
389	U Plen fl-t	2-37	1-E1508A-4
390	U Plen fl-b	2-38	1-E1508A-4
391	U Plen wall-t	2-39	1-E1508A-4
25	HR_D7-48.1	2-40	1-E1508A-5
26	HR_D7-63.9	2-41	1-E1508A-5
27	HR_D7-68.9	2-42	1-E1508A-5
28	HR_D7-79.7	2-43	1-E1508A-5
29	HR_D7-97.3	2-44	1-E1508A-5
30	HR_D7-114.9	2-45	1-E1508A-5
31	HR_D7-126.6	2-46	1-E1508A-5
32	HR_D7-139.3	2-47	1-E1508A-5
33	HR_A6-48.1	2-48	1-E1508A-6
34	HR_A6-63.9	2-49	1-E1508A-6
35	HR_A6-68.9	2-50	1-E1508A-6
36	HR_A6-79.7	2-51	1-E1508A-6
37	HR_A6-97.3	2-52	1-E1508A-6
38	HR_A6-114.9	2-53	1-E1508A-6
39	HR_A6-126.6	2-54	1-E1508A-6
40	HR_A6-139.3	2-55	1-E1508A-6
41	HR_A4-48.1	2-56	1-E1508A-7
42	HR_A4-63.9	2-57	1-E1508A-7
43	HR_A4-68.9	2-58	1-E1508A-7
44	HR_A4-79.7	2-59	1-E1508A-7
45	HR_A4-97.3	2-60	1-E1508A-7
46	HR_A4-114.9	2-61	1-E1508A-7
47	HR_A4-126.6	2-62	1-E1508A-7
48	HR_A4-139.3	2-63	1-E1508A-7

SLOT 2			
CHAN	NAME	PANEL/ INPUT #	Slot, SCP & SCP #
500	Pnl4-Therm2S	4-32	2-E1508A-4
407	Sup Ln fl	4-33	2-E1508A-4
408	Sup Ln wall	4-34	2-E1508A-4
409	Sup Ln wall	4-35	2-E1508A-4
410	Sup Ln wall	4-36	2-E1508A-4
414	St Sup fl	4-37	2-E1508A-4
415	St Sup wall	4-38	2-E1508A-4
428	St Sep fl	4-39	2-E1508A-4
73	HR_E2-50.1	4-40	2-E1508A-5
74	HR_E2-54.1	4-41	2-E1508A-5
75	HR_E2-57	4-42	2-E1508A-5
76	HR_E2-60	4-43	2-E1508A-5
77	HR_E2-65.9	4-44	2-E1508A-5
78	HR_E2-69.8	4-45	2-E1508A-5
79	HR_E2-72.8	4-46	2-E1508A-5
80	HR_E2-74.8	4-47	2-E1508A-5
81	HR_F2-4.2	4-48	2-E1508A-6
82	HR_F2-11.2	4-49	2-E1508A-6
83	HR_F2-16.2	4-50	2-E1508A-6
84	HR_F2-23.2	4-51	2-E1508A-6
85	HR_F2-29.2	4-52	2-E1508A-6
86	HR_F2-33.2	4-53	2-E1508A-6
87	HR_F2-35.2	4-54	2-E1508A-6
88	HR_F2-38.2	4-55	2-E1508A-6
89	HR_F3-50.1	4-56	2-E1508A-7
90	HR_F3-54.1	4-57	2-E1508A-7
91	HR_F3-57	4-58	2-E1508A-7
92	HR_F3-60	4-59	2-E1508A-7
93	HR_F3-65.9	4-60	2-E1508A-7
94	HR_F3-69.8	4-61	2-E1508A-7
95	HR_F3-72.8	4-62	2-E1508A-7
96	HR_F3-74.8	4-63	2-E1508A-7

Table 11-3. Instrumentation and Data Acquisition Channel List (Page 3 of 8)

SLOT 3			
CHAN	NAME	PANEL/ INPUT #	Slot, SCP & SCP #
501	Pnl5-Therm2S	5-0	3-E1508A-0
429	St Sep wall-t	5-1	3-E1508A-0
430	St Sep wall-b	5-2	3-E1508A-0
431	St Sep Dr wall-t	5-3	3-E1508A-0
432	St Sep Dr wall-b	5-4	3-E1508A-0
435	Acc wall-t	5-5	3-E1508A-0
436	Acc wall-m	5-6	3-E1508A-0
437	Acc wall-b	5-7	3-E1508A-0
97	HR_F4-79.7	5-8	3-E1508A-1
98	HR_F4-85.5	5-9	3-E1508A-1
99	HR_F4-88.5	5-10	3-E1508A-1
100	HR_F4-92.4	5-11	3-E1508A-1
101	HR_F4-94.4	5-12	3-E1508A-1
102	HR_F4-97.3	5-13	3-E1508A-1
103	HR_F4-109	5-14	3-E1508A-1
104	HR_F4-111.4	5-15	3-E1508A-1
105	HR_F5-41.2	5-16	3-E1508A-2
106	HR_F5-53.1	5-17	3-E1508A-2
107	HR_F5-55.1	5-18	3-E1508A-2
108	HR_F5-58	5-19	3-E1508A-2
109	HR_F5-63.9	5-20	3-E1508A-2
110	HR_F5-73.8	5-21	3-E1508A-2
111	HR_F5-75.7	5-22	3-E1508A-2
112	HR_F5-76.7	5-23	3-E1508A-2
113	HR_F6-4.2	5-24	3-E1508A-3
114	HR_F6-11.2	5-25	3-E1508A-3
115	HR_F6-16.2	5-26	3-E1508A-3
116	HR_F6-23.2	5-27	3-E1508A-3
117	HR_F6-29.2	5-28	3-E1508A-3
118	HR_F6-33.2	5-29	3-E1508A-3
119	HR_F6-35.2	5-30	3-E1508A-3
120	HR_F6-38.2	5-31	3-E1508A-3

SLOT 4			
CHAN	NAME	PANEL/ INPUT #	Slot, SCP & SCP #
503	Pnl7-Therm2S	7-0	4-E1508A-0
453	Qtz Win4-B	7-1	4-E1508A-0
454	Qtz Win5-A	7-2	4-E1508A-0
455	Qtz Win5-B	7-3	4-E1508A-0
456	Qtz Win6-A	7-4	4-E1508A-0
457	Qtz Win6-B	7-5	4-E1508A-0
440	Ex Pipe fl	7-6	4-E1508A-0
441	Ex Pipe wall	7-7	4-E1508A-0
145	HR_B6-4.2	7-8	4-E1508A-1
146	HR_B6-11.2	7-9	4-E1508A-1
147	HR_B6-16.2	7-10	4-E1508A-1
148	HR_B6-23.2	7-11	4-E1508A-1
149	HR_B6-29.2	7-12	4-E1508A-1
150	HR_B6-33.2	7-13	4-E1508A-1
151	HR_B6-35.2	7-14	4-E1508A-1
152	HR_B6-38.2	7-15	4-E1508A-1
153	HR_B5-41.2	7-16	4-E1508A-2
154	HR_B5-53.1	7-17	4-E1508A-2
155	HR_B5-55.1	7-18	4-E1508A-2
156	HR_B5-58	7-19	4-E1508A-2
157	HR_B5-63.9	7-20	4-E1508A-2
158	HR_B5-73.8	7-21	4-E1508A-2
159	HR_B5-75.7	7-22	4-E1508A-2
160	HR_B5-76.7	7-23	4-E1508A-2
161	HR_B4-88.5	7-24	4-E1508A-3
162	HR_B4-91.4	7-25	4-E1508A-3
163	HR_B4-93.4	7-26	4-E1508A-3
164	HR_B4-95.3	7-27	4-E1508A-3
165	HR_B4-100.2	7-28	4-E1508A-3
166	HR_B4-106.1	7-29	4-E1508A-3
167	HR_B4-111	7-30	4-E1508A-3
168	HR_B4-142.2	7-31	4-E1508A-3

Table 11-3. Instrumentation and Data Acquisition Channel List (Page 4 of 8)

SLOT 3			
CHAN	NAME	PANEL/ INPUT #	Slot, SCP & SCP #
502	Pnl6-Therm2S	6-32	3-E1508A-4
446	Qtz Win1-A	6-33	3-E1508A-4
447	Qtz Win1-B	6-34	3-E1508A-4
448	Qtz Win2-A	6-35	3-E1508A-4
449	Qtz Win2-B	6-36	3-E1508A-4
450	Qtz Win3-A	6-37	3-E1508A-4
451	Qtz Win3-B	6-38	3-E1508A-4
452	Qtz Win4-A	6-39	3-E1508A-4
121	HR_E6-50.1	6-40	3-E1508A-5
122	HR_E6-54.1	6-41	3-E1508A-5
123	HR_E6-57	6-42	3-E1508A-5
124	HR_E6-60	6-43	3-E1508A-5
125	HR_E6-65.9	6-44	3-E1508A-5
126	HR_E6-69.8	6-45	3-E1508A-5
127	HR_E6-72.8	6-46	3-E1508A-5
128	HR_E6-74.8	6-47	3-E1508A-5
129	HR_D6-103.2	6-48	3-E1508A-6
130	HR_D6-106.1	6-49	3-E1508A-6
131	HR_D6-112.9	6-50	3-E1508A-6
132	HR_D6-114.9	6-51	3-E1508A-6
133	HR_D6-116.8	6-52	3-E1508A-6
134	HR_D6-120.7	6-53	3-E1508A-6
135	HR_D6-124.6	6-54	3-E1508A-6
136	HR_D6-128.5	6-55	3-E1508A-6
137	HR_C6-41.2	6-56	3-E1508A-7
138	HR_C6-53.1	6-57	3-E1508A-7
139	HR_C6-55.1	6-58	3-E1508A-7
140	HR_C6-58	6-59	3-E1508A-7
141	HR_C6-63.9	6-60	3-E1508A-7
142	HR_C6-73.8	6-61	3-E1508A-7
143	HR_C6-75.7	6-62	3-E1508A-7
144	HR_C6-76.7	6-63	3-E1508A-7

SLOT 4			
CHAN	NAME	PANEL/ INPUT #	Slot, SCP & SCP #
504	Pnl8-Therm2S	8-32	4-E1508A-4
442	Ex Pipe wall	8-33	4-E1508A-4
443	Ex Pipe wall	8-34	4-E1508A-4
394	Pwr Sup W	8-35	4-E1508A-4
395	Pwr Sup V	8-36	4-E1508A-4
396	Pwr Sup Cur	8-37	4-E1508A-4
397	Test Sect V	8-38	4-E1508A-4
398	Test Sect Cur	8-39	4-E1508A-4
169	HR_B3-50.1	8-40	4-E1508A-5
170	HR_B3-54.1	8-41	4-E1508A-5
171	HR_B3-57	8-42	4-E1508A-5
172	HR_B3-60	8-43	4-E1508A-5
173	HR_B3-65.9	8-44	4-E1508A-5
174	HR_B3-69.8	8-45	4-E1508A-5
175	HR_B3-72.8	8-46	4-E1508A-5
176	HR_B3-74.8	8-47	4-E1508A-5
177	HR_C3-79.7	8-48	4-E1508A-6
178	HR_C3-85.5	8-49	4-E1508A-6
179	HR_C3-88.5	8-50	4-E1508A-6
180	HR_C3-92.4	8-51	4-E1508A-6
181	HR_C3-94.4	8-52	4-E1508A-6
182	HR_C3-97.3	8-53	4-E1508A-6
183	HR_C3-109	8-54	4-E1508A-6
184	HR_C3-111.4	8-55	4-E1508A-6
185	HR_D3-88.5	8-56	4-E1508A-7
186	HR_D3-91.4	8-57	4-E1508A-7
187	HR_D3-93.4	8-58	4-E1508A-7
188	HR_D3-95.3	8-59	4-E1508A-7
189	HR_D3-100.2	8-60	4-E1508A-7
190	HR_D3-106.1	8-61	4-E1508A-7
191	HR_D3-111	8-62	4-E1508A-7
192	HR_D3-142.2	8-63	4-E1508A-7

Table 11-3. Instrumentation and Data Acquisition Channel List (Page 5 of 8)

SLOT 5			
CHAN	NAME	PANEL/ INPUT #	Slot, SCP & SCP #
505	Pnl9-Therm2S	9-0	5-E1508A-0
393	UP Exit P	9-1	5-E1508A-0
406	Sup Tnk Pr	9-2	5-E1508A-0
411	Sup Ln Pr	9-3	5-E1508A-0
416	St Sup Pr	9-4	5-E1508A-0
439	Acc Pr	9-5	5-E1508A-0
444	Ex Pipe Pr	9-6	5-E1508A-0
412	Sup Ln FM	9-7	5-E1508A-0
193	HR_E3-63.9	9-8	5-E1508A-1
194	HR_E3-113.9	9-9	5-E1508A-1
195	HR_E3-115.8	9-10	5-E1508A-1
196	HR_E3-118.8	9-11	5-E1508A-1
197	HR_E3-122.7	9-12	5-E1508A-1
198	HR_E3-126.6	9-13	5-E1508A-1
199	HR_E3-131.5	9-14	5-E1508A-1
200	HR_E3-135.4	9-15	5-E1508A-1
201	HR_E4-88.5	9-16	5-E1508A-2
202	HR_E4-91.4	9-17	5-E1508A-2
203	HR_E4-93.4	9-18	5-E1508A-2
204	HR_E4-95.3	9-19	5-E1508A-2
205	HR_E4-100.2	9-20	5-E1508A-2
206	HR_E4-106.1	9-21	5-E1508A-2
207	HR_E4-111	9-22	5-E1508A-2
208	HR_E4-142.2	9-23	5-E1508A-2
209	HR_E5-63.9	9-24	5-E1508A-3
210	HR_E5-113.9	9-25	5-E1508A-3
211	HR_E5-115.8	9-26	5-E1508A-3
212	HR_E5-118.8	9-27	5-E1508A-3
213	HR_E5-122.7	9-28	5-E1508A-3
214	HR_E5-126.6	9-29	5-E1508A-3
215	HR_E5-131.5	9-30	5-E1508A-3
216	HR_E5-135.4	9-31	5-E1508A-3

SLOT 6			
CHAN	NAME	PANEL/ INPUT #	Slot, SCP & SCP #
507	Pnl11-Therm2S	11-0	6-E1508A-0
425	CT-UP DP	11-1	6-E1508A-0
433	St Sep-UP DP	11-2	6-E1508A-0
438	St Sup-Acc DP	11-3	6-E1508A-0
362	FH DP-(0-144)	11-4	6-E1508A-0
363	FH DP-(0-12)	11-5	6-E1508A-0
364	FH DP-(12-25)	11-6	6-E1508A-0
365	FH DP-(25-37)	11-7	6-E1508A-0
241	HR_D4-50.1	11-8	6-E1508A-1
242	HR_D4-54.1	11-9	6-E1508A-1
243	HR_D4-57	11-10	6-E1508A-1
244	HR_D4-60	11-11	6-E1508A-1
245	HR_D4-65.9	11-12	6-E1508A-1
246	HR_D4-69.8	11-13	6-E1508A-1
247	HR_D4-72.8	11-14	6-E1508A-1
248	HR_D4-74.8	11-15	6-E1508A-1
249	GRD2-fl-D-4/d2-b2	11-16	6-E1508A-2
250	GRD2-wall-D-4/a-2	11-17	6-E1508A-2
251	GRD3-fl-D-4/d2-b2	11-18	6-E1508A-2
252	GRD3-fl-D-2/d1-b2	11-19	6-E1508A-2
253	GRD3-fl-D-6/c3-b2	11-20	6-E1508A-2
254	GRD3-wall-E-3/c-1	11-21	6-E1508A-2
255	GRD3-wall-D-4/a-2	11-22	6-E1508A-2
256	GRD3-wall-C-5/d-3	11-23	6-E1508A-2
257	GRD4-fl-D-4/d2-b2	11-24	6-E1508A-3
258	GRD4-fl-D-2/d1-b2	11-25	6-E1508A-3
259	GRD4-fl-D-6/c3-b2	11-26	6-E1508A-3
260	GRD4-wall-E-3/c-1	11-27	6-E1508A-3
261	GRD4-wall-D-4/a-2	11-28	6-E1508A-3
262	GRD4-wall-C-5/d-3	11-29	6-E1508A-3
263	GRD5-fl-D-4/d2-b2	11-30	6-E1508A-3
264	GRD5-fl-D-2/d1-b2	11-31	6-E1508A-3

Table 11-3. Instrumentation and Data Acquisition Channel List (Page 6 of 8)

SLOT 5			
CHAN	NAME	PANEL/ INPUT #	Slot, SCP & SCP #
506	Pnl10-Therm2S	10-32	5-E1508A-4
413	Drop Inj FM	10-33	5-E1508A-4
417	St Sup FM	10-34	5-E1508A-4
445	Ex Pipe FM	10-35	5-E1508A-4
405	Sup Tnk Lvl	10-36	5-E1508A-4
426	Lg CT Lvl	10-37	5-E1508A-4
427	Sm CT Lvl	10-38	5-E1508A-4
434	St Sep Lvl	10-39	5-E1508A-4
217	HR_D5-88.5	10-40	5-E1508A-5
218	HR_D5-91.4	10-41	5-E1508A-5
219	HR_D5-93.4	10-42	5-E1508A-5
220	HR_D5-95.3	10-43	5-E1508A-5
221	HR_D5-100.2	10-44	5-E1508A-5
222	HR_D5-106.1	10-45	5-E1508A-5
223	HR_D5-111	10-46	5-E1508A-5
224	HR_D5-142.2	10-47	5-E1508A-5
225	HR_C5-63.9	10-48	5-E1508A-6
226	HR_C5-113.9	10-49	5-E1508A-6
227	HR_C5-115.8	10-50	5-E1508A-6
228	HR_C5-118.8	10-51	5-E1508A-6
229	HR_C5-122.7	10-52	5-E1508A-6
230	HR_C5-126.6	10-53	5-E1508A-6
231	HR_C5-131.5	10-54	5-E1508A-6
232	HR_C5-135.4	10-55	5-E1508A-6
233	HR_C4-88.5	10-56	5-E1508A-7
234	HR_C4-91.4	10-57	5-E1508A-7
235	HR_C4-93.4	10-58	5-E1508A-7
236	HR_C4-95.3	10-59	5-E1508A-7
237	HR_C4-100.2	10-60	5-E1508A-7
238	HR_C4-106.1	10-61	5-E1508A-7
239	HR_C4-111	10-62	5-E1508A-7
240	HR_C4-142.2	10-63	5-E1508A-7

SLOT 6			
CHAN	NAME	PANEL/ INPUT #	Slot, SCP & SCP #
508	Pnl12-Therm2S	12-32	6-E1508A-4
265	GRD5-II-D-6/c3-b2	12-33	6-E1508A-4
266	GRD5-wall-E-3/c-1	12-34	6-E1508A-4
267	GRD5-wall-D-4/a-2	12-35	6-E1508A-4
268	GRD5-wall-C-5/d-3	12-36	6-E1508A-4
269	GRD6-II-D-4/d2-b2	12-37	6-E1508A-4
270	GRD6-II-B-4/c2-a1	12-38	6-E1508A-4
271	GRD6-II-F-4/c2-b3	12-39	6-E1508A-4
272	GRD6-wall-E-3/c-1	12-40	6-E1508A-5
273	GRD6-wall-D-4/a-2	12-41	6-E1508A-5
274	GRD6-wall-G-4/b-3	12-42	6-E1508A-5
275	GRD6-wall-C-5/d-3	12-43	6-E1508A-5
276	GRD7-II-D-4/d2-b2	12-44	6-E1508A-5
277	GRD7-II-D-2/d1-b2	12-45	6-E1508A-5
278	GRD7-II-D-6/c3-b2	12-46	6-E1508A-5
279	GRD7-wall-D-4/a-2	12-47	6-E1508A-5
280	SPR1-37.2	12-48	6-E1508A-6
281	SPR1-59.1	12-49	6-E1508A-6
282	SPR1-76.8	12-50	6-E1508A-6
283	SPR1-90.7	12-51	6-E1508A-6
284	SPR1-96.6	12-52	6-E1508A-6
285	SPR1-102.5	12-53	6-E1508A-6
286	SPR1-114.4	12-54	6-E1508A-6
287	SPR1-138.2	12-55	6-E1508A-6
288	SPR13-37.2	12-56	6-E1508A-7
289	SPR13-59.1	12-57	6-E1508A-7
290	SPR13-76.8	12-58	6-E1508A-7
291	SPR13-90.7	12-59	6-E1508A-7
292	SPR13-96.6	12-60	6-E1508A-7
293	SPR13-102.5	12-61	6-E1508A-7
294	SPR13-114.4	12-62	6-E1508A-7
295	SPR13-138.2	12-63	6-E1508A-7

Table 11-3. Instrumentation and Data Acquisition Channel List (Page 7 of 8)

SLOT 7			
CHAN	NAME	PANEL/ INPUT #	Slot, SCP & SCP #
509	Pnl13-Therm2S	13-0	7-E1508A-0
296	ST. PR-R1-16.2-A	13-1	7-E1508A-0
297	ST. PR-R1-16.2-B	13-2	7-E1508A-0
298	ST. PR-R1-16.2-C	13-3	7-E1508A-0
299	ST. PR-R2-37-A	13-4	7-E1508A-0
300	ST. PR-R2-37-B	13-5	7-E1508A-0
301	ST. PR-R2-37-C	13-6	7-E1508A-0
302	ST. PR-R3-55-A	13-7	7-E1508A-0
303	ST. PR-R3-55-B	13-8	7-E1508A-1
304	ST. PR-R3-55-C	13-9	7-E1508A-1
305	ST. PR-R4-60-A	13-10	7-E1508A-1
306	ST. PR-R4-60-B	13-11	7-E1508A-1
307	ST. PR-R4-60-C	13-12	7-E1508A-1
308	ST. PR-R5-73.81-A	13-13	7-E1508A-1
309	ST. PR-R5-73.81-B	13-14	7-E1508A-1
310	ST. PR-R5-73.81-C	13-15	7-E1508A-1
311	ST. PR-R6-76-A	13-16	7-E1508A-2
312	ST. PR-R6-76-B	13-17	7-E1508A-2
313	ST. PR-R6-76-C	13-18	7-E1508A-2
314	ST. PR-R7-79.7-A	13-19	7-E1508A-2
315	ST. PR-R7-79.7-B	13-20	7-E1508A-2
316	ST. PR-R7-79.7-C	13-21	7-E1508A-2
317	ST. PR-R8-93.53-A	13-22	7-E1508A-2
318	ST. PR-R8-93.53-B	13-23	7-E1508A-2
319	ST. PR-R8-93.53-C	13-24	7-E1508A-3
320	ST. PR-R9-96-A	13-25	7-E1508A-3
321	ST. PR-R9-96-B	13-26	7-E1508A-3
322	ST. PR-R9-96-C	13-27	7-E1508A-3
323	ST. PR-R10-100-A	13-28	7-E1508A-3
324	ST. PR-R10-100-B	13-29	7-E1508A-3
325	ST. PR-R10-100-C	13-30	7-E1508A-3
326	ST. PR-R11-115.39-A	13-31	7-E1508A-3

SLOT 8			
CHAN	NAME	PANEL/ INPUT #	Slot, SCP & SCP #
511	Pnl15-Therm2S	15-0	8-E1508A-0
358	FH24-wall-129.25	15-1	8-E1508A-0
359	FH25-wall-135.18	15-2	8-E1508A-0
360	RB-IF1-fl-(-1)-A	15-3	8-E1508A-0
361	RB-IF2-fl-(-1)-B	15-4	8-E1508A-0
366	FH DP-(37-43)	15-5	8-E1508A-0
367	FH DP-(43-46)	15-6	8-E1508A-0
368	FH DP-(46-53)	15-7	8-E1508A-0
369	FH DP-(53-57)	15-8	8-E1508A-1
370	FH DP-(57-60)	15-9	8-E1508A-1
371	FH DP-(60-63)	15-10	8-E1508A-1
372	FH DP-(63-67)	15-11	8-E1508A-1
373	FH DP-(67-72)	15-12	8-E1508A-1
374	FH DP-(72-75)	15-13	8-E1508A-1
375	FH DP-(75-78)	15-14	8-E1508A-1
376	FH DP-(78-81)	15-15	8-E1508A-1
377	FH DP-(81-85)	15-16	8-E1508A-2
378	FH DP-(85-93)	15-17	8-E1508A-2
379	FH DP-(93-97)	15-18	8-E1508A-2
380	FH DP-(97-100)	15-19	8-E1508A-2
381	FH DP-(100-108)	15-20	8-E1508A-2
382	FH DP-(108-120)	15-21	8-E1508A-2
383	FH DP-(120-133)	15-22	8-E1508A-2
384	FH DP-(133-144)	15-23	8-E1508A-2
458	Rem Close	15-24	8-E1535A-3
459	Rem Start/Stop	15-25	8-E1535A-3
460	Rem Reset	15-26	8-E1535A-3
461	RELAY 3 - NO	15-27	8-E1535A-3
462	I/O Disc	15-28	8-E1535A-3
463	Pull-Up+I/O Disc	15-29	8-E1535A-3
464	Not Available	15-30	8-E1535A-3
465	Not Available	15-31	8-E1535A-3

Table 11-3. Instrumentation and Data Acquisition Channel List (Page 8 of 8)

SLOT 7			
CHAN	NAME	PANEL/ INPUT #	Slot, SCP & SCP #
510	Pnl14-Therm2S	14-32	7-E1508A-4
327	ST. PR-R11-115.39-B	14-33	7-E1508A-4
328	ST. PR-R11-115.39-C	14-34	7-E1508A-4
329	ST. PR-R12-120-A	14-35	7-E1508A-4
330	ST. PR-R12-120-B	14-36	7-E1508A-4
331	ST. PR-R12-120-C	14-37	7-E1508A-4
332	ST. PR-R13-136-A	14-38	7-E1508A-4
333	ST. PR-R13-136-B	14-39	7-E1508A-4
334	ST. PR-R13-136-C	14-40	7-E1508A-5
335	FH1-wall-10.1	14-41	7-E1508A-5
336	FH2-wall-22	14-42	7-E1508A-5
337	FH3-wall-37	14-43	7-E1508A-5
338	FH4-wall-42.95	14-44	7-E1508A-5
339	FH5-wall-46.93	14-45	7-E1508A-5
340	FH6-wall-52.9	14-46	7-E1508A-5
341	FH7-wall-55.87	14-47	7-E1508A-5
342	FH8-wall-61.85	14-48	7-E1508A-6
343	FH9-wall-67.83	14-49	7-E1508A-6
344	FH10-wall-70.82	14-50	7-E1508A-6
345	FH11-wall-73.81	14-51	7-E1508A-6
346	FH12-wall-78.78	14-52	7-E1508A-6
347	FH13-wall-84.7	14-53	7-E1508A-6
348	FH14-wall-87.65	14-54	7-E1508A-6
349	FH15-wall-90.55	14-55	7-E1508A-6
350	FH16-wall-93.53	14-56	7-E1508A-7
351	FH17-wall-96.5	14-57	7-E1508A-7
352	FH18-wall-102.48	14-58	7-E1508A-7
353	FH19-wall-108.43	14-59	7-E1508A-7
354	FH20-wall-110.43	14-60	7-E1508A-7
355	FH21-wall-111.42	14-61	7-E1508A-7
356	FH22-wall-116.38	14-62	7-E1508A-7
357	FH23-wall-120.3	14-63	7-E1508A-7

SLOT 8			
CHAN	NAME	PANEL/ INPUT #	Slot, SCP & SCP #
512	Pnl16-Therm2S	16-32	8-E1508A-4
482	Spare1	16-33	8-E1508A-4
483	Spare2	16-34	8-E1508A-4
484	Spare3	16-35	8-E1508A-4
485	Spare4	16-36	8-E1508A-4
486	Spare5	16-37	8-E1508A-4
487	Spare6	16-38	8-E1508A-4
488	Spare7	16-39	8-E1508A-4
489	Spare8	16-40	8-E1508A-5
490	Spare9	16-41	8-E1508A-5
491	Spare10	16-42	8-E1508A-5
492	Spare11	16-43	8-E1508A-5
493	Spare12	16-44	8-E1508A-5
494	Spare13	16-45	8-E1508A-5
495	Spare14	16-46	8-E1508A-5
496	Spare15	16-47	8-E1508A-5
466	PS-PWR OUTA	16-48	8-E1532A-6
467	PS-PWR OUTB	16-49	8-E1532A-6
468	IF RATEA	16-50	8-E1532A-6
469	IF RATEB	16-51	8-E1532A-6
470	CNTL3A	16-52	8-E1532A-6
471	CNTL3B	16-53	8-E1532A-6
472	CNTL4A	16-54	8-E1532A-6
473	CNTL4B	16-55	8-E1532A-6
474	CNTL5A	16-56	8-E1532A-7
475	CNTL5B	16-57	8-E1532A-7
476	CNTL6A	16-58	8-E1532A-7
477	CNTL6B	16-59	8-E1532A-7
478	CNTL7A	16-60	8-E1532A-7
479	CNTL7B	16-61	8-E1532A-7
480	CNTL8A	16-62	8-E1532A-7
481	CNTL8B	16-63	8-E1532A-7

12. CONCLUSIONS

The initial phase of the RBHT program, which aims at designing a flexible, well-instrumented rod bundle test facility for conducting reflood experiments to aid in the development of dispersed flow film boiling models for the NRC's thermal-hydraulics code, was completed and documented in this report. Based upon the results obtained in the initial phase, i.e., Task 1 through 10, the following are concluded:

1. The thermal-hydraulics heat transfer phenomena that dominates the reflood transient is dispersed flow film boiling, which is the limiting (lowest heat transfer from fuel to fluid) heat transfer situation for the LOCA transient. The RBHT program will emphasize this phase in providing specific experimental data and associated analysis to improve the understanding of the dispersed flow film boiling region.
2. The heat transfer rates in the dispersed flow film-boiling region are very low, and several competing mechanisms are responsible for the total wall heat flux. No single mechanism dominates the heat transfer process such that all the competing mechanisms must be modeled with roughly equal precision. Separate-effect data at the subcomponent levels isolating the particular contribution of each competing mechanism to the total wall heat flux will be simulated in the RBHT facility.
3. The single largest uncertainty in predicting the dispersed film boiling heat transfer is the liquid entrainment from the froth region just above the quench front. In this region, the steam generation from the rod quenching results in very large vapor velocities which entrain and shear liquid ligaments into droplets. The entrained droplets provide cooling by several different mechanisms in the upper elevations of the rod bundle where the resulting peak clad temperatures occur. To address the liquid entrainment and resulting droplet flow, specific tests are planned which will isolate the droplet behavior. Also, state-of-the art instrumentation will be used to obtain drop size and velocities as well as the local void fraction.
4. The RBHT test facility is designed permit to permit separate-effect component experiments isolating each highly ranked reflood phenomenon as best as possible so as to permit model development for particular phenomenon and to minimize the risk of introducing compensating error into the advanced reflood model package.
5. The proposed experiments to be performed in the RBHT facility will provide new data on reflood heat transfer as well as supplementing existing data for model development and code validation. They will also focus on the improvements of specific best-estimate thermal-hydraulics models of importance to the highly ranked phenomena rather than identifying licensing margin.
6. Results of the two-tier scaling analysis indicate that if prototypical fluid conditions are used in the tests and the bundle geometry is retained by using the prototypical spacer grids, there is very strong similarity between the RBHT test bundle and the PWR and BWR fuel

assemblies. The data to be obtained in the RBHT facility should be applicable to either reactor fuel assembly type.

7. The effects of the gap conductance and the rod materials differences between electrical and nuclear fuel rods are small with the possible exception of the minimum film boiling temperature. Other literature or bench type tests can determine the appropriate value for fuel rod cladding. The presence of a test housing in the proposed RBHT facility, can lead to some distortion in the tests and it should be accounted for in the test analysis.
8. One important objective of the program is to obtain new information on the mechanism of liquid entrainment at the quench front as the resulting droplet field downstream is responsible for the improved cooling at the upper elevations in the rod bundle where the clad temperature peaks. The instrumentation requirements will include detailed measurements of the local void fraction, droplet size, droplet velocity, and droplet number density in the droplet field.
9. To determine the local heat transfer, a reliable measurement of the non-equilibrium vapor temperature is needed. This has been included in the instrumentation requirements. Instrumentation will also be placed upstream and downstream of the spacer grids to see their effects. Additional instrumentation requirements have been identified using the PIRTs as a guide for the important phenomena for the different test types which the experiments must capture for the code development and validation.
10. The instrumentation plan developed in the program, which involves the use of ample instrumentation proven to perform in previous rod bundle experiments as well as state-of-the-art instrumentation specifically developed for dispersed two-phase flow measurements, represents a robust diagnostic plan that allows all the highly ranked phenomena to be either directly measured or calculated directly from the experimental data.
11. The RBHT test facility meets all the instrumentation requirements developed in Task 7 and can be used to conduct all of the planned experiments according to the test matrix developed in Task 9. It represents a unique NRC facility that can be used to provide new data at the subcomponent levels for the fundamental assessment of the physical behavior upon which the code constitutive heat transfer and flow models are based.
12. In addition to obtaining separate-effect reflood data, the RBHT facility is designed to perform mechanistic studies of the highly ranked phenomena to develop new or improved models for implementation in the NRC merged code. Thus, it will aid in the refinement of the NRC's thermal-hydraulics code and will help maintain the NRC's leadership in the reactor thermal-hydraulics safety analysis area.

Appendix A Literature Review

Appendix A1: FLECHT Low Flooding Rate Cosine Test Series

Dates When Tests Were Performed: 1974 - 1975

References:

- R1 Rosal, E. R. et al, "FLECHT Low Flooding Rate Cosine Test Series Data Report", WCAP-8651, Dec 1975.
- R2 Lilly, G.P., Yeh, H. C., Hochreiter, L. E., and N. Yamaguchi, "PWR FLECHT Cosine Low Flooding rate Test Series Evaluation Report", WCAP-8838, March 1977

Availability of Data:

Plots of selected data exist in the data report in R1. The raw data and reduced and analyzed data exists at Westinghouse on CDC 6600 and 7600 Magnetic tapes. This data has been in storage at the Westinghouse facilities. Microfiche of the raw data and analyzed data exist at the Westinghouse Engineering offices in Monroeville, PA. It is not clear if any of this data was put on the INEL data bank.

Test Facility Description, Types of Tests

The FLECHT Low Flooding Rate Cosine Test Series was a continuation of the FLECHT reflood heat transfer program started in the late 1960's and focused on low forced flooding rates tests at low pressures to provide a broader data range for the Appendix K licensing basis during the reflood period. The overall objective of the test program was to obtain data that would be useful for calculating the reflood behavior of PWRs following a postulated Loss Of Coolant Accident.

The tests were performed using a 10 by 10 rod bundle with 91 active electrical heater rods and 9 guide tube thimbles in which instrumentation was placed. The rod bundle was placed inside a thick walled (0.75-inch) square housing which was heated externally for the tests. There was excess flow area around the bundle such that the housing had to be heated to preserve the correct power-to-flow area of a PWR fuel assembly. The heater rods were 0.422-inches in diameter and were arranged on a square pitch of 0.563-inches and had a heated length of 12-feet. The electrical heater rods used a 1.66 cosine power distribution which was approximated by different pitch

heating coils. The facility layout is shown in Figure A-1.1 and the bundle geometry is given in Figure A-1.2 from R2. A radial power distribution was used in these experiments to simulate or bound the rod-to-rod power distribution in a PWR fuel assembly. One feature which was unique in this test series is that there were a large number of variable inlet flooding rates tests performed to better simulate the gravity reflood behavior of the PWR. There were also low initial clad temperature test performed to simulate lower power regions in the core that could have quenched during blowdown or during Upper Head Injection which was a newer high-pressure accumulator installed on PWRs which had Ice Condenser Containment.

The range of conditions include:

Constant Flooding Rates:	0.4 - 1.5 in/sec
Upper Plenum Pressure:	25 - 60 psia
Initial Clad Temperature (At peak location)	300 °F - 1600 °F
Initial Peak Power (At Peak Location)	0.51 - 0.95 kw/ft
Inlet Subcooling	20 °F - 180 °F
Variable Inlet Flooding Rate	Ranged from 12 - inches/sec for 5 seconds and 0.8 inches/sec onward, to 2 - inches/sec for 20 seconds and 1 - inch/sec onward.
Continuously Variable Flooding	There were two tests which simulated the average variable flooding rate from the FLECHT-SEASET Phase B systems tests.
Housing Temperature Tests	Housing initial temperature varied from 284 °F to 700 °F
FLECHT Repeat Tests	There were 6 repeat tests of previously performed FLECHT reflood tests.
Bundle and Housing Stored Energy Tests	Three different housing temperatures were used
Supplemental Entrainment	These were entrainment tests with several disconnected heater rods and failed rods over a range of flooding rates and pressures to provide additional data.

Instrumentation and Data From Tests

The heater rods were instrumentated with several thermocouples to measure the inside cladding surface temperature. The heat flux from the cladding surface was calculated from the thermocouple response using an inverse conduction computer program called DATAR. This program should still exist at Westinghouse and has been replaced by an improved version called DATARH. The thimbles shown in Figure A-2.2 were unheated tubes which receive radiant heat from the heater rods. The temperatures of the thimbles were measured using thermocouples welded to the inside of the tubes. Housing temperatures were measured along the length of the housing to characterize its heat release as the bundle quenched. The inlet flow and water temperature were measured as well as the pressure in the exit or upper plenum. There was separators and collection tanks at the exit of the test section such that the existing steam and water flows could be separated and individually measured. There were also sensitive Delta P cells every 2-feet along the housing to measure the bundle mass storage. The spacing is too sparse to obtain an accurate indication of local void fraction, however, the cells will indicate the mass stored in the bundle.

One of the more important pieces of data is the steam probe measurements at the 7, 10, and 12.5-foot elevations. These were shielded aspirating thermocouples which could measure the vapor superheat until the quench front would approach and fill the probe with water. The steam probes indicated the high degree of superheat in the dispersed two-phase flow above the quench front.

This FLECHT Test Series was the first to perform a mass and energy balance down the test section to determine the local quality conditions and the split of the heat transfer between radiation to drops, vapor and housing, and steam convection with entrained droplets. There are calculated values of the real quality for 7 tests which span the matrix at different times in the transient. The analysis indicated, for the first time, that the convection is enhanced when droplets are entrained. The analysis also indicated the importance of the radiation heat transfer. The Appendix A in Reference 1 gives the details of the calculational method.

Conclusions

The FLECHT Low Flooding Rate Cosine tests do have some data which would be of interest for improved reflood modeling. In addition to the heater rod temperatures, the measurement of the vapor temperature at the 7, 10, and 12.5 foot elevations are of value since these data indicate the degree of non-equilibrium within the flow. The pressure drop measurements are too coarse to be used as an indicator of the void fraction within the bundle. However, these measurements can be used to indicate the mass rate of accumulation within the bundle such that a complete mass balance can be calculated from the data for the tests.

The conditions which were simulated are also useful from a code analysis and validation effort since a large range of conditions were simulated, in particular a variable inlet flooding rate and a continuously variable inlet flooding rate which simulates gravity reflooding. These experiments would be useful to assess the code performance.

This is not sufficient data to make code model changes without the potential for compensating error. More detailed data is needed which identify code calculated parameters such as vapor superheat, convective enhancement, radiation to drops, rods, vapor and housing, droplet size and velocities along the bundle, and the void distribution in the froth region. These types of measurements are missing such that the code can only be compared to the cladding temperatures, quench front, and the overall mass balance.

Therefore while these tests are useful in determining the overall reflood heat transfer, they provide very limited data which can be used to assess the reflood phenomena which was identified in the PIRT. Therefore, limited effort should be spent modeling these tests.

A-5

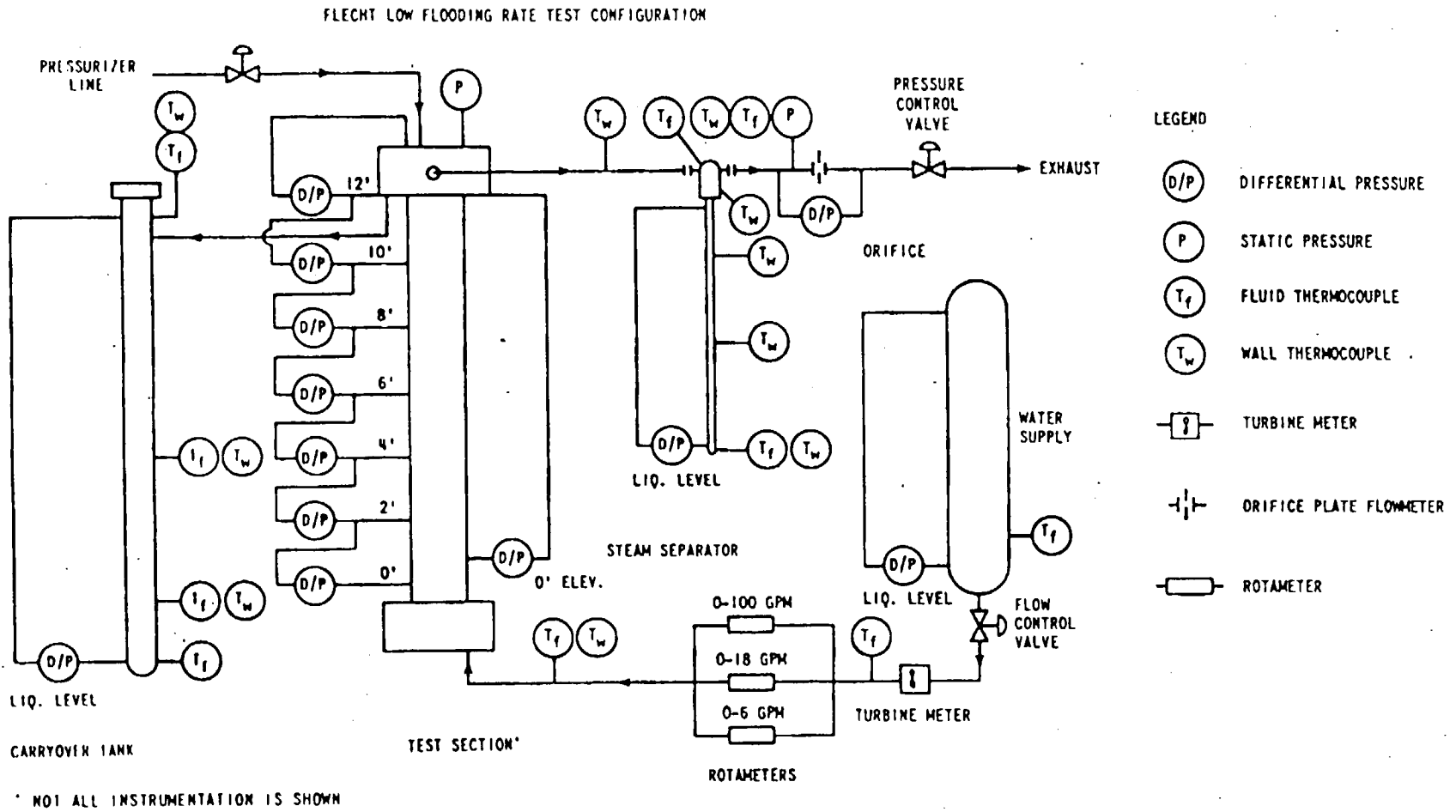
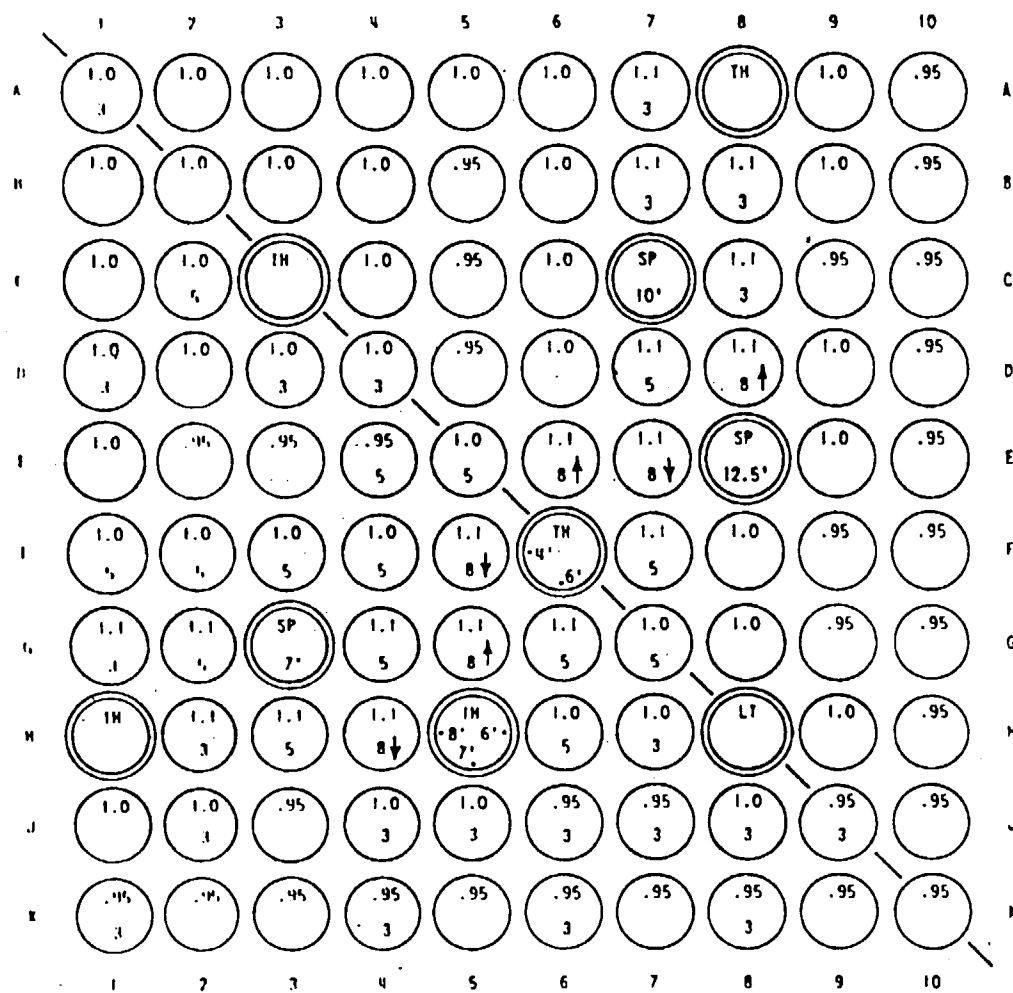


Figure A1-1. FLECHT Low-Flooding Rate Test Configuration

A-6



LEGEND:

- 1.1, 1.0, .95 RADIAL POWER DISTRIBUTION
- TH THIMBLE TUBE
- SP STEAM PROBE
- LT ANC LEVEL TRANSDUCER (0' - 6' ELEVATIONS)
- 8 ↓ INSTRUMENTED ROD WITH 8 T/C'S AT 0', 1/2', 1', 1-1/2', 2', 3', 4' & 6' ELEV.
- 8 ↑ INSTRUMENTED ROD WITH 8 T/C'S AT 6', 6-1/2', 7', 8', 9', 10', 11' & 12' ELEV.
- 5 INSTRUMENTED ROD WITH 5 T/C'S AT 2', 4', 6', 8' & 10' ELEV.
- 3 INSTRUMENTED ROD WITH 3 T/C'S AT 4', 6' & 10' ELEV.
- TH • INSTRUMENTED THIMBLE WITH WALL T/C'S

Figure A1-2. Rod Bundle Instrumentation for FLECHT Low-Flooding Rate Tests

Appendix A Literature Review

Appendix A2: FLECHT Low Flooding Rate Skewed Test Series

Dates When Tests Were Performed: 1976-1977

References:

- R3. Rosal, E. R. et al, "FLECHT Low Flooding Rate Skewed Test Series Data Report," WCAP-9108, May 1977.
- R4. Lilly, G. P., Yeh, H. C., Dodge, C. E., and S. Wong, "PWR FLECHT Skewed Profile Low Flooding Rate Test Series Evaluation Report," WCAP-9183, Nov. 1997.

Availability of Data:

Plots and tables of selected data are given in R3 for the different tests. Some of the basic quantities which were measured and calculated from the bundle mass and energy balance are also given in R4 such as the local non-equilibrium quality, portion of the rod energy which is due to radiation and convective film boiling, and energy absorbed by the drops above the quench front. Two skewed power tests and one low flooding rate cosine test were analyzed in detail, which can be used for computer code comparison purposes. A heat transfer correlation was also developed which was a function of the distance above the quench front and is given in Reference 2. The skewed profile data was also compared to the cosine power shape data for the same test conditions.

The raw test data and the analyzed test data are available at Westinghouse on CDC 7600 magnetic tapes. Some selected tests have been brought forward to the new UNIX system at Westinghouse. Microfiche exist for the measured data as well as the analyzed test data at Westinghouse Engineering Offices in Monroeville, PA. It is believed that some of the transient temperature data were placed in the NRC data bank at INEL.

Test Facility Description, Types of Tests

The FLECHT Low Flooding Rate Skewed Tests were a continuation of the FLECHT Low Flooding Rate Cosine Tests which were performed in the 1975 time frame. The rod diameter used was 0.422-inches on a square pitch of 0.563-inches. These tests were intended to provide data for supporting the Appendix K reflood heat transfer models for different possible axial

power shapes for analysis of the Loss Of Coolant Accident.

There were two unique differences in the skewed tests as compared to the earlier cosine tests. The axial power shape was skewed to the top of the bundle with a peak of 1.35 at 10 feet, and a low mass circular housing was used for the first time in the FLECHT program.

The test facility is shown in Figure A-2.1 and is similar to that for the low flooding rate cosine tests. The power shape is shown in Figure A-2.2 and the bundle cross section is given in Figure A-2.3. The bundle contained 105 electrical heater rods, six guide tube thimbles, eight metal filler rods and the ANC liquid level probe. The use of the filler rods permitted the square pitch rod array to fit into the circular housing with a minimum of excess flow area. There was additional instrumentation added to the skewed test facility as compared to the low flooding rate cosine tests. There was more extensive thermocouple instrumentation within the bundle, there were delta P cells every foot instead of every two-feet, close coupled tanks were attached to the upper plenum to collect and separate the liquid entrainment, and a more reliable exit flow measurement was used to measure the exiting steam flow from the bundle.

There was a radial power profile which was similar to the low flooding rate cosine bundle as seen in Figure 3. There were instrumentated control rod guide tubes and aspirating steam probes in the rod bundle. The steam probes were at 7-feet, 10-feet, and 11-feet. Selected guide tube thimbles were also instrumentated with wall thermocouples.

The range of conditions which were investigated were similar to the low flooding rate cosine tests and included:

Constant Flooding Rate	0.7 - 6.0 in/sec
Upper Plenum Pressure	20 - 60 psia
Initial Clad Temperature At peak location	• 507 - 1600°F
Initial Peak Power At Peak Power Location	0.45 - 1.0 kw/ft
Inlet Subcooling	8 - 100°F
Variable Inlet Flooding Rate	ranged from 6 in/sec for 5 seconds to 0.8 in/sec, to 1.5 in/sec for 100 seconds to 0.5 in/sec onward.
Cosine Overlap Tests	Tests were performed to overlap Cosine and Skewed test conditions
Hot and Cold Channel Tests	Tests were performed with portions of the bundle hot and the remainder cold

Transient Pressure and Subcooling Tests were performed in which the inlet flow, system pressure, and the inlet subcooling varied with time.

There were also repeat tests which were performed to insure that the bundle geometry was not distorted. There were a total of 75 powered experiments. Very early on in the program, two heater rods failed at the beginning of testing. Later, as the number of thermal cycles increased in the test bundle, additional heater rods failed.

Instrumentation and Data From Tests

The electrical heater rods were instrumentated with several thermocouples at the different elevation which gave good coverage for the length of the bundle. However, there were no thermocouples placed around the spacer grids which would indicate a spacer grid effect on the two-phase flow. The liquid carried out of the test section was measured as well as the exiting steam vapor. The mass storage within the test section was also measured using delta P cells at one-foot intervals along the length of the housing. From these measurements, a transient mass balance could be performed on the test to help validate the data. Typically the mass balances were within five percent.

There were three aspirating steam probes at the 7, 10, and 11-foot elevations, as well as the exit pipe of the test section, to verify that the steam flow measurement was single phase. Using the flow measurements at the bundle exit, the actual steam non-equilibrium temperature, and the integrated wall heat flux between the steam probe locations; an energy balance can be performed to obtain the local quality and therefore the local steam and liquid flow. The change in the calculated quality indicates how much of the rod bundle surface heat flux goes into evaporating the entrained liquid droplets. The calculation was carried to the quench front where the vapor temperature was assumed to be the average of the rod temperature and the saturation temperature.

A simple radiation network was developed to separate the radiation heat transfer component from the total measured wall heat flux on the heater rods. Knowing the total wall heat flux, and subtracting the radiation heat flux, the convective wall heat flux can be determined. In the dispersed flow film boiling, this is the heat flux to the superheated vapor which contains entrained liquid droplets. The Nusselt number for the convective flux was calculated and compared to the Nusselt number that typical single-phase correlations would predict. It was observed that the convective Nusselt number calculated from the test data lied significantly above the limits calculated with conventional single phase convective correlations. Also, since the flow was superheated steam at low pressure, the calculated vapor Reynolds number was quite small, from 1500 to 10,000. These data and that of the low flooding rate cosine tests indicated that the presence of entrained liquid droplets could enhance the convective nature of the single phase vapor significantly at low vapor Reynolds numbers.

Conclusion

The FLECHT Low Flooding Rate Skewed Power Tests do have data which would be of interest for improved computer code modeling for the reflood heat transfer process. In particular, the different axial power shape used in these tests is very useful for assessing computer codes which may have been “tuned” to a cosine power shape. The pressure drop measurements are improved in the skewed bundle tests such that a more local void fraction (one-foot increments), can be determined and used to assess the local heat transfer. The void fractions and overall pressure drop are also used in the test bundle mass balances along with the inlet flows and exit flows. Typically the mass balances were within five percent.

There were a large number of experiments which were performed over a wide range of conditions, some of which specifically over-lapped with the low flooding rate cosine tests. These over-lap experiments are particularly useful for code validation purposes, since the accuracy of the computer code predictions for different axial power shapes can be assessed. A Best-Estimate computer code must be able to calculate a range of different axial power shapes to determine the most limiting shape.

While the data from the skewed series of experiments as well as the data analysis of these tests was improved over the low flooding rate cosine tests; there was still the lack of sufficient vapor temperature distribution and information in the test bundle such that the axial distribution of the local qualities could be more accurately determined. The data was analyzed to determine the heat flux split between radiation heat transfer and convective-dispersed flow film boiling heat transfer using a simplified radiation network approach. When the resulting convective-film boiling heat transfer (from the data) was compared to calculated single phase heat transfer correlation at the same vapor Reynolds number, the calculated data convective-film boiling transfer was significantly higher. Since the single phase correlation used the measured vapor temperature and the calculated vapor flow rate from the quality and energy balance, it is believed that the improved heat transfer is due to the presence of the entrained droplets which can add to the turbulence level in the flow at the low vapor Reynolds numbers. This phenomena of enhanced convective-dispersed flow film boiling was identified in this report as well as in the low flooding rate report.

Therefore, the Low Flooding Rate Skewed Power reflood tests are useful in determining the overall heat transfer processes and some of individual models and phenomena which compromise the reflood heat transfer process.

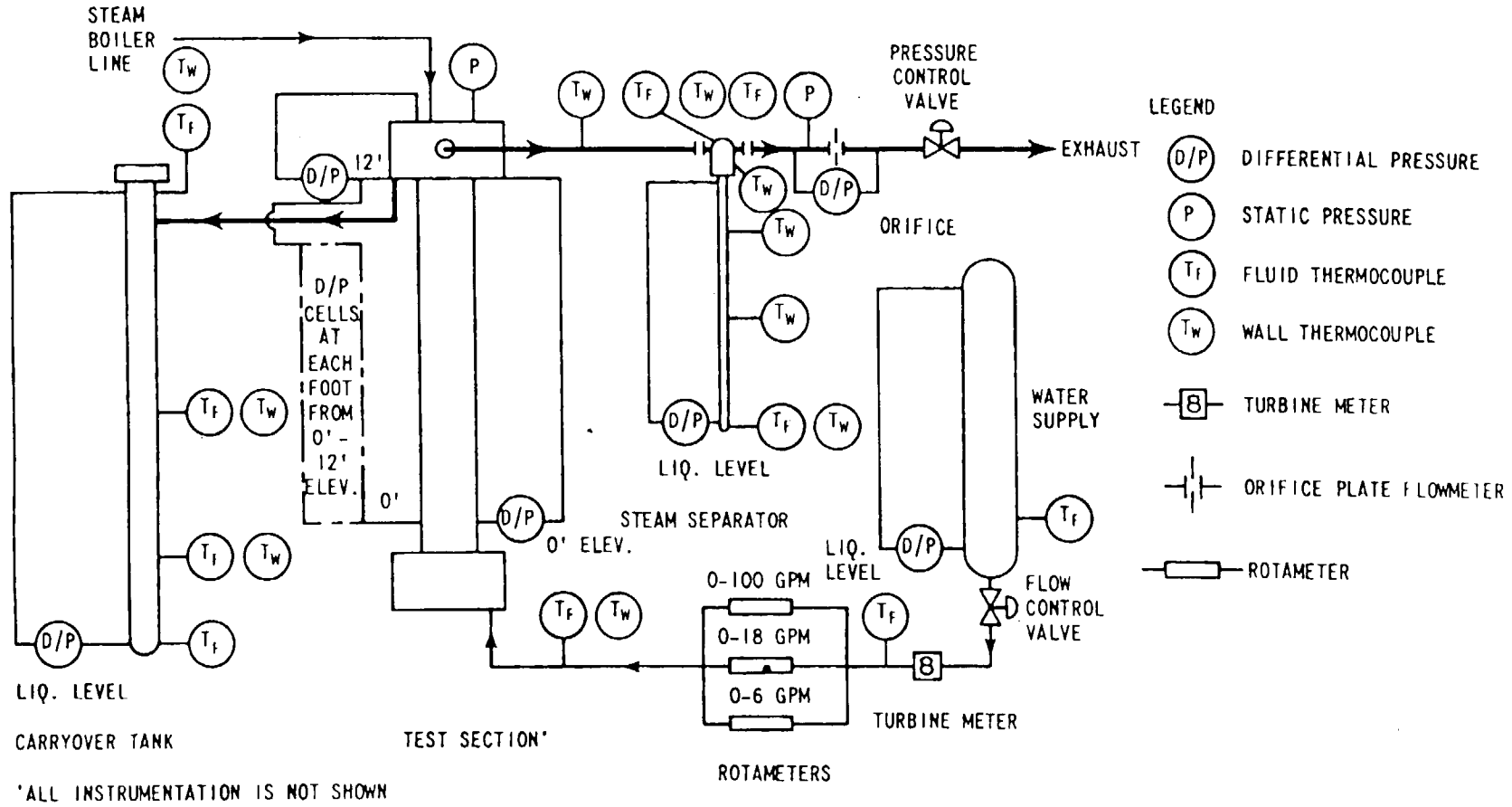


Figure A2-1. FLECHT Low Flooding Rate Test Facility Schematic

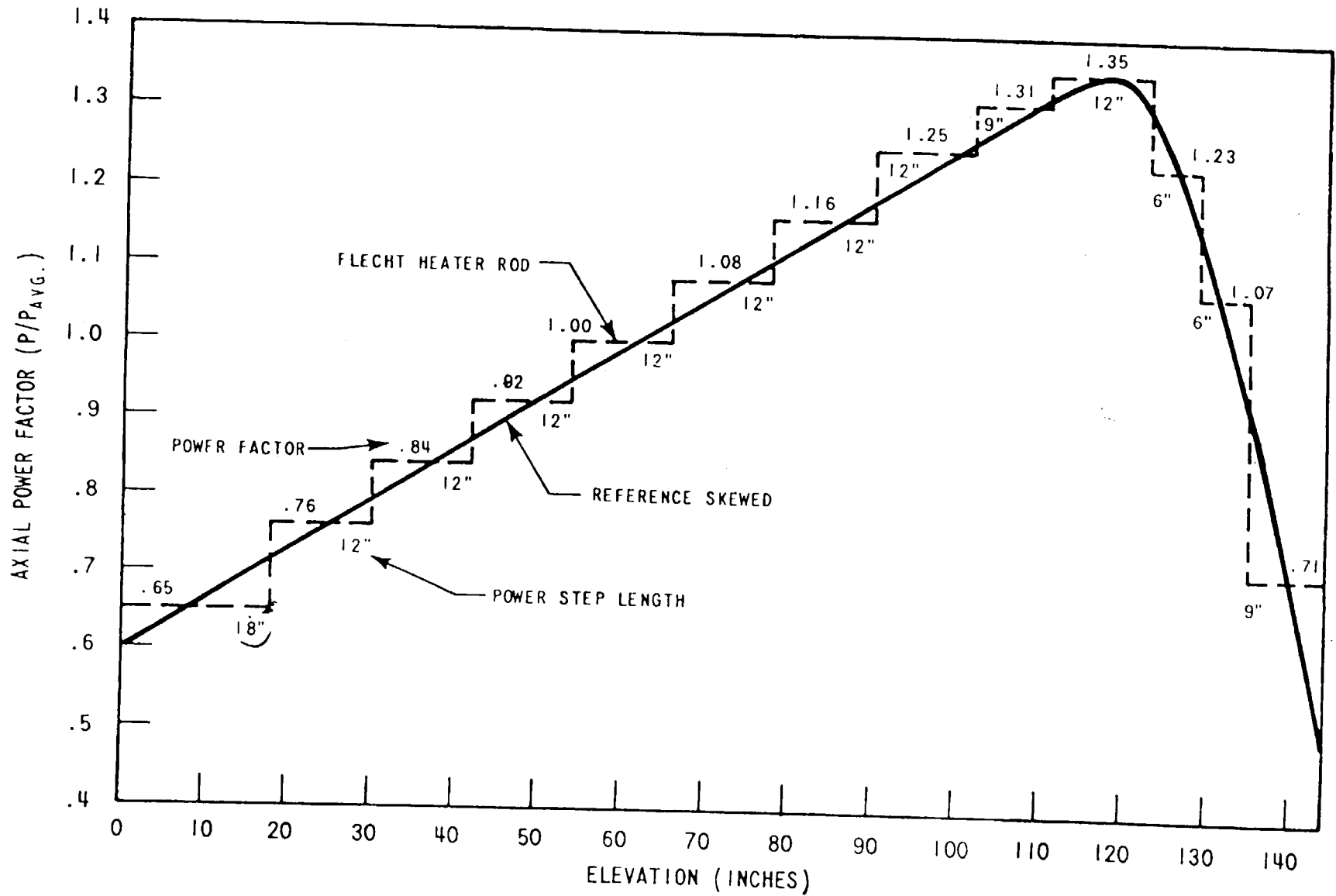
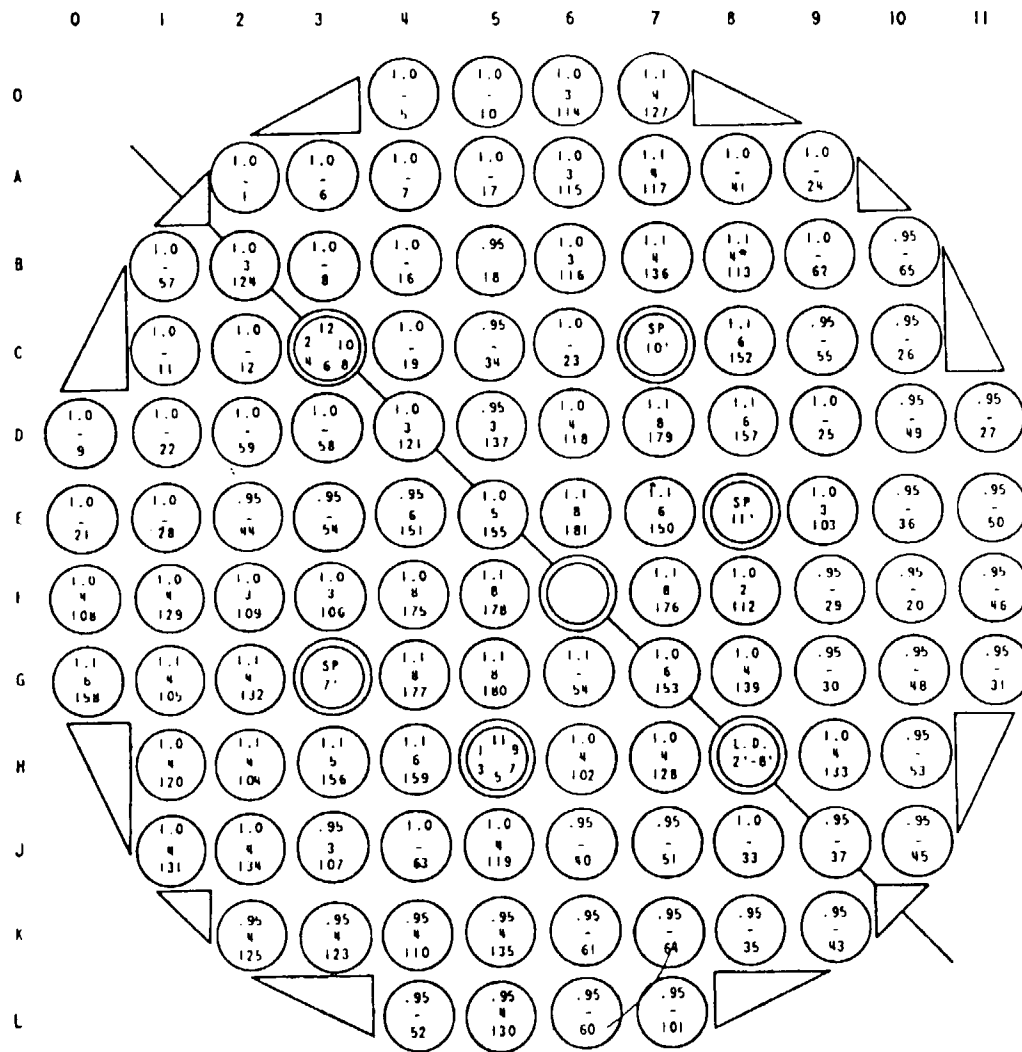


Figure A2-2. FLECHT Low Flooding Rate Test Power Shape

A2-7



LEGEND:

- 1.1, 1.0, .95 RADIAL POWER DISTRIBUTION
- TH THIMBLE
- SP STEAM PROBE
- LT ANC LEVEL TRANSDUCER (2'-8" ELEVATION)
-  INSTRUMENTED ROD WITH 8 T/C'S AT 3', 5', 7', 9', 9.5', 10', 10.5', 11' ELEVATIONS
-  INSTRUMENTED ROD WITH 6 T/C'S AT 1', 4', 6', 8', 10', 11.5' ELEVATIONS
-  INSTRUMENTED RODS WITH 5 T/C'S AT
A. 4', 6', 8', 10', 11.5' ELEVATIONS
B. 1', 4', 6', 8', 11.5' ELEVATION
-  INSTRUMENTED ROD WITH 4 T/C'S AT 2', 6', 10', 11' ELEVATIONS
-  INSTRUMENTED ROD WITH 3 T/C'S AT
A. 2', 6', 10' ELEVATIONS
B. 2', 6', 11' ELEVATIONS
C. 6', 10', 11' ELEVATIONS
D. 2', 10', 11' ELEVATIONS
- ROD 8B WITH ROUGHENED SURFACES AT T/C LOCATIONS

Figure A2-3. FLECHT Low Flooding Rate Test Rod Bundle Cross Section

**Appendix A-3
LITERATURE REVIEW**

Test Facility Name: Westinghouse FLECHT-SEASET 21 Rod Bundle Test Facility

Dates when Test were Performed: 1977-1982

References:

- R5. M. J. Loftus, et. al., "PWR FLECHT SEASET 21-Rod Bundle Flow Blockage Task Data and Analysis Report," NUREG/CR-2444, EPRI NP-2014, WCAP-992, Vol. 1. And Vol. 2, September, 1982.

Availability of Data:

Volume 1 contains data and limited analysis from the 21-Rod Bundle FLECHT-SEASET Program. Volume 2 contains sampling of data tables and plots collected for the unblocked bundle (Configuration A) and 5 blocked bundle configurations, (B, C, D, E and F). All the valid measured data are available in the NRC data bank.

Test Facility Description, Types of Tests:

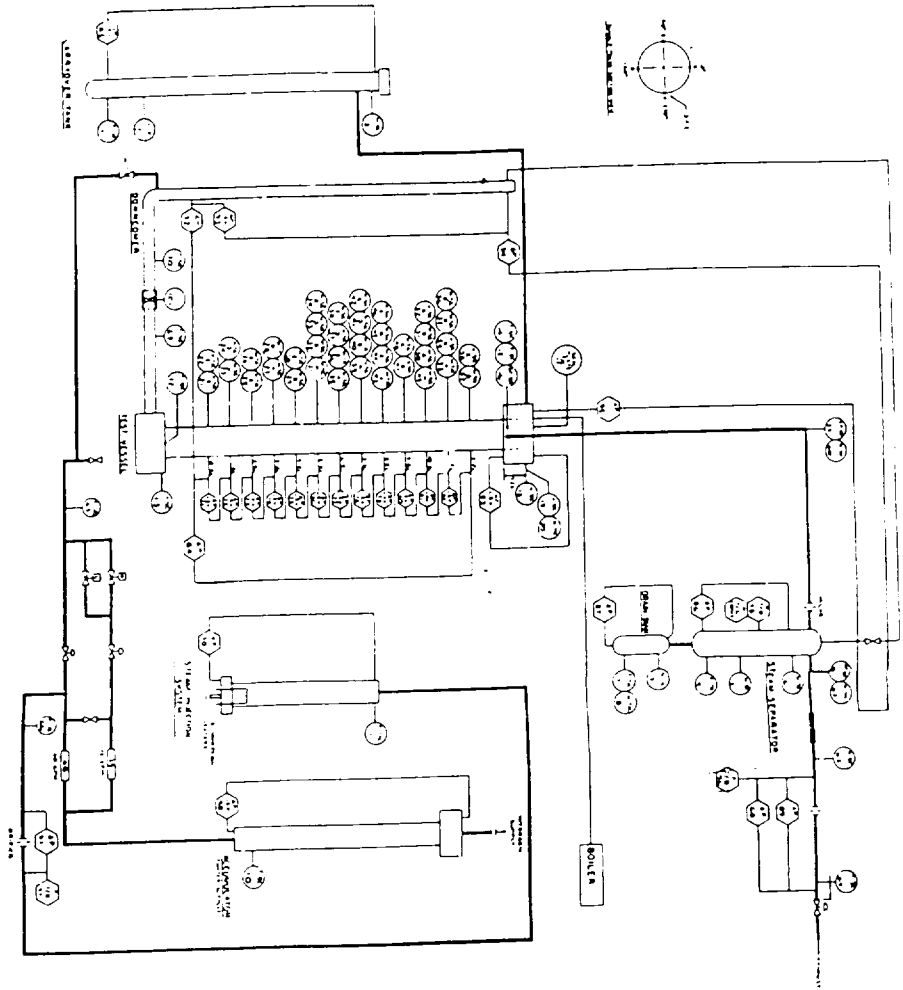
Low forced flooding rate, gravity reflood, and single phase flow tests were performed in the 21-Rod bundle FLECHT-SEASET Test Facility. The overall objectives of these tests were to determine effects of various flow blockages on reflooding behavior and to aid in development/assessment of computational models in predicting reflooding behavior of flow blockage configurations for the 163-Rod flow blockage bundle test.

The tests were performed using a 5 x 5 rod bundle array typical of a 17 x 17 power fuel assembly. The bundle contained 21 active electrical heater rods and 4 triangular shaped filler strips placed at the corners in order to minimize excess flow areas due to the circular low mass flow housing as shown in Figure A-3.1. The heater rods were 0.374 inch (0.0095m) in diameter and were arranged in a square pitch of 0.496 inches (0.0125 m) and had a heated length of 12 ft (3.42 m). The electrical heater rods used a 1.66 peak to average axial power distribution with a chopped cosine shape, which was approximately simulated by different pitch coils in the electrical heating element, as shown in Figure A-3.2. The heater rod bundle had a uniform radial power profile. Spacer grids were of a simple egg-crate style installed 21 inches (0.533 m) apart. The tests were conducted in a heavily instrumented facility as shown in Figure A-3.3.

Four types of tests were conducted: hydraulic characteristics tests, steam cooling tests, forced reflood tests, and gravity reflood tests. The hydraulic characteristic tests were performed to determine the pressure losses associated with rod friction, grids, and blockage sleeves.

The steam cooling tests were performed to measure single-phase flow heat transfer effects of unblocked and blocked configurations.

A3-2



NO.	DESCRIPTION	UNIT	SCALE	TYPE	LOCATION	STATUS
1
2
3
4
5
6
7
8
9
10
11
12
13
14
15
16
17
18
19
20
21
22
23
24
25
26
27
28
29
30
31
32
33
34
35
36
37
38
39
40
41
42
43
44
45
46
47
48
49
50
51
52
53
54
55
56
57
58
59
60
61
62
63
64
65
66
67
68
69
70
71
72
73
74
75
76
77
78
79
80
81
82
83
84
85
86
87
88
89
90
91
92
93
94
95
96
97
98
99
100

Figure A3-2 21-Rod Bundle Flow Blockage Task Instrumentation Schematic Diagram

Forced reflood tests were performed to measure the two-phase flow heat transfer effects of unblocked and blocked configurations.

The gravity reflood tests were performed to measure heat transfer effects during the PWR-simulated gravity reflood injection for unblocked and blocked configurations.

The range of conditions included

Constant flooding rates:	0.4-6.0 in/sec (10.2-152 mm/sec)
Upper plenum pressure:	20-40 psia (0.14-0.28 mpa)
Initial clad temperature: (at peak location)	500°F-1600°F (260°C-871°C)
Inlet subcooling:	5°F-140°F (3°C-78°C)
Variable in steps flooding rates:	0.8 to 6.8 in/sec (20 to 152 mm/sec)
Injection gravity reflood (variable steps)	0.2 to 1.8 lb/sec (0.09 to 0.82 kg/sec)
Housing temperature tests (at peak location)	431°F-1015°F (222°C-546°C)
Repeat tests	there were 2 repeat tests of the unblocked Configuration (A)

temperature measurement locations in the bundle. However comparisons of calculated and measured temperatures generally showed good agreement. Nusselt Numbers calculated from the steam cooling data were compared with the Dittus-Boelter heat transfer correlation as a function of Reynolds number. The results showed that, in general, the Dittus-Boelter correlation under predicts the heat transfer coefficient for Reynolds numbers less than 2500 and its in agreement for values above Reynolds numbers greater than 10000.

Differential pressure measurements along the length of the flow housing were used to determine the mass accumulation in the bundle during reflood test, but no attempt was made to calculate void fractions related to froth level and dispersed flow regions. In addition, no entrained droplets diameters and velocities were made because there were no windows to take high speed movies as it was done in the 161-rod bundle FLECHT-SEASET test.

TABLE 5
Assessment of FLECHT-SEASET Unblocked 21-Rod Bundle Test to RBHT PIRT:
A Dispersed Flow Region for Core Component

Process/Phenomena	Ranking	Basis	FLECHT-SEASET 21-Rod Bundle
Decay Power	H	Energy source which determines the temperature of the heater rods, and energy to be removed by the coolant.	Known, measured initial condition.
Fuel Rod/Heater Rod properties, ρ , C_p , k	L	The exact properties can be modeled and stored energy release is not important at this time.	Heater rod properties are known and approximate those of nuclear rod.
Dispersed Flow Film Boiling	H	Dispersed flow film boiling modeling has a high uncertainty which directly effects the PCT.	Only 2 T, measurements, and no valid α measurements were made.
• Convection to superheated vapor	H	Principle mode of heat transfer as indicated in FLECHT-SEASET experiments ⁽⁴⁾ .	Total heat transfer was measured, convective H.T. was estimated from data.
• Dispersed phase enhancement of convective flow	H	Preliminary models indicate that the enhancement can be over 50% in source cases ⁽²⁾ .	Comparisons of estimate convective H.T. to conventional correlation showed 2 ϕ enhancement. No model for this.
• Direct wall contact H.T.	L	Wall temperatures are significantly above T_{min} such that no contact is expected.	Only total heat transfer was measured, this component was not isolated.
• Dry wall contact ⁽¹²⁾	M	Hoje ⁽¹²⁾ indicates this H.T. Mechanism is less important than vapor convection.	Only total wall heat transfer was measured, this component was not isolated.
• Droplet to vapor interfacial heat transfer	H	The interfacial heat transfer reduces the vapor temperature which is the heat sink for the wall heat flux.	No measurements
• Radiation Heat transfer to: • Surfaces • Vapor • Droplets	M/H M/H M/H	This is important at higher bundle elevations (H) where the convective heat transfer is small since the vapor is so highly superheated. Very important for BWR reflow with sprays, and colder surrounding can. Large uncertainty.	Radiation to vapor was estimated.
Gap heat transfer	L	Controlling thermal resistance is the dispersed flow film boiling heat transfer resistance. The large gap heat transfer uncertainties can be accepted, but fuel center line temperature will be impacted.	Not present. Heater rods have no gap.
Cladding Material	L	Cladding material in the tests is Inconel which has the same conductivity as zircalloy nearly the same temperature drop will occur.	Used stainless steel clad
Reaction Rate	M	Inconel will not react while Zircalloy will react and create a secondary heat source at a very high PCTs, Zirc reaction can be significant	Not present
Fuel clad swelling/ballooning	L	Ballooning can divert flow from the PCT location above the ballooning region. The ballooned cladding usually is not the PCT location. Large uncertainty.	Ballooning was simulated with sleeves attached to heater rods in bundle configurations B, C, D, E and F. Enhance factors on H.T. were calculated.

TABLE 6
Assessment of FLECHT-SEASET Unblocked 21-Rod Bundle Test to RBHT PIRT:
Top Down Quench in Core Components

Process/Phenomena	Ranking	Basis	FLECHT-SEASET 21-Rod Bundle
De-entrainment of film flow	L ¹	The film flow is the heat sink needed to quench the heater rod. This has high uncertainty.	Top down quenching was observed in some tests.
Sputtering droplet size and velocity	L	The droplets are sputtered off at the quench front and are then re-entrained upward. Since the sputtering front is above PCT location, no impact. The entrained sputtered drops do affect the total liquid entrainment into the reactor system, as well as the steam production, in the steam generators.	Details at top quench front were not measured. Only total heat transfer was measured.
Fuel rod/heater rod properties for stored energy ρ , C_p , k .	L ¹	These properties are important since they determine the heat release into the coolant. However, since this occurs above PCT level, no impact.	Heater rod properties are known.
Gap heat Transfer	L ¹	Affects the rate of energy release from fuel/heater rod.	No gap in heater rods.

Note: Some of these individual items can be ranked as high (H) within the top down quenching process; however, the entire list is ranked as low (L) for a PWR/BWR since it occurs downstream of the PCT location.

TABLE 7
Assessment of FLECHT-SEASET Unblocked 21-Rod Bundle Test to RBHT PIRT:
Preliminary PIRT for Gravity Reflood Systems Effects Tests

Process/Phenomena	Ranking	Basis	FLECHT-SEASET 21-Rod Bundle
Upper Plenum - entrainment/de-entrainment	M	The plenum will fill to a given void fracture after which the remaining flow will be entrained into the hot leg, large uncertainty.	Not Measured
Hot Leg-entrainment, de-entrainment	L	The hot legs have a small volume and any liquid swept with the hot leg will be entrained into the steam generator plenums, medium uncertainty.	Not Measured
Pressurizer	L	Pressurizer is filled with steam and is not an active component- small uncertainty.	Not Measured
Steam Generators	H	The generators evaporate entrained droplets and superheat the steam such that the volume flow releases (particularly at low pressure). The result is a higher steam flow downstream of the generators-high uncertainty since a good model is needed. FLECHT-SEASET data exists for reflood.	Not Measured
Reactor Coolant Pumps	H	This is the largest resistance in the reactor coolant system which directly affects the core flooding rate-low uncertainty.	Not Measured
Cold Leg Accumulator Injection	H	Initial ECC flow into the bundle.	Not Measured, variable flows were simulated to model accumulator and pumped injection, also continuous by variable flooding rate tests were performed.
Cold Leg Pumped injection	H	Pumped injection maintains core cooling for the majority of the reflood transient.	Not measured, variable flows were simulated to model accumulator and pumped injection, also continuous by variable flooding rate tests were performed.
Pressure	H	Low pressure (20 of psia) significantly impacts the increased vapor volume flow rate, which decreases the bundle flooding rate.	Low pressure (20 psia) simulated.
Injection Subcooling	M/H	Lower subcooling will result in boiling below the quench front such that there is additional vapor to vent.	Low subcooling simulated.
Downcomer wall heat transfer	H	The heat transfer from the downcomer walls can raise the ECC fluid temperature as it enters the core, resulting in more steam generation.	Not Measured
Lower Plenum Wall Heat Transfer	M	Source effect as downcomer but less severe.	Not Measured
Break	L	Excess ECC injection spills, but break ΔP helps pressurize reactor system.	Not Measured

A3-7

TABLE 8
Assessment of FLECHT-SEASET Unblocked 21-Rod Bundle Test to RBHT PIRT:
High Ranked BWR Core Phenomena

Process/Phenomena	Ranking	Basis	FLECHT-SEASET 21-Rod Bundle
Core			
• Film Boiling		PCT is determined in film boiling period.	Total heat transfer is measured
• Upper Tie Plate CCFL		Hot Assembly is in co-current up flow above CCFL limit.	Not applicable
• Channel-bypass Leakage		Flow bypass will help quench the BWR fuel assembly core.	Not applicable
• Steam Cooling		A portion of the dispersed flow film boiling heat transfer.	Steam cooling heat transfer is estimated from data
• Dryout		Transition from nucleate boiling and film boiling.	Quench front is measured
• Natural Circulation Flow		Flow into the core and system pressure drops.	Not Measured
• Flow Regime		Determines the nature and details of the heat transfer in the core.	Not Measured
• Fluid Mixing		Determines the liquid temperature in the upper plenum for CCFL break down.	Not Measured
• Fuel Rod Quench Front		Heat release from the quench front will determine entrainment to the upper region of the bundle.	Quench front data exists
• Decay Heat		Energy source for heat transfer.	Measured as initial/boundary conditions
• Interfacial Shear		Affects the void fraction and resulting droplet and liquid velocity in the entrained flow.	Not measured
• Rewet: Bottom Reflood		BWR hot assembly refloods like PWR.	Total reflood heat transfer measured
• Rewet Temperature		Determines the quench front point on the fuel rod.	Quench temperature is measured
• Top down Rewet		Top of the hot assembly fuel will rewet in a similar manner as PWR.	Top down rewet quench front measured
• Void Distribution		Gives the liquid distribution in the bundle.	Not measured
• Two-Phase Level		Similar to quench front location, indicates location of nucleate and film boiling.	Measured by rod T/C's, collapsed level measured, 2 ϕ level estimated from DP cells.